Summer 2018

HYDROTHERMAL WATER-ROCK REACTION MODELING WITH MICROBIAL CONSIDERATIONS: RABBIT CREEK AREA, YELLOWSTONE NATIONAL PARK, WY

Shanna Law
Montana Tech

HYDROTHERMAL WATER-ROCK REACTION MODELING WITH MICROBIAL CONSIDERATIONS: RABBIT CREEK AREA, YELLOWSTONE NATIONAL PARK, WY

by

Shanna L. Law

A thesis submitted in partial fulfillment of the requirements for the degree of

Master of Science in Geoscience:
Geochemistry Option

Montana Technological University

2018

Abstract

Water-rock reactions at depth are the main control on aqueous hydrothermal chemistries of hot springs and other thermal features. Thermophilic microbes living in the hydrothermal system are a secondary control on aqueous hydrothermal chemistries and are expected to have increasing influence as spring temperatures decrease. The Rabbit Creek area of Yellowstone National Park (YNP) is an ideal case study for investigating the geologic and biologic controls on aqueous hydrothermal chemistries due to the proximity of the drill core Y-5 to geochemically diverse hydrothermal features (17.3°C to 92.2°C ± 0.1°C; field pH values 6.50 to 9.60 ± 0.05).

The modeling program EQ3/6 was used to compare expected and predicted hydrothermal aqueous chemical speciations of hydrothermal features in the Rabbit Creek area. The expected aqueous chemical speciations were found using EQ3 to speciate initial measured concentrations of dissolved major ions and trace elements from each thermal feature. EQ3/6 was used to predict local water-rock reactions by interacting local meteoric water with the summarized mineralogy of the altered rhyolitic tuff of drill core Y-5. The EQ3/6 model was cooled, depressurized, and calibrated to the aqueous chemistry of a proximal, near boiling spring expected to have negligible microbial activity (based on low extracted DNA yields of ~5 ng DNA/g of sediment). The calibrated EQ3/6 water-rock reaction model was further cooled to the measured temperature of each hydrothermal feature analyzed to predict changes in aqueous chemical speciation.

Speciated chemistries of springs were generally similar to predictions from modeled water-rock interactions, but differences increased as temperatures cooled. The EQ3/6 predictions for most springs showed deficiencies in silica, aluminum, and sulfur compared to EQ3 speciations, which could be improved by adding H_2S (g) to the system and allowing for supersaturation in the models. Variations in calcium in the thermal features were expected to be a function of plagioclase remaining unsaturated and being more variable in the Y-5 subsurface than the other minerals. Discrepancies in pH between field measurements, EQ3 speciated pH, and EQ3/6 predicted pH values for each feature represent disequilibrium. Part of the disequilibrium in cooler features (<75°C) could be due to microbial influence, but sampling time lags and occasional changes from single-stage to continuous steam separation in the Y-5 area most likely imparted the strongest control on pH values.

Archaea and bacteria were identified from DNA extracted from the sediment of the hot spring to which the EQ3/6 model was initially calibrated. The microbial community includes H_2S (g) producers, sulfur oxidizers, nitrate reducers, arsenite oxidizers, and iron reducers, in addition to a few key organisms that metabolize central carbons or oxidize hydrogen. It is not unlikely that similar organisms inhabit the other thermal features analyzed in this study, but further work would be necessary to constrain those specific microbial communities. An outlier spring at ~74°C showed the most unexpected geochemistry and is interpreted as having greater shallow meteoric influence as well as probably more microbial influence. Grizzly Pool (17.3°C ± 0.1°C, pH of 9.60 ± 0.05) has the least hydrothermal input of the analyzed features and is more affected by evaporation and microbial influence than any other feature.

Keywords: water-rock reactions, hydrothermal, aqueous chemistry, thermophilic microbes, Yellowstone, EQ3/6

Acknowledgements

Thank you to my advisor, Dr. Alysia Cox, for showing support, dedication, and patience during each step of this research. Thesis committee members Chris Gammons and Katherine Zodrow also provided supportive critique throughout the progress of this research.

The United States Geological Survey's Core Research Center permitted access to drill core Y-5 (R762) and unpublished notes by the scientists whom originally logged the core. The field research for this project was allowed by the National Park Service Permit No. YELL-2017-SCI-7008 and funded by the NASA Exobiology Award No. NNX-16AJ61G awarded to Drs. Everett Shock, Alysia Cox, Jayson Raymond, Jordan Okie, Kris Fecteau, and Grayson Boyer. Other funding sources to Alysia Cox and projects within her laboratory include: Montana Tech Faculty Development Initiative Grant to Alysia Cox and Georgia Dahlquist, the Montana Tech Faculty Seed Grant to Alysia Cox, the Montana Water Center Grant to Alysia Cox, and the Montana Research and Economic Development Initiative (MREDI) Grant to Jerry Downey, Ed Rosenberg, Hsin-Hsiung Huang, and Alysia Cox.

The field sampling was accomplished with the assistance of the 2017 Laboratory Exploring Geobiochemical Engineering and Natural Dynamics (LEGEND) field team (Mallory Nelson, Jordan Foster, Georgia Dahlquist, James Foltz, Johnathan Feldman, and Isaiah Robertson). Of special note are those who assisted in collecting the samples analyzed in this document: Nicholas Allin, Jordan Foster, Isaiah Robertson, Alaina Cox, Caitlin Cox, and Michelle Hauer. Laboratory analyses of water samples for cations, anions, and trace metals were performed by Ashley Huft and Jackie Timmer at the Montana Bureau of Mines and Geology. Renée Schmidt, Steve Parker, and Jackie Timmer kindly provided training and insight as necessary into the analysis of dissolved inorganic and organic carbon samples. LEGEND 2016 members Georgia Dahlquist, Renée Schmidt, and Jordan Foster graciously provided training and orientation to LEGEND procedures.

Many thanks go to the Group Exploring Organic Processes in Geobiochemistry (GEOPIG) under Dr. Everett Shock at Arizona State University. Notable thanks include but are not limited to: allowing the use of their high temperature dissolved oxygen meter for field sampling and providing and maintaining an internally consistent thermodynamic database for the modeling program EQ3/6 (which was most recently updated by Dr. Brian St. Clair in 2016). Dr. Kristopher Fecteau, Dr. Brian St. Clair, and James Andrew Leong graciously answered questions about EQ3 and EQ6 input files that facilitated the progress of this research.

Conversations with Dr. David Hobbs (Montana Tech), Dr. Raja Nagisetty (Montana Tech), and especially Dr. Allan Harvey (National Institute of Standards and Technology) were instrumental to calculating Henry's Law constants for use in finding temperature corrected $\log fO_2$ values for reduction-oxidation modeling constraints.

Table of Contents

List of Tables

List of Figures

List of Equations

Glossary of Terms

Term	Definition
$An_{\#}$	Percent (#) of anorthite (calcium feldspar) in plagioclase (Ca-Na feldspar)
BSA	Bovine serum albumin
CIA	Chloroform/isoamyl alcohol
Cryptoperthite	Perthitic texture on a microscopic scale.
DEB	DNA extraction buffer
DIC	Dissolved inorganic carbon
DOC	Dissolved organic carbon
DNA	Deoxyribonucleic acid
GEOPIG	Group Exploring Organic Processes in Geochemistry
HDPE	High density polyethylene
ICP-MS	Inductively coupled plasma - mass spectrometry
ICP-OES	Inductively coupled plasma - optical emission spectrometry
ka	Kilo-annum
LEGEND	Laboratory Exploring Geobiochemical Engineering and Natural Dynamics
Ma	Mega-annum
MBMG	Montana Bureau of Mines and Geology
Milli-Q	Millipore Q 18.2 MΩ/cm ultrapure water
Mr. DNA	Molecular Research DNA, Limited Partnership
$Or_{\#}$	Percent (#) of orthoclase (potassium feldspar) in perthite
PCIA	Phenol/chloroform/isoamyl alcohol
PCR	Polymerase chain reaction
Perthite	Intergrown grains of orthoclase (K feldspar) and albite (Na feldspar)
ppb	Parts per billion
ppm	Parts per million
RNA	Ribonucleic acid
rRNA	Ribosomal ribonucleic acid
SEWS	Salt ethanol wash solution
SDS	Sodium dodecyl sulfate
TBE	Tris/borate/EDTA
TDS	Total dissolved solids
USGS CRC	United States Geological Survey Core Research Center
VSMOW	Vienna Standard Mean Ocean Water
YNP	Yellowstone National Park

1. Introduction

1.1. Geology of Yellowstone National Park (YNP)

Below the surface of Yellowstone National Park (YNP) is a hot spot in the Earth's mantle (Pierce *et al.*, 1992; Christiansen *et al.*, 2002; Smith *et al.*, 2009). Due to the hot spot, basaltic magma initially erupted around the Nevada-Oregon-Idaho border about 16 Ma, and, as the North American tectonic plate moved approximately southwest over the hot spot, progressive eruptions formed the calderas and flood basalts of the eastern Snake River Plain (Pierce *et al.*, 1992; Smith *et al.*, 2009). YNP is a result of the most recent volcanic activity of the hot spot and has been dominated by rhyolitic eruptions despite the presence of bimodal volcanism (Christiansen and Blank Jr., 1972; Christiansen, 2001). There have been three caldera forming stages of predominantly rhyolitic ash-flow volcanism in YNP around 2.06 Ma, 1.29 Ma, and 0.64 Ma (Christiansen and Blank Jr., 1972; Lanphere *et al.*, 2002).

One endeavor to examine the subsurface lithology of YNP involved removing 13 drill cores from across the park in 1967-68 (White, 1975). From this, information on the conductive heat flow in the park was established (White, 1978), and a myriad of detailed studies were published on the geology of the drill core material (Honda and Muffler, 1970; Keith *et al.*, 1978; Keith and Muffler, 1978; Bargar and Beeson, 1981, 1984, 1985; Bargar and Muffler, 1982). The large scale drilling operations in YNP affected groundwater flow and the output of thermal features (White, 1975), which has limited the amount of drilling that has been allowed in YNP. The only other drill cores available from YNP, cores C-I and C-II, were removed in 1929-30 (Fenner, 1936), thus making the information gained from the removal of the latter 13 drill cores all the more valuable. Whole rock geochemistry was published for all 15 drill cores (Beeson and

Bargar, 1984), and the YNP drill cores continue to inspire research today (King *et al.*, 2016; Lowenstern *et al.*, 2016).

The YNP subsurface is observably dynamic and active due to the ongoing presence of the hot spot. There are two resurgent domes in the 0.64 Ma Yellowstone Caldera: the Sour Creek Dome in the northeast of the caldera and the Mallard Lake Dome in the southwest of the caldera (Chang *et al.*, 2007; Hurwitz and Lowenstern, 2014). These resurgent domes have displayed vertical uplift and subsidence at rates of ± 0.5 to 7 cm/yr, with increased activity in the last nine years (Chang *et al.*, 2007, 2010). Thousands of recorded earthquakes throughout YNP, including relatively recent earthquake swarms in 2009 and 2010, also demonstrate the activity of the Yellowstone subsurface (Chang *et al.*, 2010; Farrell *et al.*, 2010; Shelly *et al.*, 2013).

1.2. Water-Rock Investigations in YNP

The dynamism of the hot spot has caused fracturing and brecciation in the brittle upper crust in YNP, creating avenues for fluid flow and hydrothermal alteration in the subsurface (Dobson *et al.*, 2003). Sudden decompressional boiling in the subsurface fluid due to hydrothermal activity is often responsible for the creation of fractures and breccias seen in active hydrothermal areas (Keith and Muffler, 1978; Hedenquist and Henley, 1985; Sturchio *et al.*, 1990). These paths can be filled with precipitating minerals, thus "self sealing" and also preventing avenues for fluid flow (Keith *et al.*, 1978; Dobson *et al.*, 2003). In these ways, the dynamism of the hot spot controls the subsurface path taken by the fluid that is exuded throughout YNP in thermal features such as hot springs, mud pots, geysers, and fumaroles.

Only about 0.2 – 0.4% of the hydrothermal water that reaches the YNP surface is sourced from the magma chamber (Fournier, 1989). Instead, greater than 99% of the aqueous output of hydrothermal features in YNP is meteoric water that has been circulated through the subsurface

hydrothermal system (Fournier, 1989). Snowmelt from the Gallatin and northern Absaroka Ranges are thought to primarily recharge the YNP subsurface (Kharaka *et al.*, 2002), although local meteoric water directly infiltrates the YNP subsurface as well. Radium and radon isotopes have been used to show that a mean time frame for water-rock reactions in the YNP subsurface (in the Norris Geyser Basin) is 540 years before the hydrothermal fluid starts to ascend (Clark and Turekian, 1990). However, meteoric water exists at depth for various amounts of time, especially depending on the area within YNP. Radium isotopes have shown that different areas in YNP have time frames of subsurface meteoric water circulation ranging at least from 20 – 55 days to 25 – 1600 years (Moloney *et al.*, 2011). For example, hydrothermal features in the Rabbit Creek area of the Lower Geyser Basin were concluded to exude older hydrothermal fluid than the features in the Norris Geyser Basin or Mammoth Hot Spring areas of YNP (Moloney *et al.*, 2011). The main control on the aqueous hydrothermal chemistry of thermal features in YNP is expected to be water-rock reactions at depth in the hydrothermal system.

The extent of water-rock reactions are controlled by the temperatures and pressures at depth. The Pinedale Glaciation (47 - 15.5 ka) is a major event during which temperature and pressure were increased relative to modern times in the YNP subsurface (Bargar and Fournier, 1988; Sturchio *et al.*, 1990, 1994). Homogenization temperatures of fluid inclusions in hydrothermal quartz and fluorite from the YNP drill cores provide insight to paleo-temperature-pressure regimes (Bargar and Fournier, 1988). The temperatures of up-flow zones in YNP (including the upper part of the Y-5 drill core) were warmer by about 20°C - 50°C and up to 155°C during and possibly before the Pinedale Glaciation (Bargar and Fournier, 1988). In the Rabbit Creek area, subsurface temperatures were between 131°C to 275°C during the Pinedale Glaciation (Bargar and Fournier, 1988). It is thought that during (and/or before) the Pinedale

Glaciation, much of the hydrothermal alteration represented in the YNP drill cores occurred (Bargar and Fournier, 1988).

Previous investigations into the specifics of water-rock reactions in YNP used data from the YNP drill cores. Dobson *et al.*(2004) generated reactive transport models using the summarized mineralogy of YNP drill core Y-8 and the Lawrence Livermore National Laboratory modeling program TOUGHREACT to correctly predict the observed assemblage of most alteration minerals in the drill core (except zeolites). King *et al.*(2016) modeled multireaction chemical equilibria geothermometry using the summarized mineralogy of YNP drill core Y-3 and nearby aqueous hydrothermal chemistry. There have been no other published models on the YNP drill cores, leaving much room for further research.

Other analyses of water-rock reactions in YNP have focused on tracing components of the aqueous hydrothermal fluid. As rhyolitic rocks in the YNP subsurface are hydrothermally altered, boron decreases in the rocks (Shaw and Sturchio, 1992). The opposite has been observed for lithium, which tends to be incorporated into alteration minerals (Shaw and Sturchio, 1992; Sturchio and Chan, 2003). While there is an inverse relationship between boron and lithium in altered rhyolitic rocks, there has been an observed average B/Li ratio of ~3 for YNP thermal waters (Shaw and Sturchio, 1992).

1.3. Thermophilic Microbes in YNP

It is well known that extremophile microbes inhabit thermal features and have metabolisms that influence the aqueous chemistry of thermal features (ex: Brock, 1967; Reysenbach *et al.*, 2000; Meyer-Dombard *et al.*, 2005; Boyd *et al.*, 2007; Wagner and Wiegel, 2008; Shock *et al.*, 2010; Cox *et al.*, 2011; Saltikov, 2011; Brock, 2012; Inskeep *et al.*, 2013; Alsop *et al.*, 2014). Microbes in all three kingdoms of life (Eukaryota, Bacteria, and Archaea)

have been found in YNP thermal features, and many deep-branching thermophilic archaea are likely representative of the early evolution of life (Blank *et al.*, 2002; Meyer-Dombard *et al.*, 2005; Wagner and Wiegel, 2008). A variety of metabolisms and electron acceptors are represented in hydrothermal systems, including relatively common electron acceptors (ex: oxygen, nitrate, nitrite, sulfide, sulfate, carbon monoxide, carbon dioxide) and relatively uncommon electron acceptors (ex: arsenate and arsenite) (Shock *et al.*, 2010; Saltikov, 2011). Specific microbial communities vary between thermal features and are controlled by geochemical parameters. For example, the ability of photosynthetic microbes to survive in YNP thermal features is controlled by the interplay of pH, temperature, and sulfide concentrations (Cox *et al.*, 2011). While there is much that can be said on this topic, for the scope of this thesis, it is most important to note that the microbial communities of thermal features are secondary controls on aqueous hydrothermal chemistries and should be taken into consideration when studying thermal features.

1.4. Thesis Objectives

The overall goal of this study was to examine the extent of abiotic and biotic controls on the aqueous hydrothermal chemistries of YNP thermal features. This was accomplished by comparing known hydrothermal aqueous chemistries of YNP thermal features with hydrothermal aqueous chemistries predicted from modeled subsurface water-rock reactions. Water-rock reactions were modeled specific to the temperature of each thermal feature analyzed and assumed that the thermal features were all primarily fed by the same hydrothermal fluid. It was expected that the observed aqueous hydrothermal chemistries of the analyzed YNP thermal features would be different from the predicted aqueous hydrothermal chemistries, at least in part due to the presence of thermophilic microbes in the hydrothermal system. Of the thermal features

analyzed in this thesis, Grizzly Pool was expected to contain a larger contribution from shallow meteoric water than the other thermal features. One of the goals of this thesis was to determine how much detectable hydrothermal input there was to this feature.

1.5. Study Site

Drill core Y-5 was removed from the Lower Geyser Basin in 1967 (White, 1975). The Y-5 drill core was originally chosen to be representative of the Midway part of the Lower Geyser Basin, and its location was ideal due its simultaneous ease of access and absence from the public eye (White, 1975). The location of Y-5 is also situated on the northwestern edge of the Mallard Lake resurgent dome (Fig. 1).

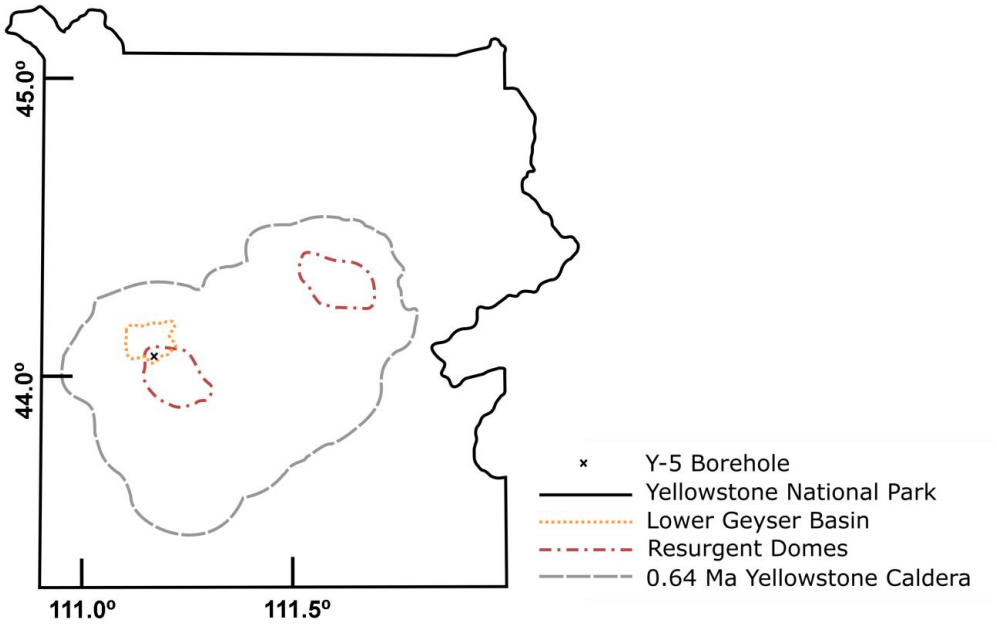

Figure 1: Y-5 borehole location within YNP.
YNP and the Lower Geyser Basin boundaries were drawn from White, 1975. The 0.64 Ma caldera and resurgent dome boundaries were drawn from Chang *et al.*, 2007.

Keith and Muffler (1978) extensively studied the mineralogy and lithology of Y-5. They correlated the rhyolitic tuffs of Y-5 as part of the Lava Creek Tuff, which is the uppermost part of the Yellowstone Group (Keith and Muffler, 1978). K-Ar dating of Y-5 material indicated that the rock has an age of 577 ± 30 ka (Keith and Muffler, 1978).

The Y-5 borehole is located in the Rabbit Creek area, broadly southeast of Grand Prismatic Hot Spring and north of Old Faithful Geyser. There are several loosely defined thermal areas within the Rabbit Creek area, which have been analyzed by the Group Exploring Organic Processes in Geochemistry (GEOPIG) at Arizona State University and the Laboratory Exploring Geobiochemical Engineering and Natural Dynamics (LEGEND) at Montana Technological University. The unofficially named Rabbit Creek thermal areas, with distances relative to the Y-5 borehole, are: Rabbit Creek North (~1.5 km northeast), Rabbit Creek South (~1.6 km southeast), and Tomato Soup (~1.75 km northeast) (Fig. 2).

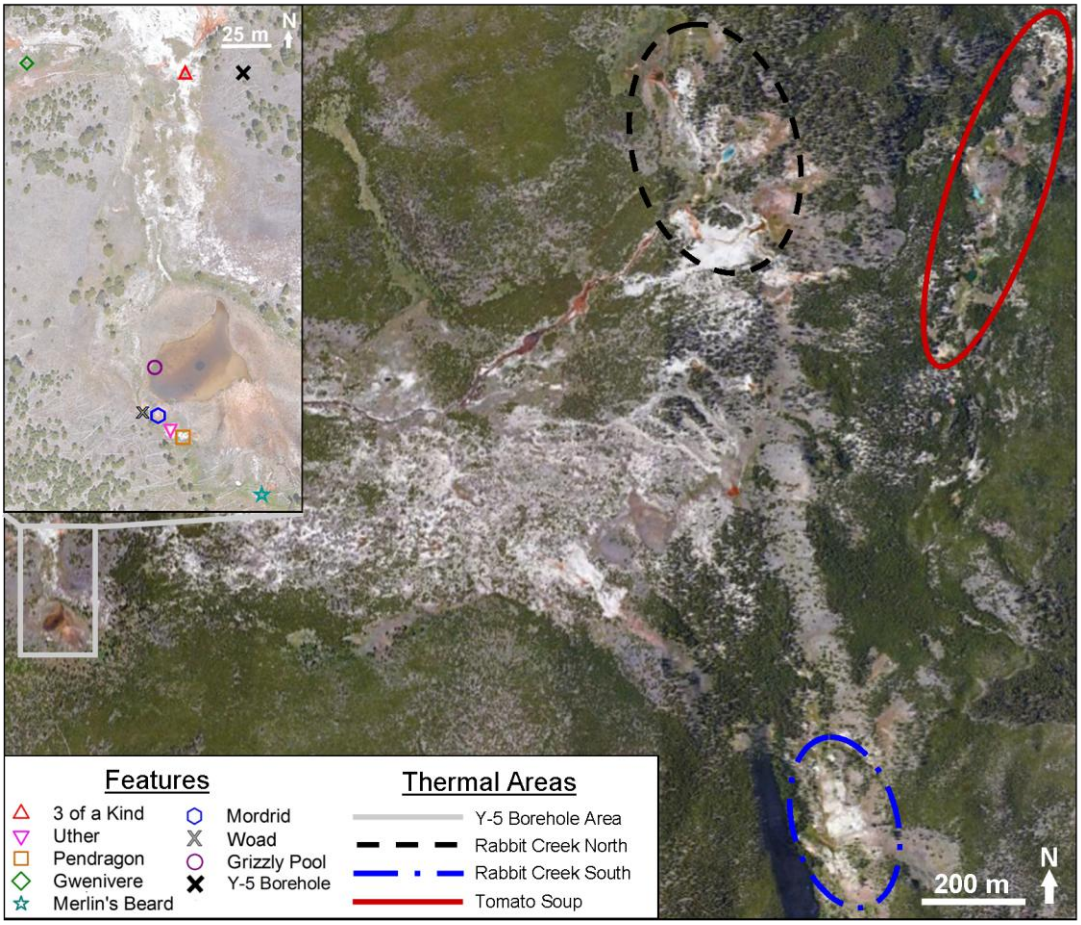

Figure 2: Thermal areas within the Rabbit Creek vicinity.
The features around the Y-5 borehole are paid special attention. Satellite imagery from Google Earth, 2017.

Rabbit Creek North contains the deeply sourced, alkaline chloride Rabbit Creek Source Pool, and the Rabbit Creek Source outflow travels southwest toward the Y-5 borehole area (Fig. 2). In contrast, the Rabbit Creek South area contains some springs that are essentially boiling meteoric water (Dahlquist, 2017). Tomato Soup is characterized by springs with red water that look like tomato soup, hence the area's name. The diversity of thermal features within the Rabbit Creek area made it essential that the thermal features compared to the Y-5 borehole be as close to the actual borehole as possible in order to minimize error due to the variability of the area.

There are two deeply sourced hot springs proximal to the Y-5 borehole, unofficially named in this thesis as "3 of a Kind" and "Gwenivere" (Fig. 2-3). Gwenivere is ~110 m west of the Y-5 borehole and 3 of a Kind is ~30 m west of the Y-5 borehole (Fig. 2-3). Other thermal features in the vicinity of the Y-5 borehole are diverse and include: Till Geyser (southwest of Gwenivere and northwest of Woad, not pictured), a hot spring with red water (west of Gwenivere, not pictured), 5 unnamed hot springs within ~70 m of each other but ranging 48.8°C in temperature (unofficially labeled in this document as "Uther", "Pendragon", "Merlin's Beard", "Mordrid", and "Woad"; Fig. 2-3), and Grizzly Pool (a ~17°C body of water ~50 m across; Fig. 2-3). These features are all within 300 m of the Y-5 borehole. The only springs without outflow channels are Uther, Mordrid, and Woad.

Grizzly Pool does not have an active outflow channel, and looks more similar to a meteoric water body than a hydrothermal spring at first glance, despite being surrounded by obvious thermal features (Fig. 3). Even though satellite imagery clearly reveals a hole in the center of Grizzly Pool, which could be an avenue for hydrothermal fluid into the body of water, Grizzly Pool is nonetheless an outlier from the other features (Fig. 2-3). As previously mentioned, one of the goals of this thesis was to determine how much detectable hydrothermal

input there currently is to this feature. The other five features south of Grizzly Pool are of modeling interest because they are obvious hydrothermal features and thus more similar to 3 of a Kind and Gwenivere, despite being separated geographically by the anomalous Grizzly Pool. Even though the thermal features closest to the Y-5 borehole show much variability, as does the entire Rabbit Creek area, focusing on this small area was still the most relevant to the geology revealed by the Y-5 borehole.

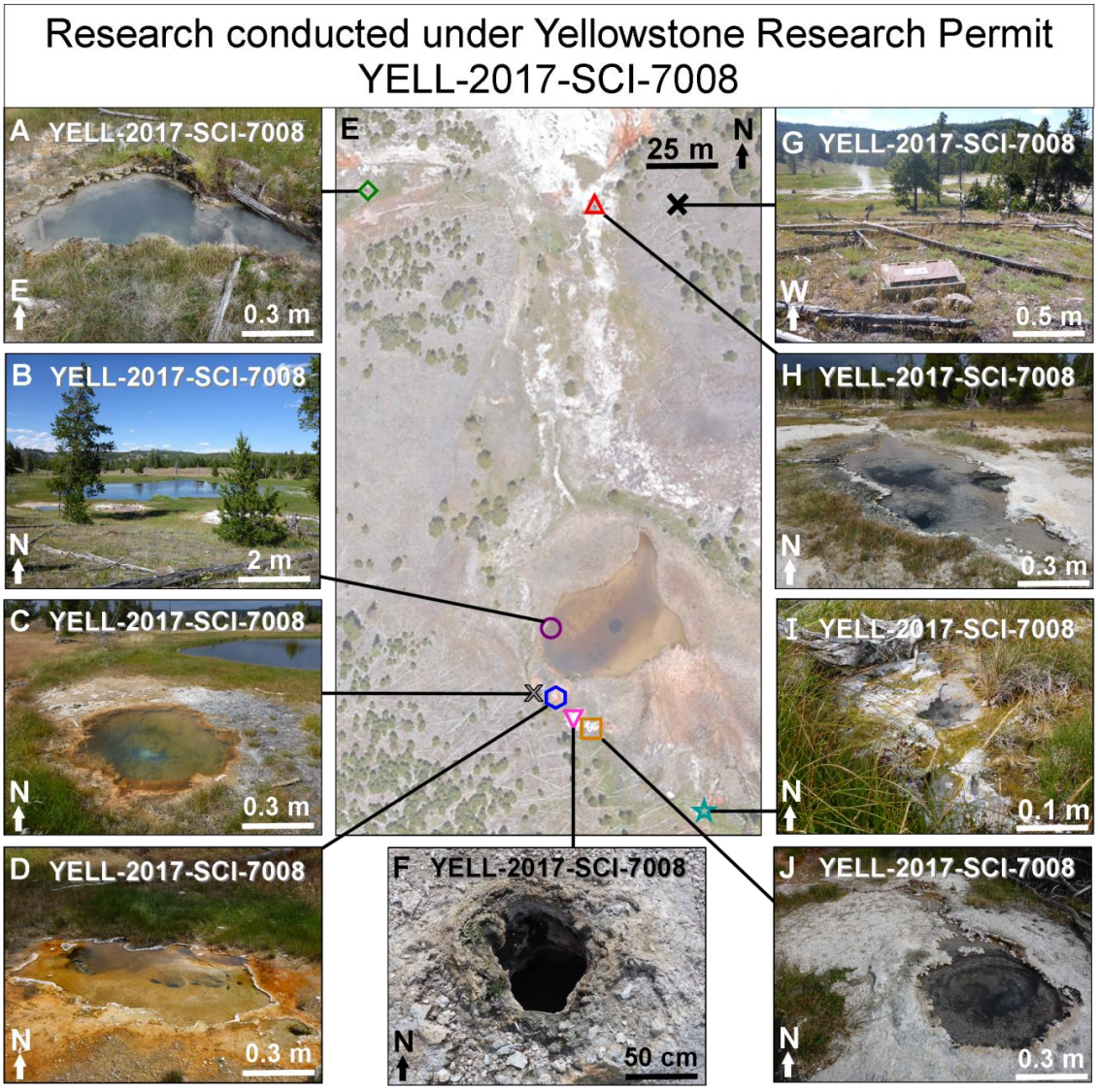

Figure 3: Y-5 borehole and surrounding thermal features: locations and images.
(A) Gwenivere, (B) Grizzly Pool, (C) Woad, (D) Mordrid, (E) Satellite image from Google Earth, 2017 with plotted sample locations, (F) Uther, (G) Y-5 borehole, (H) 3 of a Kind, (I) Merlin's Beard, and (J) Pendragon. Unofficial names are used, except for Grizzly Pool.

2. Methods

2.1. Drill Core Analysis

Drill core Y-5 is housed at the United States Geological Survey's Core Research Center (USGS CRC) in Lakewood, Colorado. This drill core had already been thoroughly logged and analyzed in the 1960-70s, along with the other YNP drill cores. The main scientists who originally studied Y-5 were T. E. C. Keith, L. J. P. Muffler, and C. N. Bargar, and they left hundreds of pages of handwritten notes detailing their results from visual inspection, petrography, and X-ray diffraction (Keith *et al.*, 1968-78). For this study, both the unpublished notes and published conclusions (Keith and Muffler, 1978) were scrutinized concurrently with visual inspection of drill core Y-5 (Core Library Number R762) at the USGS CRC for one week in January, 2017. Color photographs of representative sections of the drill core were taken, and a summarized core log was generated. Estimated bulk mineralogical proportions were deduced to use as input to EQ6 models.

Previously published whole rock geochemistry of Y-5 included trace element concentrations, weight percents of major elements as oxides, and normative mineral calculations (Beeson and Bargar, 1984). The published weight percents of the Y-5 rock (SiO_2, Al_2O_3, Fe_2O_3, FeO, MgO, CaO, Na_2O, K_2O, P_2O_5) were used to calculate the aluminum-saturation index, the alkalinity index, the iron index, and the modified alkali-lime index as outlined by Frost and Frost, 2008. All four indices plot against SiO_2 (wt. %) to classify igneous rocks.

The aluminum-saturation index (ASI) is defined as:

$$\mathrm{ASI} = \frac{\mathrm{Al}}{\mathrm{Ca} - 1.67\mathrm{P} + \mathrm{Na} + \mathrm{K}} \quad (1)$$

where elemental masses are calculated from the weight percents using molecular weights (Frost and Frost, 2008). An ASI value above one indicates that the rock is peraluminous, and an ASI value less than one indicates that the rock is metaluminous (Na + K < Al) or peralkaline (Na + K > Al) (Frost and Frost, 2008). A peraluminous rock has more aluminum than is necessary to form feldspars (Frost and Frost, 2008). A portion of phosphorus is subtracted from the calcium to correct for the probable presence of calcium phosphates, like apatite, which is a common igneous accessory mineral.

The alkalinity index (AI) is defined as:

$$AI = Al - (K + Na) \tag{2}$$

where elemental masses are calculated from the weight percents using molecular weights (Frost and Frost, 2008). An AI value greater than one means that the rock is peraluminous or metaluminous, whereas an AI value less than one means that the rock is peralkaline (Frost and Frost, 2008). This index is most helpful for alkaline rocks (Frost and Frost, 2008).

The iron index (Fe-index) is defined as:

$$Fe\ index = \frac{\mathrm{FeO_T}}{\mathrm{FeO_T + MgO}} \tag{3}$$

where

$$FeO_T = \mathrm{FeO} + (0.9)(\mathrm{Fe_2O_3}) \tag{4}$$

The Fe-index defines a rock as ferroan or magnesian (Frost and Frost, 2008).

The modified alkali-lime index (MALI) is defined as:

$$MALI = Na_2O + K_2O - CaO \tag{5}$$

which defines a rock as calcic, calc-alkalic, alkali-calcic, or alkaline (Frost and Frost, 2008).

2.2. Measured Water Chemistries

2.2.1. Laboratory Preparation

Storage containers for field-filtered water samples required extensive in-laboratory preparation before field sampling occurred. Separate bottles were prepared to store filtered sample water for analysis of: stable water isotopes ($\delta^{18}O$ and δD), total dissolved inorganic carbon (DIC), total dissolved organic carbon (DOC), major cations, major anions, and trace elements. Procedures were similar to those in Dahlquist, 2017 and Schmidt, 2017.

10 mL glass vials were prepared to store water to be analyzed for stable water isotopes. Each vial was rinsed with Millipore Q 18.2 MΩ/cm ultrapure water (aka Milli-Q) seven times, wrapped in tin foil, and dried in a muffle furnace at 450°C for four hours. Each bottle lid was rinsed with Milli-Q water seven times and dried on previously muffled tin foil in a positive pressure HEPA hood (Envirco Corp, filter model 69600S-00HPLXX) (Dahlquist, 2017). The bottles were capped in the HEPA hood and then were ready to store sample water.

40 mL glass vials were prepared to store water to be analyzed for DIC and DOC. Each bottle was rinsed with Milli-Q water seven times and allowed to soak in a bath of ~10% HCl (v/v) for 72 hours. Afterwards, each bottle was rinsed seven times with Milli-Q water, wrapped in tin foil, and dried in a muffle furnace at 450°C for four hours. Each bottle lid was washed in the same manner as the bottles but dried on previously muffled tin foil in a positive pressure HEPA hood. The bottles were capped in the HEPA hood, and then the DIC bottles were ready to store sample water. Each vial for DOC was subsequently preserved with 85 µL 85% phosphoric acid and then were also ready to store sample water.

30 mL high density polyethylene (HDPE) Nalgene bottles were prepared to store water to be analyzed for major cations, major anions, and trace elements. Each bottle was individually

filled with ~1% (v/v) Citranox soap and allowed to soak for 24 hours, flipped to continue soaking for 24 hours, filled with ~10% HCl (v/v) to soak for 72 hours, flipped to continue soaking for 72 hours, filled with ~pH 2 HCl to soak for 72 hours, and flipped to continue soaking for 72 hours. Each bottle was rinsed with Milli-Q water seven times in between each cleaning solution and at the beginning and end of the procedure. Trace metal grade HCl was used, and trace metal clean gloves were worn throughout the process. After the washing procedure, the final Milli-Q rinse was poured over a pH strip to ensure sufficient acid removal. The final droplets of rinse water were thoroughly removed by flicking the open bottles. Bottles to store sample for analysis of major cations and major anions were filled with fresh Milli-Q for storage. Bottles to store sample for analysis of trace elements were preserved with 1% (v/v) (300 µL) undiluted trace metal grade nitric acid. The same trace-metal-clean washing procedure for HDPE 30 mL bottles was used to prepare field equipment used to collect and field-filter water samples: 1 L HDPE Nalgene bottles, 150 mL syringes, and tygon tubing. New polycarbonate stop cocks were acid washed with an abbreviated procedure: rinsed with Milli-Q water three times, soaked in ~10% HCl overnight, rinsed seven times with Milli-Q water, soaked in ~pH 2 HCl overnight, and rinsed seven times with Milli-Q water .

2.2.2. Field Sampling

We sampled the water of the Y-5 area thermal features on August 13, 2017, using multiple field techniques (*in situ* meters, water filtration, and field spectrophotometry). Other thermal features in the Rabbit Creek area, including in the thermal areas RC North, RC South, and Tomato soup, were similarly sampled throughout the middle of August, 2017.

In the Y-5 area, for the hot springs 3 of a Kind, Gwenivere, and Merlin's Beard, all samples were taken from the same location within the water body in immediate succession or

concurrently. For Uther, Pendragon, Mordrid, and Grizzly Pool, the *in situ* meter measurements were taken up to a few hours earlier than the full water samples were collected due to the availability of field hands and equipment. Full water samples were collected from the same location within each feature as the *in situ* meter measurements. Due to time constraints, the spring Woad was only sampled for *in situ* meter measurements with one collected sample for stable water isotopes.

We also collected two snow samples from the Rabbit Creek area on April 26, 2017, approximately one kilometer south-southwest of the Y-5 borehole. The snow samples were collected from the top few centimeters of remnant snow pack. The collected samples were melted in closed, trace metal clean HDPE collection bottles using ambient heat in the interior of a vehicle for expediency. The snow was sampled using *in situ* meters and water filtration for later laboratory analyses.

2.2.2.1. *In situ* Meters

Hand held meters and probes were used to measure *in situ* pH (WTW 3110 ProfiLine meter with Sentix 41-3 probe), conductivity (YSI 30 meter), and dissolved oxygen (Presens Fibox 4 meter with fiber optic oxygen dipping probe). Each meter also measured temperature, but the temperature measurement utilized for analysis and modeling was measured using the Presens Fibox 4 meter with temperature probe. The errors on these instruments were reported as the fluctuation of the measured value in the field, which is often greater than the instrumental error under ideal conditions. If instrumental error was greater than field fluctuation, the instrumental error was reported instead (pH ± 0.005; conductivity ± 0.2%; temperature ± 0.1°C).

2.2.2.2. Field Spectrophotometry

Dissolved silica and reduction-oxidation active chemical species of interest (dissolved sulfide and ferrous iron) were measured on-site using a portable field spectrophotometer (Hach DR/1900). The compounds were measured as absorbance and converted to concentration using calibration curves produced in the lab and saved to the instrument.

Fresh, unfiltered hot spring water was measured for total dissolved sulfide using the Methylene Blue Method 10254 after Cline, 1969 and similar to Cox *et al.*, 2011, Dahlquist, 2017, and Schmidt, 2017. This method is Hach test #691, which measures total dissolved sulfide at a wavelength of 665 nm and has a range of 0.31 to 2.19 µmol/L for a sample volume of 10 mL. Hach sulfide reagents 1 (sulfuric acid and N,N-dimethyl-p-phenylenediamine) and 2 (potassium dichromate) were added in 0.5 mL increments in rapid succession to a 10 mL blank of Milli-Q water and to the10 mL sample, where various sulfide species reacted for five minutes with N,N-dimethyl-p-phenylenediamine sulfate to form methylene blue. The final color intensity was proportional to sulfide concentration. Test interferences included high turbidity, high concentrations of barium or sulfide, or the presence of strong reducing agents (ex: sulfite, thiosulfate, hydrosulfite). The interference of concern is mild turbidity in samples 170813FA Merlin's Beard and 170813GA Grizzly Pool. This test was performed immediately after sample collection directly next to each sample site to prevent movement of the sample or subsequent loss of sulfide. No dilutions were necessary, which helped prevent sulfide loss. The reported precision of the method at ideal lab conditions is 5 µg/L (0.16 µmol/kg), which is assumed here to be up to seven times greater (35 µg/L; 1.12 µmol/kg) due to field and sample conditions.

Fresh, filtered (0.2 µm) sample water was measured for ferrous iron using the 1,10-phenanthroline method after St. Clair, 2017, and similar to Dahlquist, 2017. This method

measures Fe(II) at a wavelength of 510 nm and has a range of 0.35 to 44.8 µmol/L. To 10 mL of filtered (0.2 µm) sample water, 100 µL of 0.178 mol/L 1,10-phenanthroline monohydrate was added and allowed to develop for 1 minute. The blank was 10 mL of filtered (0.2 µm) sample water with no added reagent. Test interferences include Cu (II) and Hg in concentrations greater than 10^{-3} mol/L or 10^{-7} mol/L respectively. Later measurements of copper in the samples show that Cu (II) is not of concern. While Hg was not measured in these samples, thermal waters in the general Rabbit Creek area have been reported to have Hg concentrations on the order of magnitude of 10^{-4} to 10^{-5} mol/L, which suggests that there could be interference from Hg (Ball *et al.*, 2010). No dilutions were necessary. The precision of the method is 10 µg/L (0.18 µmol/kg) under ideal lab conditions or 20 µg/L (0.36 µmol/kg) under field conditions (St. Clair, 2017). It was helpful to measure for ferrous iron in the field to compare to dissolved iron (ferrous + ferric) data obtained through ICP-MS analysis of water filtered in the field (see sections 2.2.2.3 and 2.2.3.3).

Filtered (0.2 µm) sample water was measured for dissolved silica using Silicomolybdate Method 8185, also used by Schmidt, 2017. This method is Hach test #656, which measures dissolved silica at a wavelength of 452 nm and has a range of 16.6 to 1664.3 µmol/L. To 10 mL of filtered (0.2 µm) sample water, Hach molybdate and Hach acid reagents were added to develop silicomolybdic and phosphomolybdic acid complexes for 10 minutes. The Hach citric acid reagent was added to destroy the phosphomolybdic acid complexes for 2 minutes before analysis. The remaining yellow color of the solution was proportional to the concentration of silica. The blank was 10 mL of filtered (0.2 µm) sample water with no added reagent. Test interferences include turbidity, sulfides, and the presence of slow reacting forms of silica. The interference of concern is mild turbidity in samples 170813FA Merlin's Beard and 170813GA

Grizzly Pool. Samples measured for silica had a dilution factor of five. The reported precision of the method under ideal lab conditions is 1 mg/L (16.6 µmol/kg), which is assumed here to be up to seven times greater (7 mg/L; 116.2 µmol/kg) due to field and sample conditions.

2.2.2.3. Water Filtration

Sample water was filtered on-site into storage bottles for geochemical analysis. Each water sample was retrieved with a 2 m long HDPE sampling dipper (triple rinsed with sample) and poured into a 1 L HDPE Nalgene bottle (originally washed to trace metal cleanliness (see section 2.2.1) and triple rinsed with sample). A 150 mL syringe with tygon tubing and polycarbonate stop cock (originally trace metal cleaned or acid washed (see section 2.2.1) and triple rinsed with sample) were used to filter water from the sample bottle, through PALL® Acrodisc® Supor® membrane sterile filters (1.2 µm and 0.8 µm/0.2 µm), and into storage bottles. The sample collection bottle, syringe, stop cock, and tubing were re-used for each sample (after triple rinsing with each new sample), but a new set of six collection bottles were used to store the filtered water from each sample (see section 2.2.1). The first field sample was a field blank, which consisted of filtered, trace metal clean Millipore Q 18.2 MΩ/cm ultrapure water (aka Milli-Q) that had been brought to the field in a trace metal clean 1 L HDPE Nalgene bottle.

Six sample storage bottles were filled in the field for each sample, each bottle having been previously prepared in a laboratory for a final intended laboratory analysis (see section 2.2.1). For each sample, the bottles were consistently filled in the following order: stable water isotopes, major cations, major anions, DIC, DOC, and trace elements. Glass bottles (for stable water isotopes, DIC, and DOC) were filled to the upper meniscus, whereas HDPE bottles (for major cations, major anions, and trace elements) were filled to the shoulder. Samples for stable water isotopes and trace elements were stored at room temperature until laboratory analyses.

Samples for DIC and DOC analyses were stored at 4°C until laboratory analyses. Samples for major cations and major anions were stored at 4°C in the field and at -20°C in the laboratory until laboratory analyses.

2.2.3. Laboratory Analyses

Laboratory analyses were required for each bottle of filtered water collected for each sample. All sample analyses were performed on equipment at the Montana Bureau of Mines and Geology (MBMG). DIC and DOC samples were analyzed by LEGEND, and the rest of the samples were analyzed by MBMG chemists.

2.2.3.1. Stable Water Isotopes

Stable water isotopes ($\delta^{18}O$ and δD) were analyzed by chemists at the Montana Bureau of Mines and Geology (MBMG) on a Picarro Isotopic Water Analyzer L2130-i. Values were reported as $\delta^{18}O$ and δD relative to the Vienna Standard Mean Ocean Water (VSMOW), which are in units of per mille (‰). Instrumental errors were ± 0.01‰ for $\delta^{18}O$ and ± 0.1‰ for δD.

2.2.3.2. Dissolved Inorganic and Organic Carbon

Total DIC and DOC concentrations were analyzed by LEGEND at the MBMG using the Aurora 1030W Total Carbon Analyzer with Autosampler 1088. To analyze for DIC, 8.00 mL of sample was interacted with 1.50 mL of ~5% phosphoric acid. The reaction occurred at 70°C for 1.5 minutes to convert the dissolved inorganic carbon to gaseous carbon dioxide. The carbon dioxide gas was detected at 70°C for 3.5 minutes, and the concentration of carbon dioxide was proportional to the concentration of dissolved inorganic carbon. Standard solutions of lithium carbonate and sodium bicarbonate were made in-house at four concentrations each (eight solutions in total) and added to the autosampler before and after the samples. The data from the standard solutions were used to build a standard curve, and the standards were included at the

beginning and end of the analysis to monitor instrumental drift throughout the course of the analysis. Each solution (standard or sample) was analyzed in triplicate, and 10.00 mL of deionized water was rinsed through the instrument between each sample or standard. Lab blanks of Milli-Q water were included as necessary between the standard solutions and the samples to allow for extra clean up between solutions of vastly different concentrations.

To measure for DOC, 8.00 mL of sample was interacted with 1.00 mL of ~5% phosphoric acid at 70°C for 1.5 minutes and held at 70°C for 3.0 minutes. The solution was sparged with nitrogen gas for 2.0 minutes to remove the dissolved inorganic carbon as gaseous carbon dioxide. Next, 1.50 mL of ~10% sodium persulfate was added to the sample to oxidize the dissolve organic carbon into gaseous carbon dioxide. The reaction occurred at 97°C for 2.0 minutes, and the carbon dioxide gas was detected at 97°C for 3.0 minutes. The concentration of carbon dioxide gas was proportional to the concentration of dissolved organic carbon. Standard solutions of potassium hydrogen phthalate and sucrose were made in-house at four concentrations each (eight solutions in total) and added to the autosampler before and after the samples. The data from the standard solutions were used to build a standard curve, and the standards were included at the beginning and end of the analysis to monitor instrumental drift throughout the course of the analysis. Each solution (standard or sample) was analyzed in triplicate, and 10.00 mL of deionized water was rinsed through the instrument between each sample or standard. Lab blanks of Milli-Q water were included as necessary between the standard solutions and the samples to allow for extra clean up between solutions of vastly different concentrations.

The raw DIC and DOC data from the instruments were reported as integrated areas of signal peaks, which were then converted to units of parts per million (ppm) using the calibration

curves from the standard solutions run with each analysis. Values were converted from ppm to molality assuming solution density of 1 g/cm^3. Instrumental error for DIC was reported for each sample as the standard deviation of the three replicate analyses. Total DIC was speciated into CO_2 (aq), HCO_3^-, and CO_3^{-2} using equations from Eby (2004), and using the geochemical modeling program CHNOSZ to determine temperature appropriate $\log K_{a1}$ and $\log K_{a2}$ values for relevant reactions (Appendix A). A few DOC samples were only able to be analyzed for one replicate (170813GA Grizzly Pool, 170813HA Uther) due to a loss of sample. The instrumental error for DOC was reported as the average standard deviation from solutions with replicate analyses measured in the same run. The exception is Mordrid, whose own standard deviation was greater than the average standard deviation and reported as error for this sample.

2.2.3.3. Major Cations, Major Anions, and Trace Elements

Major cations (Li^+, Na^+, K^+, Ca^{+2}, and Mg^{+2}) were analyzed by chemists at the MBMG using EPA method 300.0 on a Thermo Scientific iCAP 6000 Series inductively coupled plasma optical emission spectrometer (ICP-OES). Major anions (F^-, Cl^-, NO_2^-, NO_3^-, Br^-, PO_4^{-3}, SO_4^{-2}) were analyzed by chemists at the MBMG using EPA method 300.1 on a Metrohm Compact Ion Chromatography Plus. Major cation and anion data were reported in ppm and values were converted to molality assuming a solution density of 1 g/cm^3. Instrumental error was provided as percent error on each ion, which was derived from replicate analyses of standards for each ion (Appendix E).

Trace elements (Be, B, Al, Ti, V, Cr, Mn, Fe, Co, Ni, Cu, Zn, Ga, As, Se, Rb, Sr, Zr, Nb, Mo, Pd, Ag, Cd, Sn, Sb, Cs, Ba, La, Ce, Pr, Nd, W, Tl, Pb, Th, and U) were analyzed by chemists at the MBMG using EPA method 200.8 on a Thermo Scientific iCAP Q inductively coupled plasma mass spectrometer (ICP-MS). Trace element data were reported in parts per

billion (ppb), and these data were converted to molality assuming a solution density of 1g/cm^3 and using isotopic correction factors provided by the MBMG for each relevant element. Instrumental error was provided as percent error on each element, which was derived from replicate analyses of standards for each element (Appendix E).

2.3. Geochemical Model Development

The geochemical modeling program used was EQ3/6 version 8.0a (updated 12-13-2010) (Wolery, 2010). This program was designed by Thomas J. Wolery at the Lawrence Livermore National Laboratory to model geochemical interactions between aqueous solutions, solids, and gases relevant to the Yucca Mountain Project (Wolery and Jarek, 2003). The EQ3/6 program has two main modeling components: (1) EQ3, which uses thermodynamic data to predict the chemical speciation of a given solution, and (2) EQ6, which is a reaction path code for modeling water-rock reactions (Wolery, 2010).

Both EQ3 and EQ6 utilize pre-Newton-Raphson optimization and then a Newton-Raphson iteration to solve sets of equations for concentrations of unknown chemical species (Wolery and Jarek, 2003). The pre-Newton-Raphson optimization converges rapidly far from the solution, and is used to define primary iteration variables only within one order of magnitude of the final solution (Wolery and Jarek, 2003). The Newton-Raphson iteration then converges quickly once the solution is near, and is used to define the final variables (Wolery and Jarek, 2003). For this project, EQ3 and EQ6 calculated all activity coefficients using the B-dot equation, which is a form of the extended Debye-Hückel equation. The pH scale was calculated using the Bates-Guggenheim equation.

The thermodynamic database used for all calculations was based on the internally consistent SUPCRT92 database originally compiled by Drs. James Johnson (Lawrence

Livermore National Laboratory), Eric Oelkers (University of California, Berkeley), and Harold Helgeson (University of California, Berkeley) (Johnson *et al.*, 1992). This database has been periodically updated for EQ3/6 by Dr. Everett Shock and others from the Group Exploring Organic Processes in Geobiochemistry (GEOPIG) at Arizona State University. The most recent version of this database, which was used for the models presented in this document, was updated by Dr. Brian St. Clair in 2016. The thermodynamic data in this EQ3/6 database are defined from 0°C to 350°C and from 1 bar to 165.21 bars.

2.3.1. EQ3 Models – Chemical Speciation of Thermal Features

EQ3 models were built for each thermal feature of interest. The input file for each thermal feature included the following geochemical data measured from the relevant field sample: water temperature, pH, dissolved oxygen, dissolved silica, dissolved sulfide, major cations and anions (PO_4^{-3} as HPO_4^{-2}), HCO_3^- from speciated DIC, and trace elements (see section 3.2.1, section 3.2.2, Appendix A, and Appendix E). Only trace elements that were measured above detection limit in at least one sample were included in the models (Be, B, Al, Ti, V, Mn, Fe, Cu, Zn, Ga, As, Se, Rb, Sr, Nb, Mo, Sb, Cs, Ba, W, Tl, Th, and U). These trace elements were included in all models for internal comparison and were valued at the lower detection limit (which were maximum values) for relevant samples (see Appendix E). Even though the modeled speciation of the trace elements measured below the lower detection limit in some samples were not relevant in terms of magnitude, they were relevant in terms of relative abundance, especially for comparison between samples. Ions and elements that were below the lower detection limit for all samples were omitted from the models (NO_2^-, Cr, Co, Ni, Zr, Pd, Ag, Cd, Sn, La, Ce, Pr, Nd, and Pb). Initial speciation of the trace elements for the EQ3 input files were chosen to be the basis species for each element as defined in the EQ3/6 database. Each EQ3 input file also

included a value for ammonium cited from literature for Yellowstone springs of similar pH, temperature, and location to each sample (see section 3.2.2; Holloway *et al.*, 2011).

For each EQ3 file, the overall reduction-oxidation condition was specified as $\log fO_2$. The fugacity of oxygen was approximately equated to the partial pressure of oxygen, which was calculated using Henry's Law. The Henry's Law calculation for each thermal feature required the *in situ* dissolved oxygen measurement and a temperature corrected Henry's Law constant. Temperature corrected Henry's Law constants were calculated using equation 15 from Fernández-Prini *et al.* (2003), which required temperature specific water vapor pressures calculated from Wagner and Pruss (1993) and temperature specific water densities from Kell (1975). Because the calculated values for $\log fO_2$ utilized *in situ* dissolved oxygen measurements, the reduction-oxidation constraint was unique for each sample. This was deemed the most appropriate reduction-oxidation constraint for the samples because the samples varied widely in temperature (and thus in dissolved oxygen), allowing for overall oxidation of the samples to be clearly differentiated by $\log fO_2$.

Certain reduction-oxidation pairs (HS^-/SO_4^{-2} and NH_4^+/NO_3^-) were additionally specified in the geochemical inputs. It did not seem reasonable to specify overall reduction-oxidation constraints based on either of these reduction-oxidation pairs because HS^- and NO_3^- were measured below the lower detection limit in some samples. However, it was relevant to constrain the values for both the oxidized and reduced forms of nitrogen and sulfur because these elements are nutrients essential to microbial life. For the samples that had values measured above the detection limit for both sides of one or both of the reduction-oxidation couples, it was important to use the measured values. In an effort to keep the input files consistent, the values for HS^- and NO_3^- were specified at their lower detection limits as necessary according to the data with the

understanding that these were maximum values for those samples (see section 3.2.2 and Appendix E for details).

EQ3 model sensitivity was tested for bulk geochemistry and reduction-oxidation conditions. The measured values for the geochemical data have error associated with them, so, for the main hot spring of interest, 3 of a Kind, EQ3 models were run using the upper, mid, and lower values of geochemical data based on error. EQ3 sensitivity to reduction-oxidation conditions was tested by similarly running the 3 of a Kind EQ3 model for the calculated $\log fO_2$ ± 0.5 log bars.

When possible, the EQ3 models were run without allowing the program to charge balance the system. However, many of the thermal features required a charge balance (Uther, Pendragon, Gwenivere, Mordrid, and Grizzly Pool), and setting the model to balance charge on H^+ actually yielded outputs with pH values closer to field pH than when the charge was balanced on other ions.

2.3.2. EQ3/6 Models – Water-Rock Reactions

Water-rock reactions were modeled in two parts. First, an EQ3 model was executed for local meteoric water (Rabbit Creek area snow) using the same chemical components included in the EQ3 inputs for the thermal features (see Appendix F). For geochemical components that were not measured from the snow (dissolved silica, sulfide, ammonium), dilute concentrations were chosen as initial values (10^{-5}, 10^{-6}, and 10^{-7} mol/kg, respectively). Second, the EQ3 pick-up file generated after running EQ3 was interacted with an idealized mineralogical composition of YNP drill core Y-5 using EQ6 (see section 3.1.3). The chemistry of the water in the EQ6 output after water-rock reactions is referred to as the EQ3/6 output in this thesis.

The EQ6 models were run as fluid-centered flow-through open systems in true kinetics time mode. This allowed for the irreversible water-rock reactions to start at elevated pressure and temperature at depth before the solution was depressurized and cooled to the measured surficial temperature and approximate atmospheric pressure of each analyzed thermal feature. During the ascent of fluid, minerals that were precipitated out of solution were no longer able to react with the final solution as it moved forward in time.

The forward rate laws for each mineral in the model were specified using relative rate constants proportional to the abundance of each mineral, which is a "good rule of thumb" suggested by Wolery and Jarek (2003) (see section 3.1.3). EQ6 uses a truncated second-order Taylor's series for relative rate calculations, where the specified relative rate constant in the EQ6 input file is used as the first constant in the Taylor's series (Wolery and Jarek, 2003). Backward rate laws were specified to be in partial equilibrium with the system, which allows for precipitation rates to be calculated as necessary to prevent supersaturation of dissolved components (Wolery and Jarek, 2003). This approach to backward rate laws has been done historically for modeling geochemical reaction paths (Helgeson *et al.*, 1970; Wolery and Jarek, 2003).

The starting temperature for the water-rock reactions was chosen as 167.8°C, which was the greatest temperature measured in the Y-5 borehole (White, 1975). This temperature was comfortably between the range of historical temperatures expected in the Rabbit Creek area subsurface based on fluid inclusion microthermometry (131°C to 275°C) (Bargar and Fournier, 1988). A sensitivity analysis for the starting temperature was performed at 250°C and 350°C.

The water-rock reactions were modeled over a time frame of 1.5 ka. Although 1.5 ka is a geologically short time frame, it is fitting based on previous radium isotope studies. Radium

isotopes suggest that the hydrothermal fluid of thermal features in the Rabbit Creek area is relatively old compared to other YNP areas, such as the Norris Geyser Basin, although the definition of "old" is vague (Moloney *et al.*, 2011). Meteoric water in the Norris Geyser Basin is thought to have reacted with rocks in the subsurface hydrothermal system for a mean age of 540 years before ascent (Clark and Turekian, 1990), and Moloney *et al.* (2011) suggests that in YNP, meteoric water can react with rocks in the YNP subsurface for up to 25 to 1600 years. A sensitivity analysis for the length of time was performed for time frames of 0.5 ka and 2.5 ka.

The geochemical inputs to EQ3 and mineralogical inputs to EQ6 were edited until the final geochemistry of the water in the EQ3/6 output was calibrated (i.e. matched) to the EQ3 speciation of the water of 3 of a Kind. The water-rock reaction model output (i.e. EQ3/6 output) was calibrated to the EQ3 speciation of 3 of a Kind because this spring is the closest thermal feature to the Y-5 borehole and exudes hot (92.2°C), deeply sourced fluid, meaning its aqueous hydrothermal chemistry is most likely to represent water-rock reactions relatively unaffected by microbes. The starting composition of the EQ3 meteoric water was the measured chemistry of 2017 snow from the Rabbit Creek area, which was calibrated by shifting starting concentrations of select chemical species. The starting mineralogy of the rocks was estimated mineral proportions based on Y-5 drill core analysis, which was calibrated by changing the relative forward rate constants for the dissolution of the minerals. The moles of each mineral were proportionally determined from the calibrated relative rate laws, and the molar proportions were normalized to 10,000 moles. Carbon dioxide gas was included in the model to help control the pH of the system, which was relevant because the majority of gas from Midway Geyser Basin thermal features is CO_2 (Fournier, 1989). CO_2 (g) was inputted in a similar manner to the mineral constituents, and was included in the molar normalization.

The EQ3 and EQ6 inputs (meteoric water chemistry and summarized Y-5 mineralogy respectively) were calibrated in the above manner for relevant species of the key elements (H, C, F, Na, Al, Si, S, K, and Ca). Only these elements (H, C, F, Na, Al, Si, S, K, and Ca) were focused on in the calibration because they are stoichiometrically present in the Y-5 drill core minerals, which allowed their aqueous concentrations to be controlled by mineral dissolution. The chemical species considered for each element in the calibration were the species that contained the elements that could be calibrated (ex: NaCl (aq) was excluded because Cl is not stoichiometrically in any inputted mineral, but NaF (aq) was included because Na and F are in Y-5 minerals). Calibration was performed via trial-and-error until: (1) the aqueous chemical species concentrations outputted from EQ3/6 matched the aqueous concentrations of the chosen 3 of a Kind calibration species as best as possible and (2) no EQ3/6 aqueous species concentrations were more than one order of magnitude different from the EQ3 aqueous species concentrations in 3 of a Kind water.

The calibrated EQ3/6 model was then cooled and depressurized to the field temperatures of Pendragon, Gwenivere, Merlin's Beard, and Mordrid for comparison to the EQ3 speciation of those thermal features. Starting assumptions for these models included: (1) all of the Y-5 thermal features are fed by the same hydrothermal source fluid due to their proximity to each other and (2) the differences in their fluid chemistries are primarily controlled by their differences in temperature.

2.4. Biological Analysis

A main assumption of the calibrated EQ3/6 model is that there are no noticeable changes to the speciation of the 3 of a Kind aqueous hydrothermal fluid due to microbes. To investigate the validity of this assumption, the microbial community of 3 of a Kind sediment was

determined. LEGEND extracted DNA from 3 of a Kind sediment, which Molecular Research (Mr. DNA) in Shallowater, TX, amplified and sequenced.

2.4.1. Sediment Collection

Sediment was collected from the bottom of each hot spring using a 2 m long HDPE sampling dipper. In the field, the sediment was homogenized and aliquoted from a sterile Dynarex specimen container into 2.0 mL centrifuge tubes (pre-sterilized in the lab using an autoclave) using a scoopula (field sterilized with 70% ethanol). Tubes were filled approximately ½ to ¾ full. During sample collection, a thin layer of sample water was kept on the sediment in order to reduce stress on the microorganisms in the sample. The water was drained from the sample right before the sample was frozen on dry ice in the field. About one week after sample collection, the samples were stored at -80°C until DNA extraction.

2.4.2. Laboratory Analyses

2.4.2.1. DNA Extraction

DNA was extracted from the sediment from the hot spring 3 of a Kind following the procedure outlined by Dahlquist, 2017 with minor modification. Only sediment from 3 of a Kind was analyzed due to temporal constraints. Most pipetting steps in the extraction procedure were performed in a positive pressure HEPA hood.

Sediment from two 2.0 mL centrifuge tubes was redistributed into six 2.0 mL centrifuge tubes (UV sterilized). DNA extraction buffer (DEB) with pH 8 was added to each tube in a ratio of 1000 µL DEB:1 g sediment. Each tube was vortexed and then put through three freeze-thaw cycles (-80°C to 65°C) with vortexing between each cycle. Each freeze-thaw cycle lasted approximately 12 minutes. After the freeze-thaw cycles, each aliquot was sonicated on ice (three

minutes of sonication, followed by three minutes of rest, with a final four minutes of sonication). The sonication was an addition to the Dahlquist, 2017 procedure.

After sonication, lysozyme (50 mg/mL) was added to each aliquot in a ratio of 18 µL lysozyme: 1 mL sample+DEB. Each aliquot was incubated at 37.0°C and 500 rpm for 30 minutes. Sodium dodecyl sulfate (SDS) (20 wt. %) was added to each sample in a ratio of 45 µL SDS: 1 mL sample+DEB. Next, proteinase K (20 mg/mL) was added to each sample in a ratio of 22.5 µL proteinase K: 1 mL sample+DEB. The addition of SDS and proteinase K was followed by an one hour incubation at 65.0°C and 500 rpm. After this incubation, all tubes were inverted by hand for 10 minutes and centrifuged for five minutes at room temperature and 14,000 x g.

After centrifugation, the supernatant from each aliquot was transferred to a new, UV sterilized 2.0 mL centrifuge tube and the pellets were discarded. Phenol/chloroform isoamyl/ alcohol (PCIA) (equal parts by volume) was added to each aliquot in a ratio of 1 mL PCIA: 1 mL supernatant. Each tube was inverted by hand and then centrifuged for one minute at room temperature and 14,000 x g. After centrifugation, the aqueous phase was transferred to new UV sterilized 2.0 mL tubes and the non-aqueous phase was discarded. Chloroform isoamyl/alcohol (equal parts by volume) (CIA) was added to each aliquot in a ratio of 1 mL CIA: 1 mL aqueous phase. Each tube was inverted by hand and then centrifuged for one minute at room temperature and 14,000 x g. After centrifugation, the aqueous phase was transferred to new UV sterilized 2.0 mL tubes and the non-aqueous phase was discarded. All pipetting involving PCIA and CIA were performed in a fume hood (sterilized with 70% ethanol) due to hazardous fumes.

In a HEPA hood, sodium acetate (3M) was added to each aliquot in a ratio of 1 µL sodium acetate: 1 mL transferred supernatant (aqueous phase). Isopropyl alcohol was added until full. All tubes were incubated at -20°C for approximately 36 hours.

Following precipitation, the tubes were combined into two 15 mL Falcon tubes (DNA/RNAse free) with the three tubes from each original sample tube being kept together. To each Falcon tube, sodium chloride (5 M) was added in a ratio of 1 mL NaCl: 1 mL sample. 1.0 mL of binding matrix was added to each tube. The tubes were inverted by hand for 10 minutes before being centrifuged for five minutes at room temperature and 3,260 x g. The supernatant was decanted until only ~750 µL of supernatant + pellet was left in each tube, which were homogenized and transferred to spin filter tubes. The samples were centrifuged for one minute at room temperature and 14,000 x g. Flow through was discarded, 500 µL of FastDNA® SPIN Kit salt water ethanol solution (SEWS) was added, and the pellets were re-suspended before another round of centrifugation (one minute, room temperature, 14,000 x g). Flow through was discarded before a second round of centrifugation (two minutes, room temperature, 14,000 x g). Flow through was discarded, and then the addition of SEWS with two subsequent centrifugations was repeated. The filters were transferred to UV sterilized 2.0 mL centrifuge tubes and allowed to dry with open lids in a positive pressure HEPA hood for five minutes. After the pellets had dried, 150 µL of sterile water was added to each sample. Each sample was shaken with extreme gentleness before the closed tubes were incubated for five minutes at 55.0°C. A final round of centrifugation (one minute, room temperature, 14,000 x g) was used to separate the eluant from the solids.

The filters were discarded and the eluant was kept. The DNeasy PowerClean Cleanup Kit, including the optional rinse with 100% ethanol, was used to clean the eluant from each sample. The final volume of each sample was concentrated to 50 µL. Nanodrop nucleic acid concentrations were below the lower detection limit (reported as negative values), and 260/280 ratios were poor (between 0.70 and 0.90). Qubit 3.0 was used to determine final DNA

concentrations for each sample. Qubit 3.0 is a fluorometer, and the Invitrogen double stranded DNA high sensitivity assay was used to attach fluorescent tags to the extracted DNA before determining DNA concentration. The two extracted sample volumes were later combined, and the average concentration was calculated to be approximately 0.26 ng/µL, which is about 5.2 ng DNA/g wet 3 of a Kind sediment. An aliquot of each sample was stored at 4°C for in-house polymerase chain reaction (PCR) and gel electrophoresis to test for DNA amplification. The remainder of each sample was stored at -80°C until the samples were combined and sent off campus for sequencing.

2.4.2.2. Polymerase Chain Reaction

LEGEND performed polymerase chain reaction (PCR) to ensure that the extracted DNA could be amplified. The 16S and 18S genes were targeted using primers from Integrated DNA Technologies: Universal (515F, 806R), Bacterial (1100F, 1429R), Archaeal (344F, 915R), and Eukaryotic (A7F, 570R). PCR was performed for each of the two samples of extracted DNA from 3 of a Kind sediment. For each sample, reagents were added to 0.2 mL UV sterilized tubes after Boyd *et al.*, 2010: 10.5 µL sterile water, 12.5 µL master mix, 0.4 µL forward primer (25 µM), 0.4 µL reverse primer (25 µM), and 1.2 µL sample. This was done for each primer for each sample. The master mix was comprised of: 80 µL of 50 mM $MgCl_2$, 80 µL of 5000 nM bovine serum albumin (BSA), 400 µL of 10 x PCR buffer, 24 µL of taq polymerase, 4 µL of each dNTP, and 1400 µL of sterile water (Dahlquist, 2017; Schmidt, 2017). A set of positive controls was prepared with added *M. smegmatis* and a set of negative controls was prepared with sterile water used as "sample". All tubes were put into an Eppendorf Mastercycler® gradient, and PCR settings were after Boyd *et al.*, 2010, Dahlquist, 2017, and Schmidt, 2017.

2.4.2.3. Gel Electrophoresis

In house gel electrophoresis was performed on the products of PCR after the methods in Dahlquist, 2017, and Schmidt, 2017. A 1% agarose gel was made for this purpose. To make the gel, 1.20 g agarose and 120 mL 1% TBE (54 g/L tris - 27.5 g/L borate - 37.2 g/L EDTA) were combined and microwaved until clear (~two minutes) (Dahlquist, 2017; Schmidt, 2017). To the mixture, 1.2 µL ethidium bromide (10 mg/mL) was added before the liquid was poured into a mold with combs added to create wells. After the gel set (~one hour), the combs were removed and the gel was covered with 1% TBE. The first and last well in each row of wells was filled with a ladder mixture (0.5 µL 1 kb DNA ladder, 1 µL 6x loading dye, 5.5 µL sterile water). The rest of the wells were filled with 1 µL of 6x loading dye and 5 µL sample (PCR product). The gel was run under 110 V for about one hour, after which the gel was visualized under ultraviolet light.

2.4.2.4. Sequencing

The two 3 of a Kind sediment DNA extracts were combined and sent to Molecular Research (Mr. DNA) in Shallowater, TX, where PCR amplification and 16S and 18S rRNA gene sequencing were performed for Bacteria and Archaea. Mr. DNA used the same PCR primers as used in-house (Bacterial: 1100F, 1429R; Archaeal: 344F, 915R) and used PCR reagents from the HotStarTaq Plus Master Mix Kit (Dahlquist, 2017; Schmidt, 2017). The PCR product was checked with a 2% agarose gel (Dahlquist, 2017; Schmidt, 2017). Sample separation was based on molecular weight and DNA concentration, and the sample was purified using Ampure XP beads (Dahlquist, 2017; Schmidt, 2017). A MiSeq was used to sequence the data from the sample, and the Mr. DNA analysis pipeline was used to process the data (removed sequences <150 base pairs, removed barcodes, deleted ambiguous base calls, and joined overlapping

sequences) (Dahlquist, 2017; Schmidt, 2017). The sequences were further cleaned for background noise, had chimeras removed, and had operational taxonomic units clustered at 3% divergence (97% similarity) before being taxonomically classified using the nucleotide Basic Local Alignment Search Tool (BLASTn) (Dahlquist, 2017; Schmidt, 2017). BLASTn was used in conjuncture with the curated database from the Ribosomal Database Project (RDP-II) and National Center for Biotechnology Information (NCBI) (Dahlquist, 2017; Schmidt, 2017).

3. Results

3.1. Drill Core Y-5

3.1.1. Primary Lithology

The Y-5 core is a shallow core extending only 164.0 m below the surface of the Earth (elevation 2,219 m) (Keith and Muffler, 1978). The first 11.9 m below the surface of the earth are summarized here as "messy deposits," which includes obsidian sand and gravel (mostly uncemented), pebble conglomerate (Fig. 4A), and breccia (Fig. 4B). The unconsolidated deposits predominantly lack evidence of hydrothermal alteration, and are interpreted as being deposited by the Pinedale Glaciation (Keith and Muffler, 1978). The underlying conglomerate and breccia have a green matrix composed of α-cristobalite, β-cristobalite, montmorillonite, clinoptilolite, and at least one known instance of erionite (Keith and Muffler, 1978). The clasts are rhyolite and pumice.

The vast majority of the rest of the core is classified as rhyolitic ash flow tuff that is correlated by Keith and Muffler (1978) as being part of the 577 ± 30 ka Lava Creek tuff. From 11.9 m to 34.9 m, the tuff has a "vapor-saturated" zone (Keith and Muffler, 1978). The upper portion of the "vapor-saturated" zone is a soft, porous tuff (Fig. 4C), which grades into a welded tuff by the bottom of this zone (Fig. 4D). The "vapor-saturated" tuff contains abundant phenocrysts and lithic fragments. The rest of the core from 34.9 m to 164.0 m is densely welded ash flow tuff. This tuff is crystal rich except for 99.1 m to 118.9 m, which predominantly contains lithic fragments (Keith *et al.*, 1968-78; Fig. 4H,I). The lithic-rich section of the densely welded tuff does still contain phenocrysts, which remain abundant at the top and bottom of the lithic-rich section (Fig. 4I) even though the lithic fragments are dominant in the middle of the lithic-rich section (Fig. 4H). Zircon is a minor accessory volcanic mineral throughout the tuff.

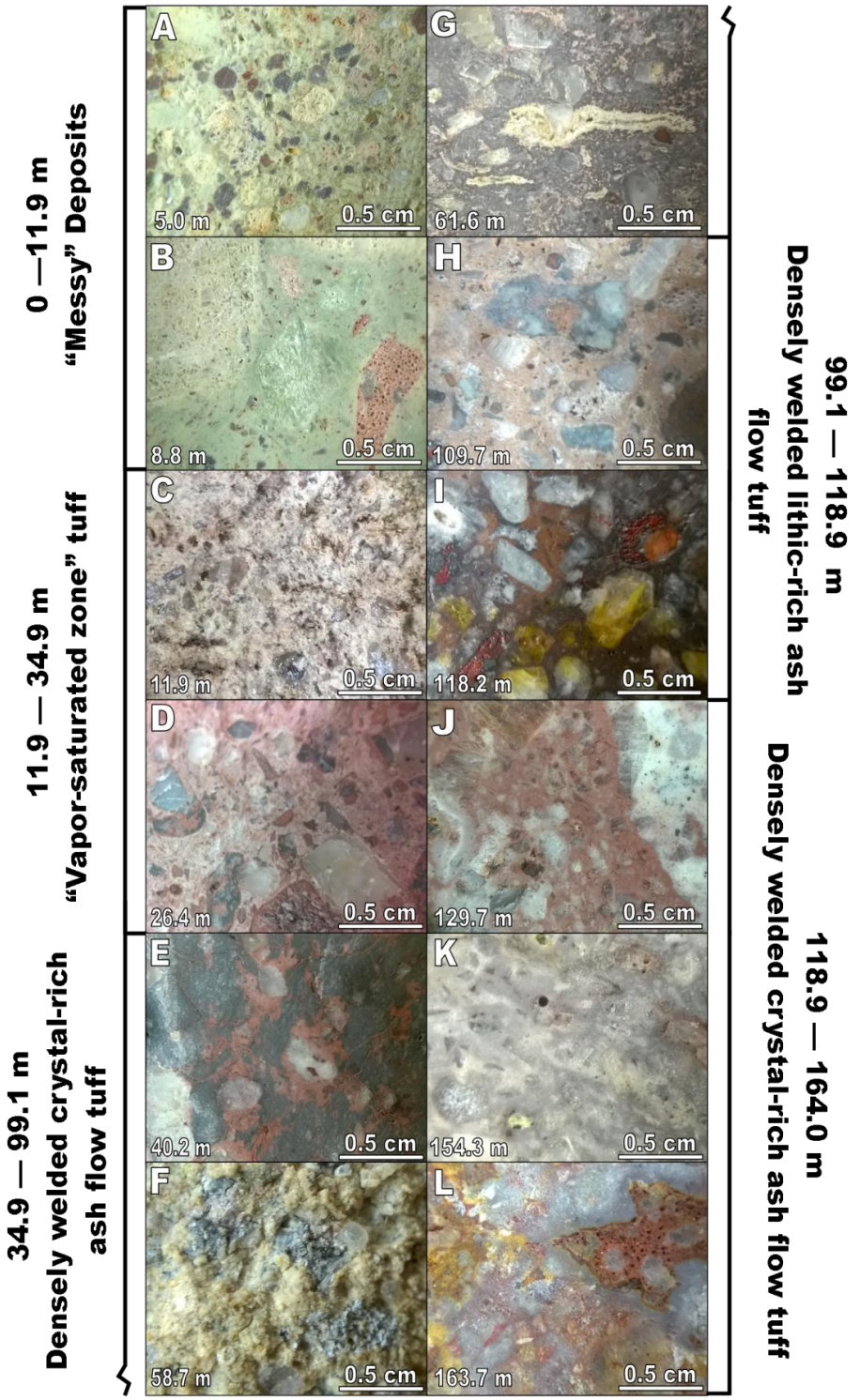

Figure 4: Representative photographs of the Y-5 drill core primary lithology with depth. (A) Pebble conglomerate. (B) Volcanic breccia. (C) Soft porous tuff with phenocrysts and lithic fragments. (D) Welded tuff with phenocrysts and lithic fragments. (E) Crystal-rich pink-grey tuff. (F) Soft matrix-dominated volcanic conglomerate. (G) Crystal-rich grey tuff with pumice fragments. (H) Lithic-rich pink tuff. (I) Grey-brown lithic rich tuff with iron-oxides and staining. (J) Crystal-rich pink tuff. (K) Crystal-rich grey tuff. (L) Crystal-rich pink tuff with iron staining.

Even though the majority of the core is comprised of ash flow tuff, there is striking visual variation in the core (Fig. 4C-L). The tuff groundmass is often pink (Fig. 4C, D, H, J) or grey (Fig. 4G, K), although there are areas where the groundmass contains both grey and pink (Fig. 4E, L). The pink groundmass generally has greater hydrothermal alteration, and contains dominant quartz and subordinant α-cristobalite (Keith *et al.*, 1968-78). The grey groundmass conversely contains subordinant quartz and is dominated by either α-cristobalite or tridymite (Keith *et al.*, 1968-78). An exception to this is when tuff with a tridymite dominated groundmass also contains microscopic grains of oxidized iron (often below 122 m), causing instead a pink color again (Keith and Muffler, 1978). See Appendix B for the distribution of pink, grey, and pink/grey groundmass throughout the core. The quartz and α-cristobalite are the result of devitrification during post-emplacement cooling (Keith *et al.*, 1968-78). There is negligible β-cristobalite in the ash flow tuff.

The phenocrysts throughout tuff are comprised of quartz, sanidine, and plagioclase. The sanidine phenocrysts are completely cryptoperthitic (Or_{48-56}) above 83.3 m and are either partially cryptoperthitic or completely sanidine below 83.3 m (Keith and Muffler, 1978). The plagioclase phenocrysts are calcic oligoclase with an average composition of $An_{23\pm5}$, although the average composition in the top ~61 m of the core is An_{18-24} whereas the average composition below ~61 m is An_{20-30} (Keith *et al.*, 1968-78). Pumice fragments throughout the tuff are recrystallized to sanidine and α-cristobalite, particularly in the vapor-phase zone (Keith and Muffler, 1978) (Fig. 4G). Rare pseudomorphs exist where hematite + goethite ± montmorillonite consumed clinopyroxene (Keith *et al.*, 1968-78; Fig. 4I).

The lithic fragments are grey, red, and brown and include rhyolite, recrystallized pumice laths, and welded porphyritic tuffs from older Yellowstone Group tuffs (Keith *et al.*, 1968-78).

These fragments are predominantly angular with some subangular fragments, and they range in size from microscopic to three centimeters (Keith *et al.*, 1968-78).

3.1.2. Hydrothermal Alteration: Textures and Secondary Mineralogy

The unconsolidated obsidian sand in the first 4.7 m of the drill core is unaltered, but there is some weak opal cement between the obsidian grains starting after ~4.7 m (Keith and Muffler, 1978). The "messy deposits" below that begin to show fracturing containing secondary clays (montmorillonite, illite) and forms of silica (opal, β-cristobalite) with occasional clinoptilolite and pyrolusite (Keith *et al.*, 1968-78; Keith and Muffler, 1978).

Most of the intense fracturing exists in the ash flow tuff below ~45 m. The fractures extend in a myriad of directions relative to the core axis from near horizontal (Fig. 5A, C) to near vertical (Fig. 5C) with just about any angle in between (Fig. 5A, E, F). Sometimes there are networks of veins (Fig. 5C) and sometimes there are isolated veins (Fig. 5A, F). The fractures range in width from millimeters (Fig. 5C) to several centimeters (Fig. 5A).

Almost all fractures are filled with secondary mineral deposition. These fractures are commonly filled with red/brown chalcedony + iron oxide (red hematite ± goethite at shallower depths but only brown goethite deeper in the core) (Keith *et al.*, 1968-78). Later mineralization in fractures is comprised of white-pink chalcedony ± montmorillonite (Fig. 5A, C) (Keith *et al.*, 1968-78). Fracture fill is frequently layered, especially in larger fractures (Fig. 5A). Occasionally, veins are filled with a brecciation composed of local angular tuff fragments in a matrix of iron oxide + chalcedony ± montmorillonite (Fig. 5E). There are several instances of larger scale brecciation with a similar matrix (Fig. 5D).

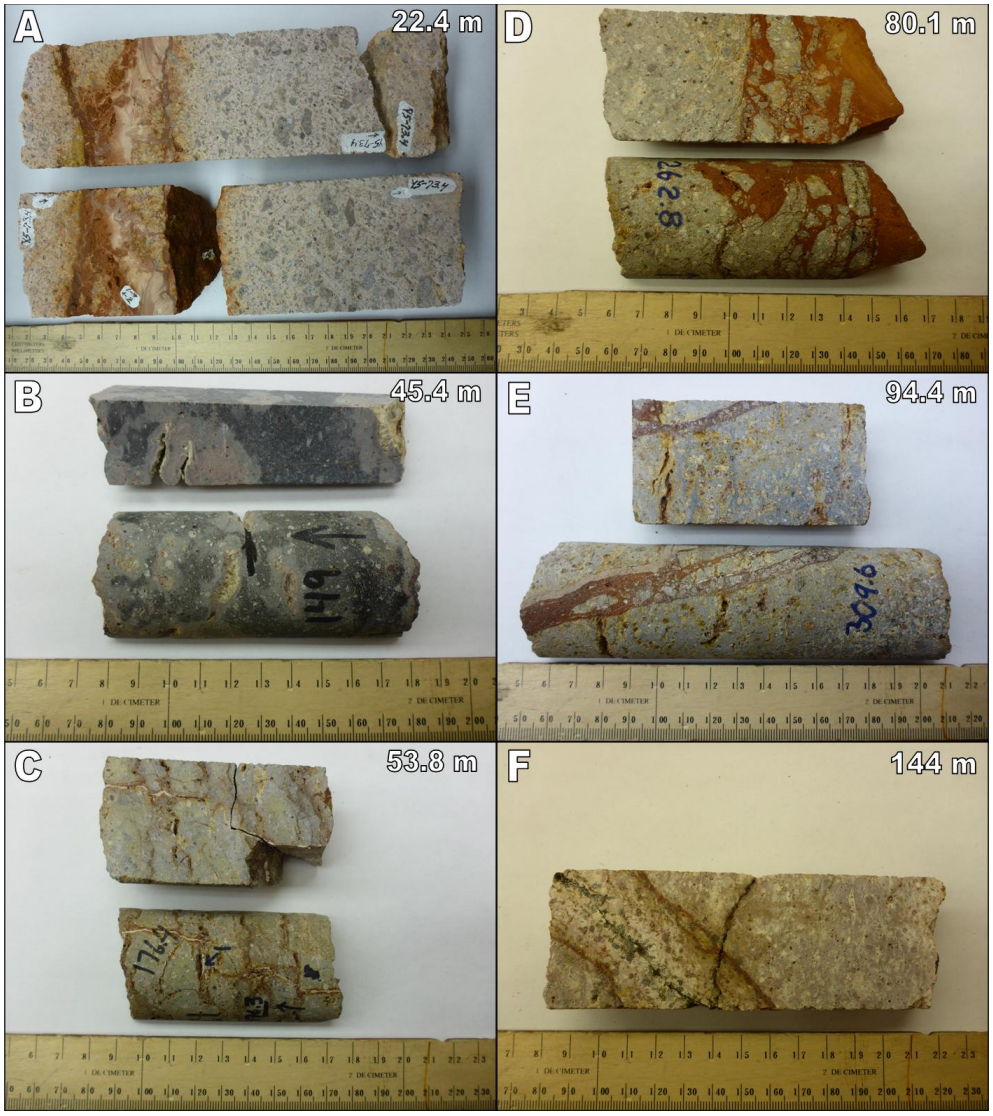

Figure 5: Representative photographs of fractures, brecciation, and cavities in the Y-5 drill core. Mineral identification originally by Keith *et al.*, 1968-78. (A) "Vapor-saturated zone" tuff with horizontal fracture filled with red goethite + chalcedony with later white chalcedony. (B) Ash flow tuff with cavities filled with secondary quartz + montmorillonite + mordenite ± fluorite. (C) Ash flow tuff with small scale fractures filled with red iron stained chalcedony and later white montmorillonite + chalcedony. (D) Ash flow tuff with brecciation composed of angular local tuff in a matrix of goethite + chalcedony with additional montmorillonite closer to the contract with the intact tuff. (E) Ash flow tuff with brecciation in fractures containing a goethite + chalcedony matrix with additional montmorillonite in smaller related fractures. (F). A fracture with alteration (dominantly goethite spheres and staining) constrained within the adjacent tuff.

Deeper fractures sometimes do not have fracture fill as seen earlier in the core, even though the hydrothermal mineral suite is the same. Fig. 5F shows a fracture only a few millimeters wide with goethite spheres grown in the tuff immediately adjacent to the fracture. Goethite staining extends ~2.5 cm in the tuff in all directions from the fracture, accumulating

most obviously at ~2.5 cm from the fracture itself. The iron oxide staining is apparent in the primary lithology as yellow staining on sanidine phenocrysts, which can be seen throughout the core (Fig. 4I).

Fractures not completely sealed host cavities. The core sometimes breaks at wide (greater than 4.5 cm) partially filled fractures, revealing the inner surface. Fig. 6A, E, and G show small scale photographs of the representative fracture fill mineralogy and petrogenesis: chalcedony ± iron oxide, chalcedony ± montmorillonite, and late quartz (prismatic and saccharoidal), mordenite fibers, octahedral fluorite, and bladed calcite (not pictured) (Keith *et al.*, 1968-78). Occasional mordenite fibers are often more abundant than seen in Fig. 6A and E, and Fig. 6F shows the best example of abundant mordenite in the core.

Isolated cavities appear both with and without nearby fractures (Fig. 5B, C, E). The cavities appear much more sporadically than fractures, but similarly exist mostly below ~45 m. Most cavities are only a few millimeters to a few centimeters wide and long, and most cavities are longer than they are wide. The cavities are either simply open space in the primary tuff or inside of devitrified pumice fragments.

The cavities frequently host tabular K-feldspar, often iron stained yellow or orange, with later quartz growth (Fig. 6B, C). Secondary hydrothermal quartz occurs both as euhedral crystals (Fig. 6B, C) and as saccharoidal coverings (Fig. 6B). Rare magnetite octahedrons are less than a millimeter in width and look like black flecks at first glance (difficult to see on saccharoidal quartz in Fig. 6B). Deeper in the core, there is much less secondary K-feldspar and more abundant goethite, which is botryoidal in some well formed cavities (Fig. 6H). The only sulfide found in the core is cubic pyrite, which is rarely as abundant as in Fig. 6D.

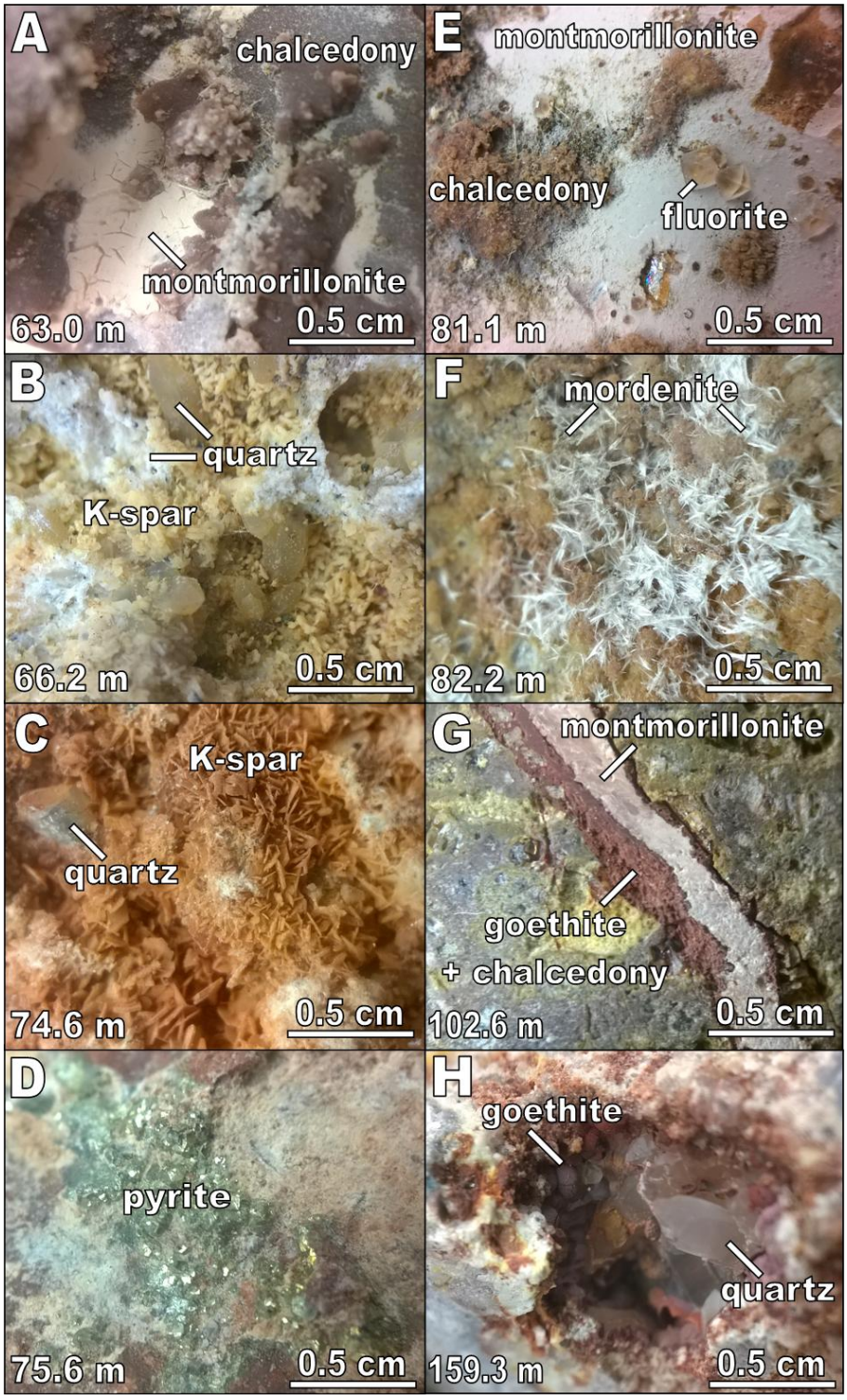

Figure 6: Representative photographs of secondary mineralogy in the Y-5 drill core. (A) Cracked montmorillonite on chalcedony. (B) K-feldspar combs, euhedral quartz, and saccharoidal white quartz ± magnetite. (C) Iron stained K-feldspar combs with euhedral quartz. (D) Pyrite. (E) Octahedral fluorite on montmorillonite on chalcedony. (F) Mordenite "fibers". (G) Fracture fill of goethite + chalcedony and montmorillonite. (H) Cavity filled with botryoidal goethite and euhedral quartz.

3.1.3. EQ6 Mineralogical Inputs

Table I summarizes the primary and secondary mineralogy of the Y-5 drill core. Ideally, all of the minerals in Table I would be part of the EQ6 mineralogical input. However, the EQ3/6 database does not contain the following minerals: tridymite, zircon, montmorillonite, illite, erionite, clinoptilolite, mordonite, pyrolusite, or hollandite.

Table I: Primary and secondary minerals and amorphous solids in the Y-5 drill core.

Primary Minerals and Amorphous Solids		Secondary Hydrothermal Minerals	
Quartz Polymorphs		**Iron Minerals**	
α–cristobalite	SiO_2	magnetite	$FeFe_2O_4$
β–cristobalite	SiO_2	hematite	Fe_2O_3
quartz	SiO_2	goethite	$\alpha\text{-}Fe^{3+}O(OH)$
tridymite	SiO_2	pyrite	FeS_2
Amorphous Silica		**Quartz Polymorphs**	
obsidian	Am. SiO_2	quartz	SiO_2
opal	$SiO_2 \cdot nH_2O$	chalcedony	SiO_2
Feldspars		**Clays**	
plagioclase	$NaAlSi_3O_8$-$CaAl_2Si_2O_8$	montmorillonite	$(Na,Ca)_{0.33}(Al,Mg)_2(Si_4O_{10})(OH)_2 \cdot nH_2O$
alkali feldspar	$(Na,K)AlSi_3O_8$	illite	$K_{0.65}Al_{2.65}Si_{3.35}O_{10}(OH)_2$
sanidine	$KAlSi_3O_8$	**Zeolites**	
K-feldspar	$KAlSi_3O_8$	erionite	$Ca_3K_2Na_2(Al_{10}Si_{26}O_{72}) \cdot 30\ H_2O$
Other		clinoptilolite	$(Ca,Na,K)_{2\text{-}3}Al_3(Al,Si)_2Si_{13}O_{36} \cdot 12H_2O$
zircon	$ZrSiO_4$	mordonite	$(Na_2,Ca,K_2)_4(Al_8Si_{40})O_{96} \cdot 28H_2O$
		Other	
		pyrolusite	MnO_2
		hollandite	$Ba(Mn^{4+}{}_6Mn^{3+}{}_2)O_{16}$
		K-feldspar	$KAlSi_3O_8$
		fluorite	CaF_2
		calcite	$CaCO_3$

The final mineral assemblage (plus carbon dioxide gas) used in the EQ6 input is summarized in Table II. To help represent the alteration products in the Y-5 drill core, kaolinite

and muscovite were used in the EQ6 input instead of montmorillonite and illite, respectively. There were no zeolites in the database of similar enough composition to erionite, clinoptilolite, or mordonite to justify using them as substitutes in the model. There also were no relevant minerals that could have been substituted in the model for the two manganese bearing minerals, pyrolusite and hollandite, but these minerals were present in the drill core in such small quantities that they would have been negligible. Similarly, there were no similar minerals to zircon, which was unconcerning due to its role as an accessory igneous mineral. Although tridymite was not able to be included in the model, there were enough other forms of silica in the model.

Table II: Calibrated EQ6 input (minerals + CO_2 (g)).
"Ideal plagioclase" refers to the name of the mineral in the EQ3/6 database (as opposed to plagioclase, low).

Input	Stoichiometry	Moles	Relative Forward Rate Constant
quartz	SiO_2	3.60E+03	2.75E+14
α-cristobalite	SiO_2	3.60E+03	2.75E+14
β-cristobalite	SiO_2	6.55E-03	5.00E+08
chalcedony	SiO_2	1.05E-06	8.00E+04
amorphous silica	SiO_2	2.62E-03	2.00E+08
ideal plagioclase (An_{23})	$NaAlSi_3O_8$-$CaAl_2Si_2O_8$	1.31E-05	1.00E+06
sanidine-ss (Or_{80})	$(K,Na)AlSi_3O_8$	1.31E+03	1.00E+14
sanidine, high	$KAlSi_3O_8$	1.49E+03	1.14E+14
magnetite	Fe_3O_4	2.62E-09	2.00E+02
hematite	Fe_2O_3	5.24E-07	4.00E+04
goethite	FeOOH	6.55E-07	5.00E+04
pyrite	FeS_2	2.62E-09	2.00E+02
kaolinite	$Al_2Si_2O_5(OH)_4$	4.58E-07	3.50E+04
muscovite	$KAl_3Si_3O_{10}(OH)_2$	6.55E-09	5.00E+02
fluorite	CaF_2	5.24E-05	4.00E+06
calcite	$CaCO_3$	1.31E-06	1.00E+05
carbon dioxide gas	CO_2	3.14E-01	2.40E+10

3.1.4. Trace Elements

The trace elements in the hydrothermal fluids originate from the rocks and enter the fluid through water-rock reactions. However, The EQ3/6 model can only remove elements from rocks that are included in the stoichiometries of the mineral inputs (Table II). Because of this, the trace elements in the Y-5 system are underrepresented in the EQ3/6 models. However, trace elements were previously measured directly from powered samples of the Y-5 drill core at various depths (Beeson and Bargar, 1984).

The average concentration of the trace elements in the rocks was calculated from seven depths in the Y-5 drill core for which bulk geochemical analysis was performed (24.8 m, 35.2 m, 36.5 m, 36.9 m, 42.4 m, 80.9 m, and 160.2 m) (Beeson and Bargar, 1984). Figure 7 considers only the trace elements that were measured in *both* the Y-5 drill core material and the water of the surrounding thermal features (Appendix C). Trace elements measured below the detection limit for all rock and water samples were not graphed (Ni, Ag, Sn, Pd, Cd, Pr, and Tl). Other trace elements measured in the drill core material were consistently below the detection limit (values not reported) of the instrument(s) for all the YNP drill cores: Ge, As, Ru, Rh, Pd, Cd, In, Te, Pr, Sm, Tb, Dy, Ho, Tm, Lu, Hf, Ta, W, Re, Ir, Pt, Au, Tl, Bi, Th, and U (Beeson and Bargar, 1984).

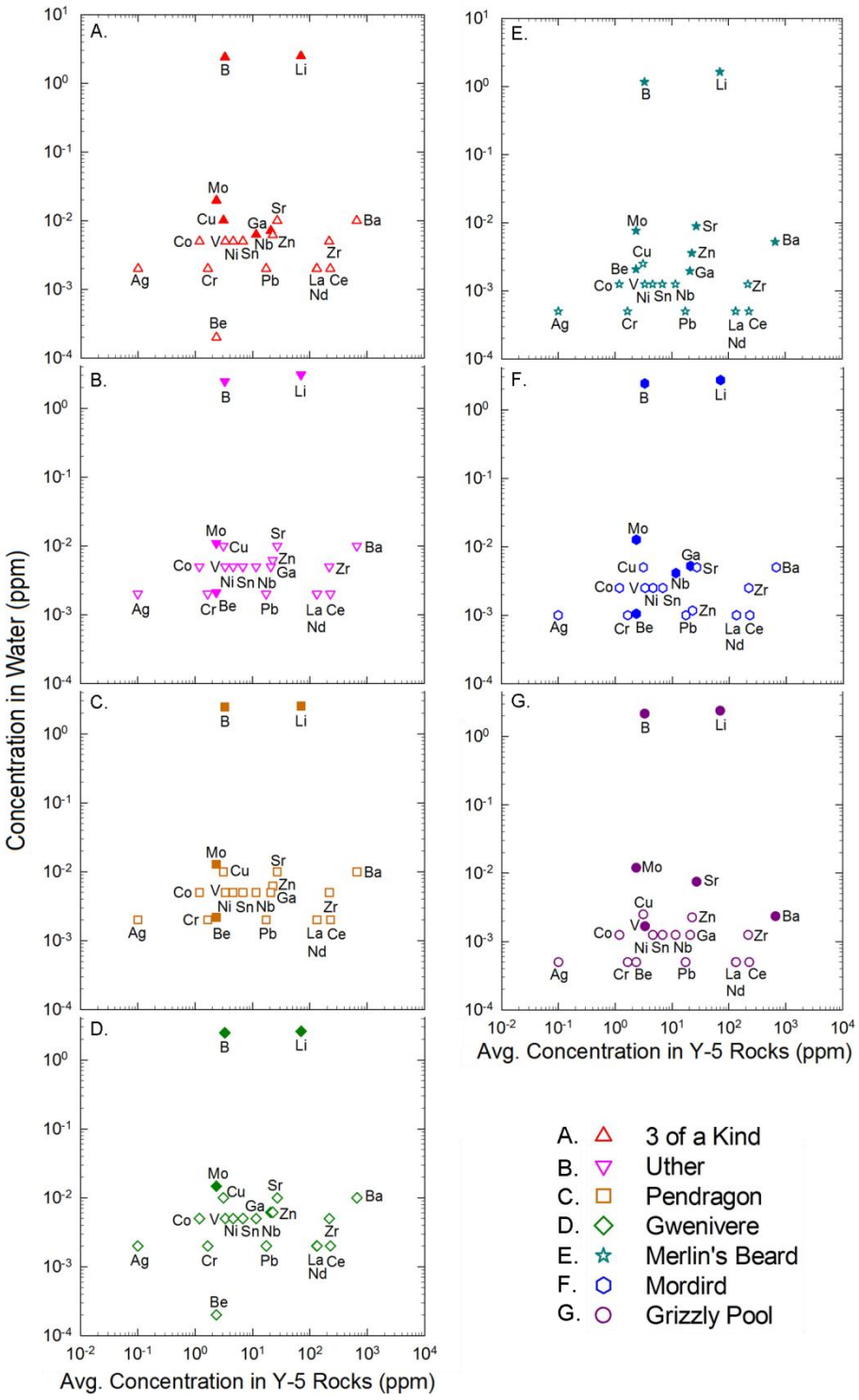

Figure 7: Trace elements in the Y-5 drill core (Beeson and Bargar, 1984) and nearby thermal features. Closed symbols represent values above the detection limit for trace elements in the thermal feature water. Open symbols represent values below the lower detection limit for trace elements in the thermal feature water (plotted at their detection limits). Error bars for the aqueous trace elements are within the size of the symbols. Error bars for the trace elements in the rock (unreported in Bargar and Beeson, 1984) are assumed to be within the symbol size.

The direct comparison between trace elements in the Y-5 drill core material and the surrounding thermal features showed no obvious trends (Fig. 7). Several of the trace elements in the thermal feature waters had similar or identical values within or between springs (ex: Co-V-Nb; Cr-Pb-La-Nd-Ce) (Fig. 7), but this was only due to several elements being commonly below the lower detection limit of the instrument used to analyze for those elements (Appendix C). Because several of the trace elements that were detectable in the Y-5 rocks were not detectable in many of the thermal features, the exceptions are notable. For example, Merlin's Beard had the greatest number of elevated trace element concentrations in its thermal water, when looking at the select trace elements in Fig. 7. Also, boron, lithium, and molybdenum were the elements consistently measured above the lower detection limit in all of the thermal feature waters in this comparison (Fig. 7). Although, only boron and lithium had concentrations orders of magnitude greater than the other trace elements in the thermal waters (Fig. 7). See section 3.3.2 for more complete information on the trace elements measured above detection limit in the thermal feature waters.

3.1.1. Petrologic Characterization

Weight percents of major element oxides (SiO_2, Al_2O_3, Fe_2O_3, FeO, MgO, CaO, Na_2O, K_2O, P_2O_5,) in the YNP drill cores were used to calculate the aluminum-saturation index, the alkalinity index, the iron index, and the modified alkali-lime index (Frost and Frost, 2008) (Appendix D; Fig. 8). It is important to note that these indices are meant to apply to igneous rocks, whereas here they are applied to hydrothermally altered igneous rocks. However, it is still helpful to look at these indices in regard to the Y-5 rocks because the overall chemistry of the Y-5 rocks is what is reacting with water at depth in the YNP hydrothermal system. At all analyzed

depths, the Y-5 rocks were peraluminous and ferrous (Fig. 8). The rocks generally changed from calcic to calc-alkaline and alkali-calcic with increasing depth (Fig. 8).

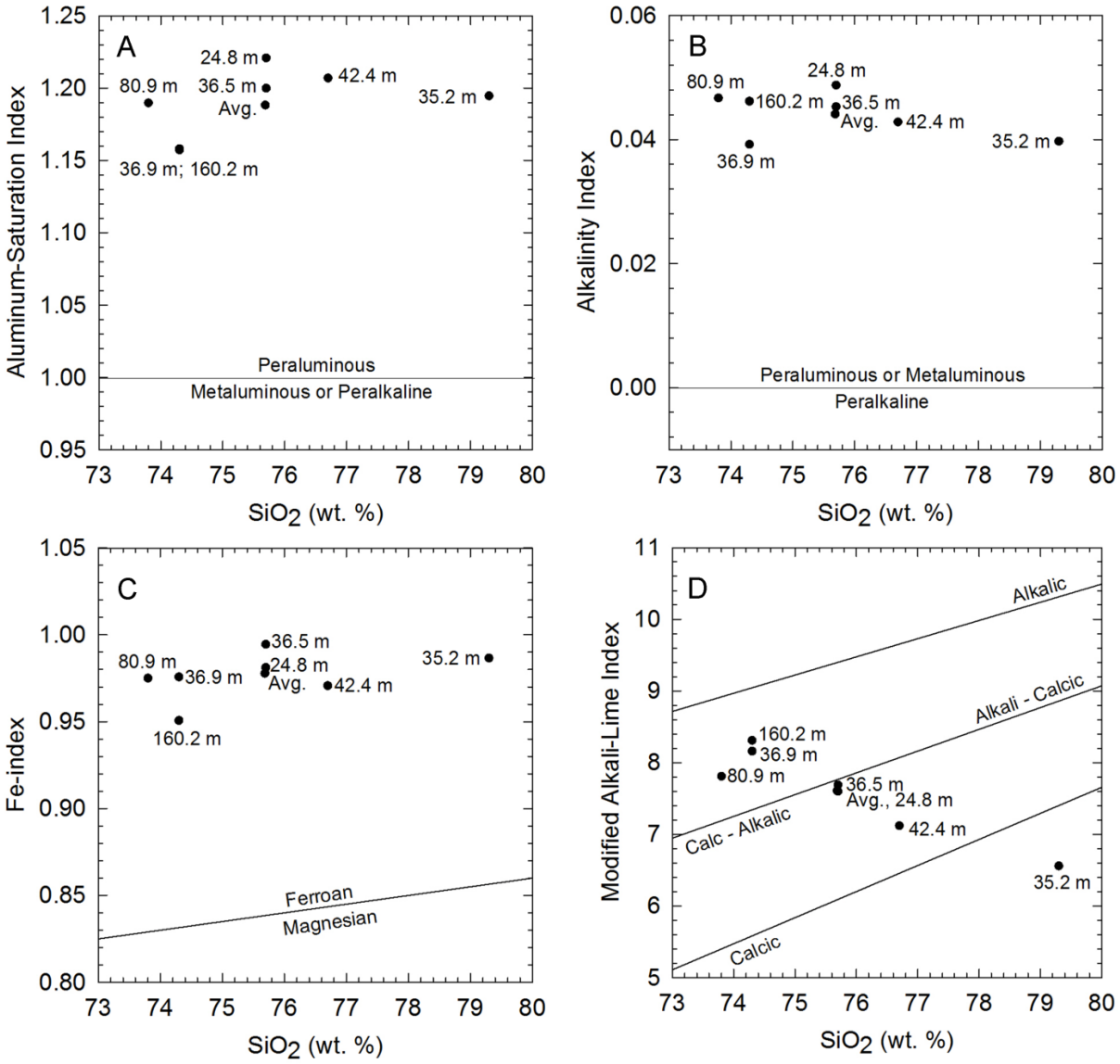

Figure 8: Petrologic characterization of the Y-5 drill core.
Data from Bargar and Beeson, 1984, plotted using Frost and Frost, 2008 methods show that the rocks are: peraluminous, based on aluminum-saturation index (A) and alkalinity index (B); ferroan, based on iron index (C); and (D) calcic, calc-alkalic, and alkali-calcic, based on the modified alkali-lime index.

3.2. Water Chemistries

3.2.1. Characterization of Y-5 Area Thermal Features

Stable water isotope values (δD and $\delta^{18}O$) from thermal features throughout the Rabbit Creek area (Fig. 2) were compared (Appendix E; Fig. 9). The stable water isotopes from the overall Rabbit Creek area follow a trend line with equation $\delta D = 2.7\delta^{18}O - 97.7$ ($R^2 = 0.9445$) (Fig. 9). The trend line for the Rabbit Creek thermal features had a slope much lower than the meteoric water lines (Craig, 1961; Kharaka *et al.*, 2002) and slightly lower than the thermal water line for YNP thermal features sampled by LEGEND in July 2016 (Dahlquist, 2017) (Fig. 9). Stable water isotope values of thermal features near the Y-5 borehole generally overlapped with values of thermal features in Rabbit Creek North (Fig. 9).

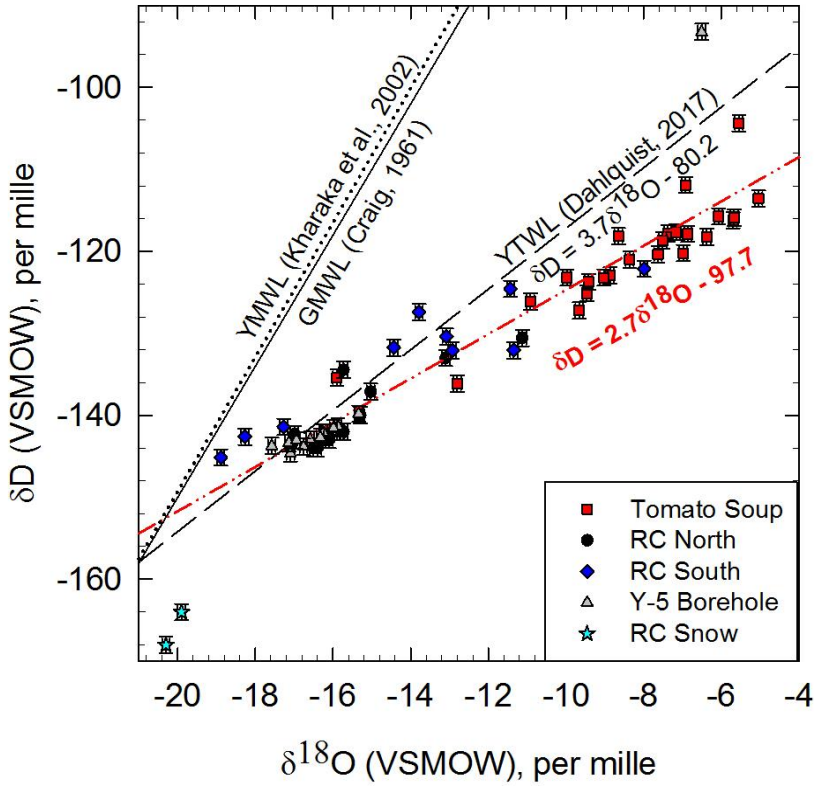

Figure 9: δD vs $\delta^{18}O$ of thermal features throughout the Rabbit Creek area. GWML = Global Meteoric Water Line $\delta D = 8\delta^{18}O + 10$ (Craig, 1961). YMWL = Yellowstone Meteoric Water Line $\delta D = 8.2\delta^{18}O + 14.7$ (Kharaka *et al.*, 2002). YTWL = Yellowstone Thermal Water Line $\delta D = 3.7\delta^{18}O - 80.2$ (Dahlquist, 2017). The trend line through the Rabbit Creek area data is the red line with equation $\delta D = 2.7\delta^{18}O - 97.7$. Error bars represent instrumental error (δD ± 1‰, $\delta^{18}O$ ± 0.1‰).

The two snow samples from the Rabbit Creek area unsurprisingly did not graph near any of the thermal features (Fig. 9). The snow samples, which were collected from snow pack and not from freshly fallen snow, also did not plot directly on either the Yellowstone meteoric water line or global meteoric water line (Fig. 9). However, the stable water isotopes of the snow samples did fit well within the range of snow samples used to build the YMWL: $\delta^{18}O$ = -12.5‰ to -23.9‰ and δD = -88‰ to -178‰ (Kharaka *et al.*, 2002).

Within the Y-5 area, stable water isotope values clustered between $\delta^{18}O$ = -18‰ and -15‰ and δD = -138‰ and -146‰ (Fig. 9, 10). The exception was Grizzly Pool ($\delta^{18}O$ = -6.5‰, δD = -93‰), which was also the outlier from the entire Rabbit Creek area (Fig. 9, 10). The trend line for the Y-5 area (excluding Grizzly Pool) was $\delta D = 1.9\delta^{18}O - 111.1$ ($R^2 = 0.9141$) (Fig. 10).

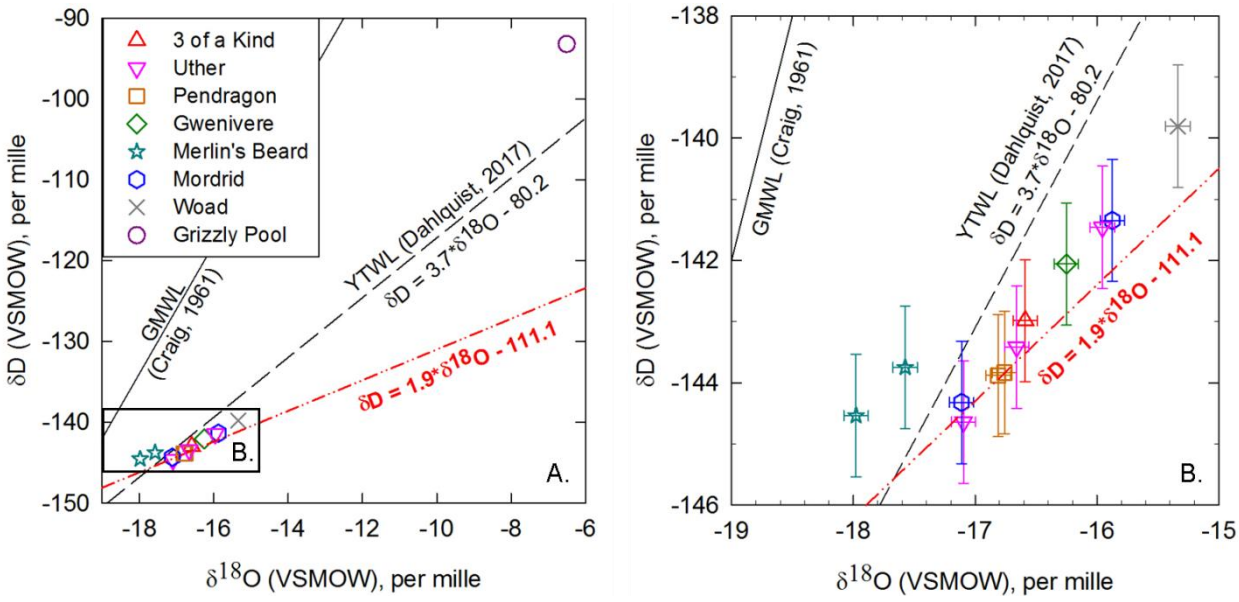

Figure 10: δD vs. $\delta^{18}O$ of the Y-5 thermal features.
GWML = Global Meteoric Water Line (Craig, 1961). YTWL = Yellowstone Thermal Water Line (Dahlquist, 2017). The trend line through the Y-5 thermal feature data (excluding Grizzly Pool) is the red line with equation $\delta D = 1.9*\delta^{18}O - 111.1$. Error bars represent instrumental error (δD ± 1‰, $\delta^{18}O$ ± 0.1‰). (A) All Y-5 features, including duplicate spring samples. Error bars are within the symbol size. (B) All Y-5 features except Grizzly Pool.

Four of the Y-5 thermal features (Uther, Pendragon, Merlin's Beard, and Mordrid) had duplicate water isotope samples collected at different times during the sampling day (Fig. 11). Duplicates for each sample overlapped with their counterparts for δD ± 1‰, except for the duplicates of Mordrid (Fig. 11). Two of the duplicate samples of Uther did not overlap for δD ± 1‰ (samples collected at 14:38 and 11:00), but both of these samples overlapped for δD ± 1‰ with the third Uther duplicate (sample collected at 10:49). The duplicate samples for Pendragon overlapped with each other for $\delta^{18}O$ ± 0.1‰, but the duplicate samples from the other three thermal features did not overlap with their counterparts for $\delta^{18}O$ ± 0.1‰ (Fig. 11). Interestingly, for $\delta^{18}O$ ± 0.1‰, the two samples from Mordrid overlapped with two of the samples from Uther that also did not overlap for δD ± 1‰ (samples collected at 14:38 and 11:00) (Fig. 11).

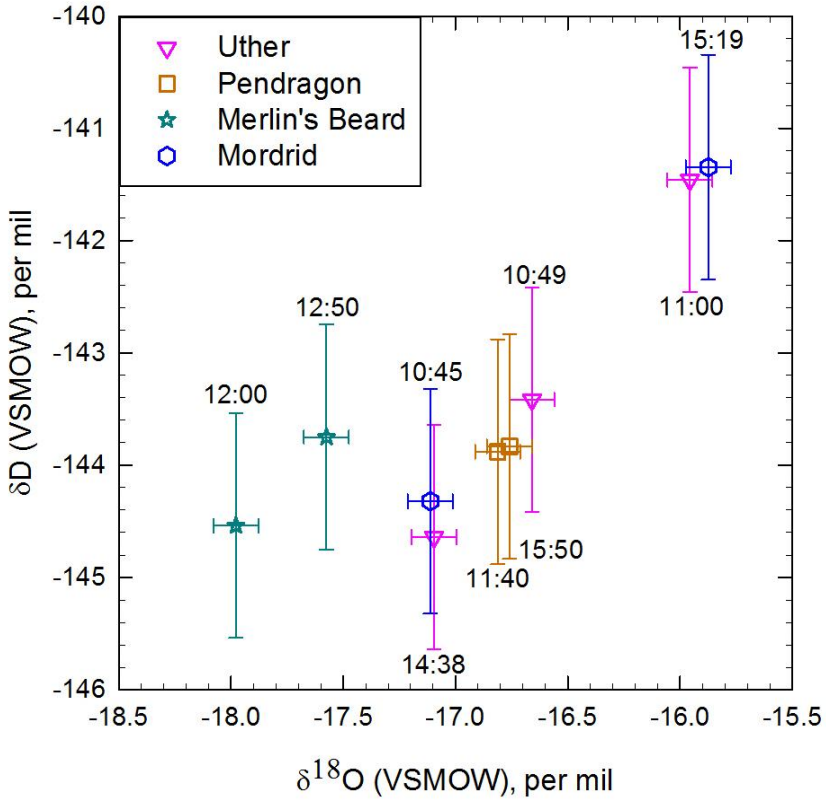

Figure 11: δD vs. $\delta^{18}O$ of duplicate samples of the Y-5 thermal features. Error bars represent instrumental error (δD ± 1‰, $\delta^{18}O$ ± 0.1‰). Next to each value is the time of sample collection.

The features around the Y-5 borehole demonstrated a wide range in temperature from 17.3°C (Grizzly Pool) to near-boiling at 92.2°C (3 of a Kind and Pendragon) (Fig. 12). Along with the wide range of temperature, the springs also demonstrated variations in pH, dissolved oxygen, conductivity, and dissolved silica (Fig. 12).

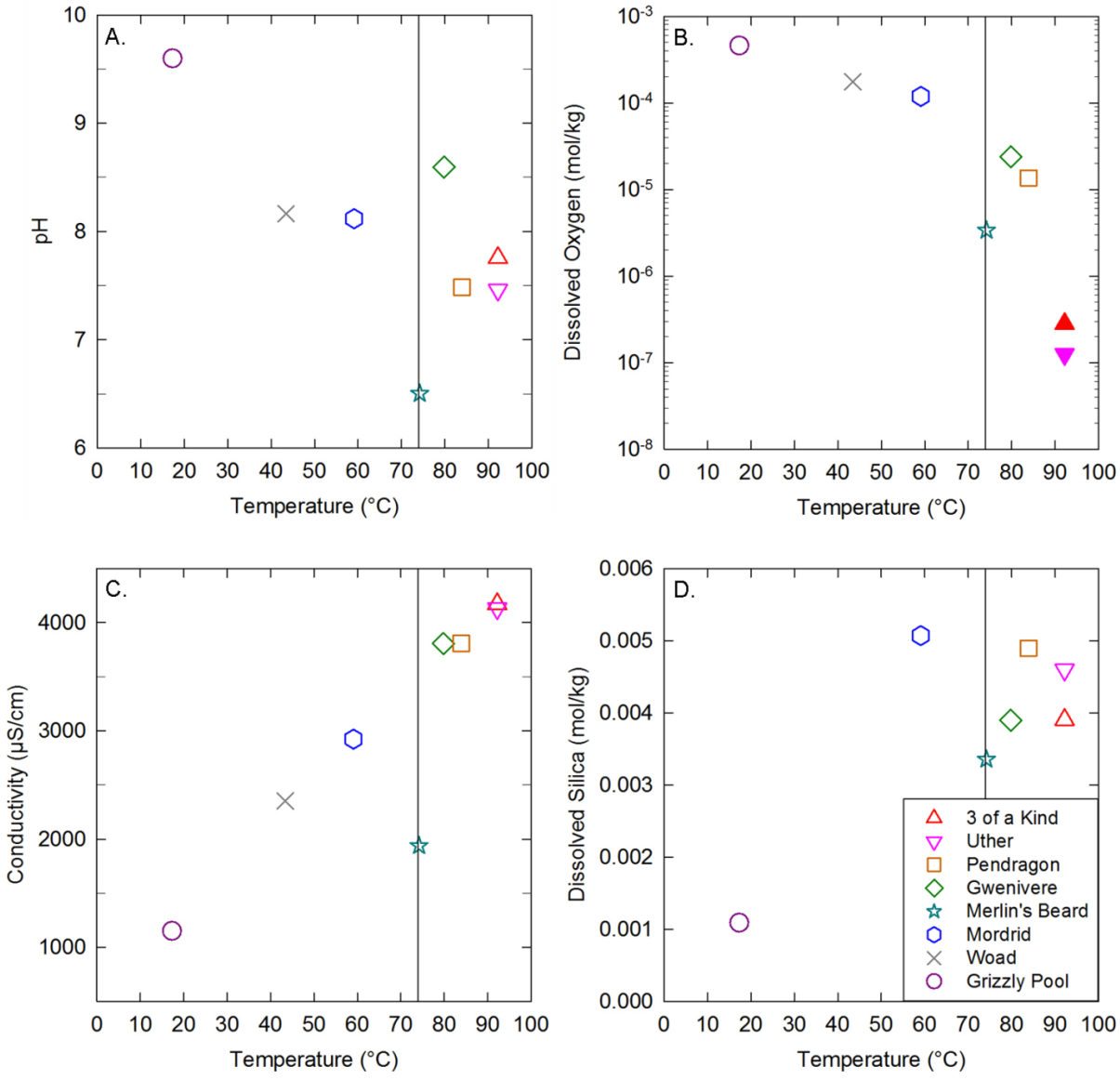

Figure 12: Temperature trends between thermal features.
Open symbols represent values above the detection limit and filled in symbols represent values below the detection limit. All error bars lie within the size of the symbols (Appendix E). The vertical lines at 74°C represent the limit to photosynthesis (Brock, 1967; Cox *et al.*, 2011), which is also the temperature of Merlin's Beard (74.2°C ± 0.2°C). A) pH vs. temperature. B) Dissolved oxygen (logarithmic scale) vs. temperature. C) Conductivity vs. temperature. D) Dissolved silica vs. temperature (no dissolved silica datum for Woad).

There were clear trends for conductivity and dissolved oxygen with temperature (Fig. 12B, C). Conductivity increased nearly linearly with temperature whereas dissolved oxygen decreased logarithmically with temperature, except for Merlin's Beard in both cases (Fig. 12B, C). Trends with pH and dissolved silica with temperature were less clear (Fig. 12A, D). In general, pH decreased with increasing temperature whereas dissolved silica increased with increasing temperature (Fig. 12A, D). Merlin's Beard generally fit within these trends, although Merlin's Beard did have the lowest measured pH of the features (Fig. 12A). The temperature of Merlin's Beard was close to the upper temperature limit for photosynthesis (Fig. 12), which may or may not be relevant to its difference from the other features. The Y-5 features were circum neutral to basic (Fig. 12A). The speciated total dissolved inorganic carbon (DIC) shows that the dominant carbon species in these alkaline features was bicarbonate (Appendix A; Fig. 13).

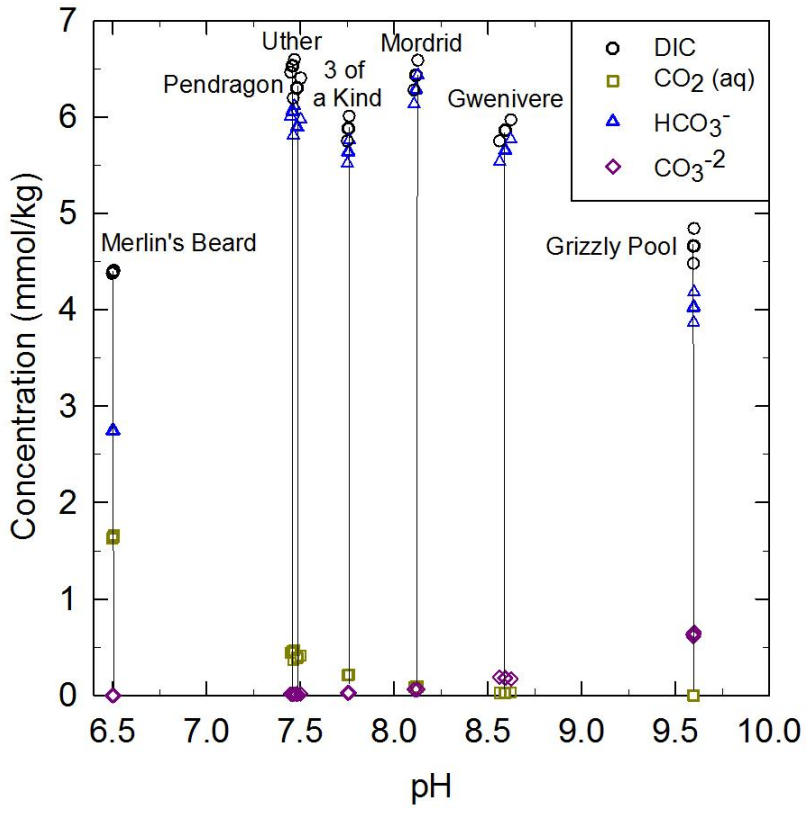

Figure 13: Speciation and concentration of dissolved inorganic carbon (DIC) vs pH in Y-5 thermal features.

Subordinant concentrations of CO_2 (aq) decreased with increasing pH while subordinant concentrations of CO_3^{-2} increased with increasing pH (Fig. 13). Merlin's Beard and Grizzly Pool had noticeably less DIC than the other thermal features, and Merlin's Beard had more similar concentrations of HCO_3^- and CO_2 (aq) due to its lower pH (Fig. 13). The errors on the DIC values and pH values were used to generate high and low values for both DIC and pH, which were used to also generate high and low values for the inorganic carbon species (Appendix A; Fig. 13). This method shows an inconsistent amount of error in the inorganic carbon species in the different samples (Fig. 13), which is due to the inconsistent amount of error between samples.

Total dissolved organic carbon (DOC) decreased with increasing temperature (Fig. 14). DOC was negligible for all features above 70°C; the only features with elevated DOC were Mordrid and Grizzly Pool (Appendix E; Fig. 14).

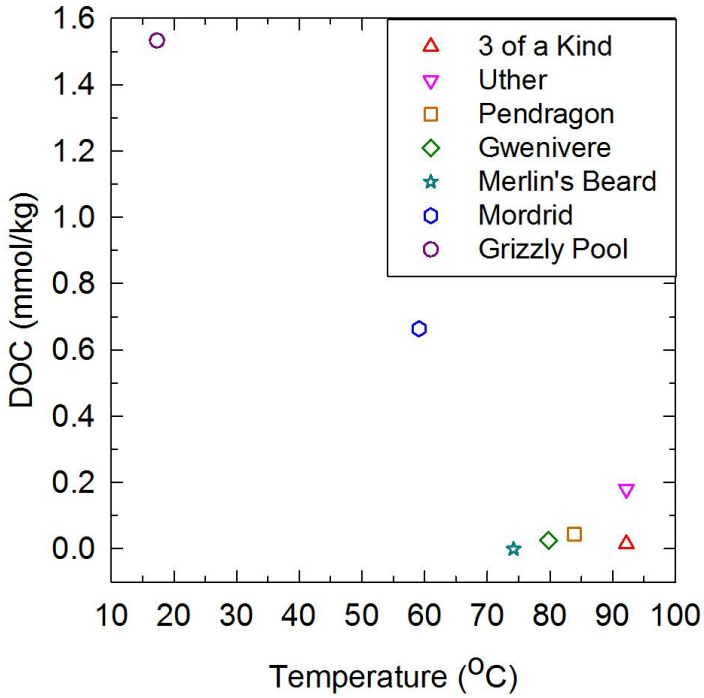

Figure 14: DOC vs. temperature for Y-5 thermal features.
Error bars are within symbol size. DOC was corrected for the blank value (Appendix E).

3.2.2. EQ3 Geochemical Inputs

EQ3 models were built for each thermal feature using the data tabulated in Appendices A and D with additional model inputs as shown in Table III. The geochemical inputs for each thermal feature are presented in Figure 15. There were orders of magnitude differences between the geochemical parameters, but for many individual parameters, the concentrations were often similar between Y-5 features (Fig. 15). The inputs that were the most different between features include H^+, O_2 (aq), HS^-, Ca^{+2} (Fig. 15).

Table III: Additional parameters for EQ3 inputs for Y-5 thermal features.

Sample	T (^{0}C)	logfO_2 (log bars)	NH_4^+ (mol/kg)	Sample ID for referenced NH_4^+ (Holloway *et al.*, 2011)
3 of a Kind	92.2	-3.43	1.40E-05	06WA116
Uther	92.2	-3.79	1.40E-05	06WA116
Pendragon	83.9	-1.76	1.40E-05	06WA116
Gwenivere	79.8	-1.52	1.65E-05	Averaged 06WA114 & 06WA115
Merlin's Beard	74.2	-2.37	1.40E-05	NA*
Mordrid	59.1	-0.86	1.00E-05	06WA115
Grizzly Pool	17.3	-0.50	1.40E-05	NA*

*There were no thermal features similar to Merlin's Beard or Grizzly Pool, so the NH_4^+ value used for those springs is the most common value cited for the Y-5 borehole area: 1.40E-05 mol/kg.

The initial geochemical input for the EQ3 part of the calibrated EQ3/6 model was the averaged meteoric water chemistry from the two Rabbit Creek area snow samples (Appendix F), which was edited as necessary until calibration. The final geochemical inputs to the EQ3 part of the calibrated EQ3/6 model are summarized in Figure 15.

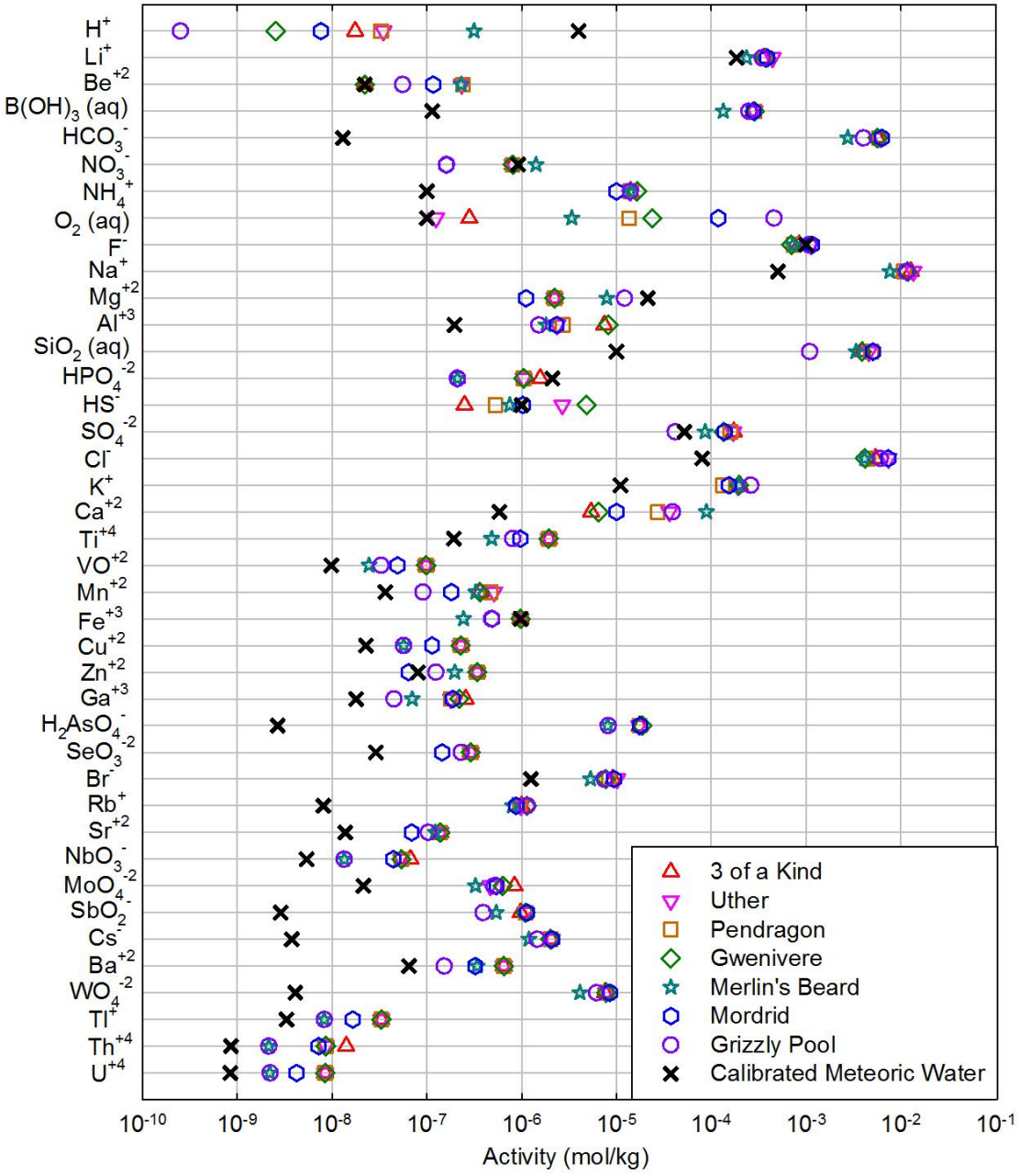

Figure 15: Geochemical inputs for all EQ3 models.
Error bars are within the symbol size. See Appendix E for values measured below lower detection limit.

In Fig. 15, it is misleading that there seems to be order of magnitude differences between features for individual trace elements. Different samples required different dilution factures for laboratory analysis, which led to different reported lower detection limits, even when a trace element was measured below the lower detection limit for most samples. Iron is a good example

of this because Grizzly Pool was the only sample where iron was measured above the detection limit, but the iron lower detection limit for samples with greater dilution was greater than the iron value for Grizzly Pool (Appendix E, Fig. 15). Unfortunately, the data valued at the lower detection limits could not be clearly demonstrated on Figure 15. See Appendix E for details.

As noted in section 2.3, only trace elements that were measured above the lower detection limit in at least one thermal feature were included in the models. Those trace elements (those in Fig. 15) were then included in all models for internal comparison and were valued at the lower detection limit (which were maximum values) for relevant samples (see Appendix E). Even though the magnitudes of the species of the trace elements which were modeled at their lower detection limit were not relevant, their relative abundances were relevant, especially for comparison between samples.

3.3. Modeling Outputs

Model sensitivity analyses are summarized in Appendix G. The EQ3 models were more sensitive to the error on the geochemical inputs than to fluctuations in the overall reduction-oxidation constraint ($\log fO_2 \pm 0.5$ log bars). An estimated error of 7% was used for the cited ammonium values. There was no good way to quantify the error for the cited value, so this magnitude of error was chosen because it enabled error bars to fit within the symbol size for graphs like Figure 15 while still being greater than most of the given instrumental errors.

EQ6 models were much more sensitive to changes in the starting water chemistry and mineral proportions/forward rate constants than anything else, which is why these parameters were edited to calibrate the model. EQ6 was relatively insensitive to changes in starting temperature and time length. With changes in starting temperature and time, there were

numerical changes in the final speciation of some elements, but often the changes were orders of magnitude less than the values themselves (Appendix G).

3.3.1. Water-Rock Reactions

The chemical speciation of 3 of a Kind (1) from the EQ3 speciation of the measured water chemistry and (2) predicted from the calibrated EQ3/6 model were closely aligned (Fig. 16). The largest discrepancies were that there were not enough silicon, aluminum, or sulfur species activities in the EQ3/6 predictions. This also resulted in the deficiency of $CaSO_4$ (aq) in the prediction (Fig. 16). Conversely, there was slightly too much CO_3^{-2} predicted from EQ3/6, resulting in greater amounts of $NaCO_3^-$ and KCO_3^- being predicted (Fig. 16). 100% of the predicted species were calibrated within one order of magnitude of the expected EQ3 speciation of 3 of a Kind, and 58% of the species were calibrated within half of an order of magnitude of the expected chemical speciation.

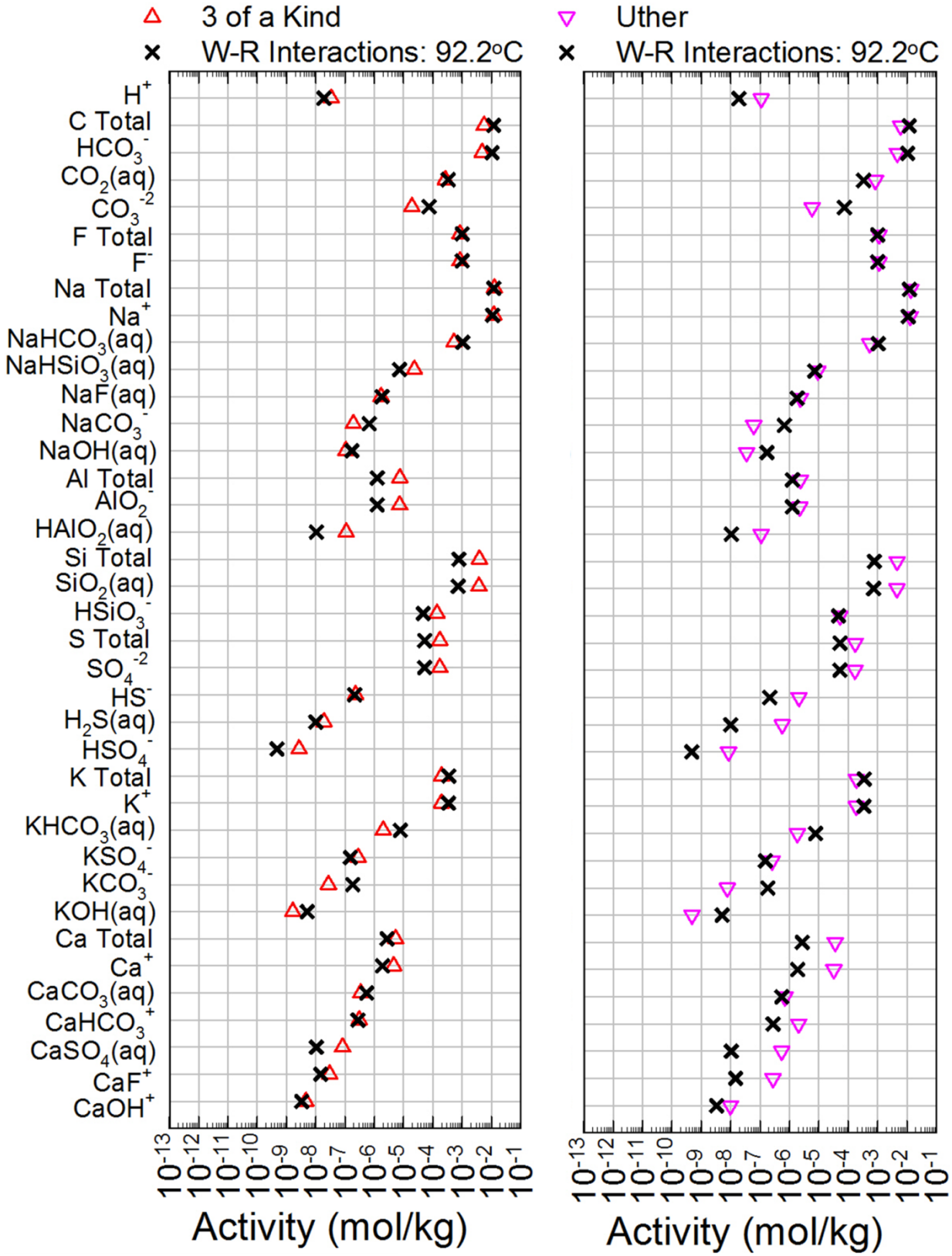

Figure 16: EQ3/6 predictions (water-rock reactions) and EQ3 speciation of 3 of a Kind and Uther.

The EQ3/6 predicted chemical speciation at 92.2°C, which was also the temperature of Uther, fits the EQ3 speciation of Uther slightly less than it does the EQ3 speciation of 3 of a Kind (Fig. 16). The main differences were that Uther had a greater amount of total calcium and more H^+ than 3 of a Kind. Because Uther had more H^+ than 3 of a Kind, the EQ3 speciation of aqueous hydroxides were lower in Uther than what was predicted with EQ3/6 at 92.2°C (Fig. 16). Otherwise, the 92.2°C EQ3/6 calibration fits Uther similarly with the largest discrepancies again being in under-predicted silicon, aluminum, and sulfur species and over-predicted CO_3^{-2} (Fig. 16).

As the EQ3/6 model was cooled to the temperatures of the springs, the EQ3/6 predictions were more similar to each other than to any of the EQ3 speciations of the Y-5 thermal features. There were changes in the EQ3/6 predictions as it was cooled, which were especially noticeable in pH predictions (Fig. 16-18; Appendix H). The EQ3/6 models were overall more sensitive to changes in final temperature than changes in starting temperature (Appendices G, H).

The 83.9°C EQ3/6 predictions actually fit the EQ3 speciation of Pendragon better than the 92.2°C EQ3/6 predictions fit the EQ3 speciation of Uther because the activity of H^+ was better aligned (Fig. 17). The 83.9°C EQ3/6 predictions were again deficient in silicon, aluminum, and sulfur species and had extra CO_3^{-2} (Fig. 17). The activities of calcium species in Pendragon were more similar to Uther than to 3 of a Kind or to the 83.9°C EQ3/6 predictions (Fig. 16, 17).

The 79.8°C EQ3/6 predictions fit the EQ3 speciation of Gwenivere similarly to how the 92.2°C EQ3/6 predictions compared with the EQ3 speciation of 3 of a Kind (Fig. 16, 17). One main difference was that the CO_3^{-2} prediction was closer to what was expected in Gwenivere whereas the CO_2 (aq) prediction was greater than expected in Gwenivere (Fig. 17).

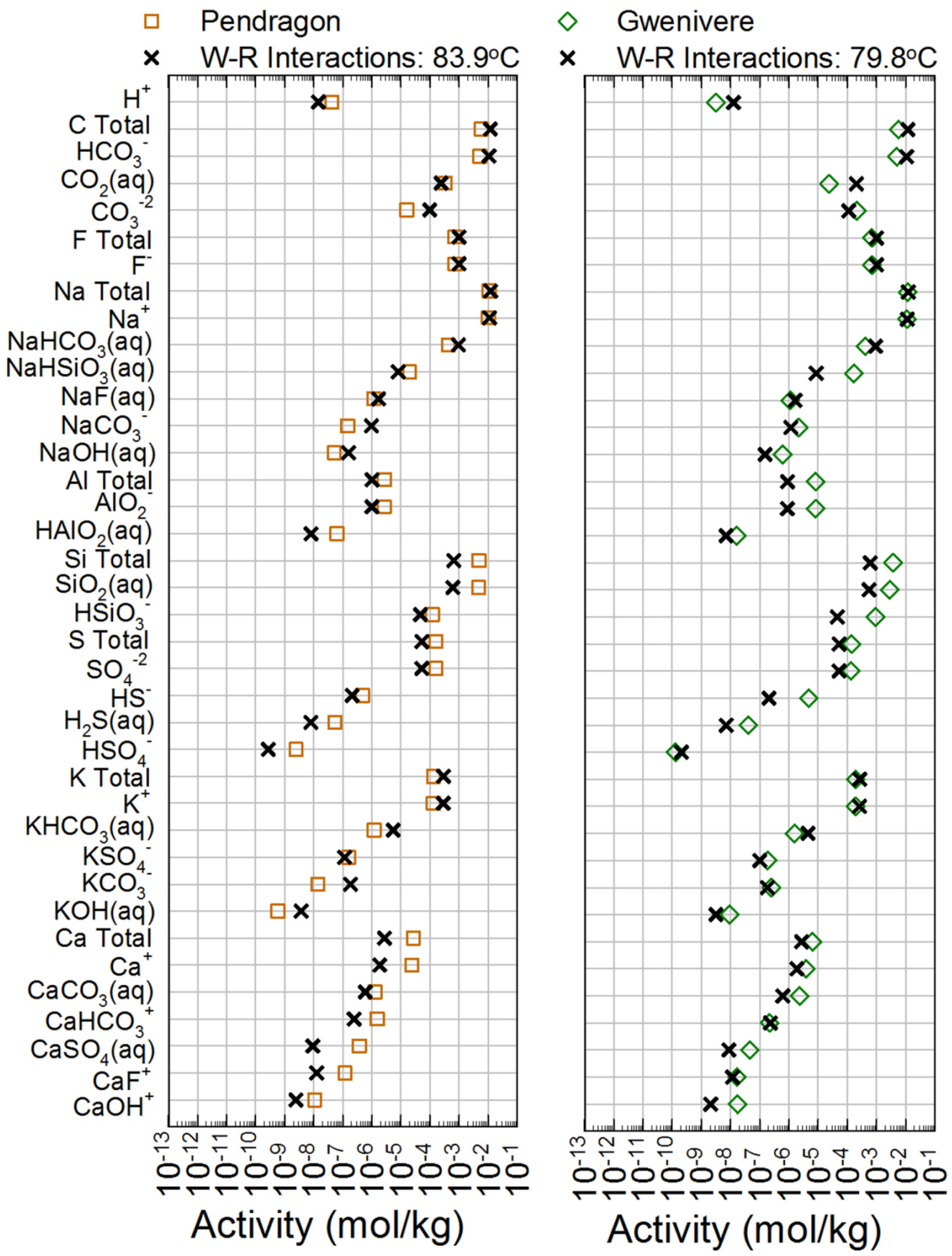

Figure 17: EQ3/6 predictions (water-rock reactions) and EQ3 speciation of Pendragon and Gwenivere.

The 79.8°C EQ3/6 predicted H^+ activity was greater than in the EQ3 speciation of Gwenivere, which led to lower predicted activities of NaOH (aq) and KOH (aq) (Fig. 17). The activities of calcium species were under-predicted for Gwenivere, but not as severely as they were for Pendragon or Uther (Fig. 16, 17). Similar deficiencies in predicted silicon, aluminum, and sulfur species were seen again in the 79.8°C EQ3/6 predictions.

The 74.2°C EQ3/6 predictions fit the EQ3 speciation of Merlin's Beard worse than the warmer predictions matched the warmer EQ3 speciations (Fig. 16-18). A major difference in the relationships between the 74.2°C EQ3/6 prediction and the EQ3 speciation of Merlin's Beard was that the total carbon, bicarbonate, and carbonate were all predicted above what was expected (Fig. 18). Due to the under-prediction of H^+ activity and the over-prediction of carbon, there was an over-prediction of species containing bicarbonate, carbonate, and hydroxide ($NaHCO_3$ (aq), $NaCO_3^-$, NaOH (aq), $KHCO_3$ (aq), KCO_3^-, and KOH (aq)) (Fig. 18). Although there was still a deficiency of total silicon and dissolved silica, there was the closest alignment of total aluminum, AlO_2^-, $HSiO_3^-$, total sulfur, and SO_4^{-2} between the model outputs (Fig. 18). However, there was the largest deficiency in the activities of calcium species yet predicted (Fig. 18).

The greatest differences between an EQ3/6 prediction and expected EQ3 speciation at the same temperature was seen for Mordrid and the EQ3/6 model cooled to 59.1°C (Fig. 16-18). There were two orders of magnitude less H^+ predicted than expected in Mordrid, resulting in mismatches between the predicted and expected activities of all carbon-bearing species (despite a relatively closely aligned value for total carbon) (Fig. 18). There were again deficiencies for aluminum, silicon, and sulfur species (except for HS^-) (Fig. 18). A deficiency in predicted total calcium was similar to the calcium deficiency seen in the prediction for Gwenivere (Fig. 17, 18).

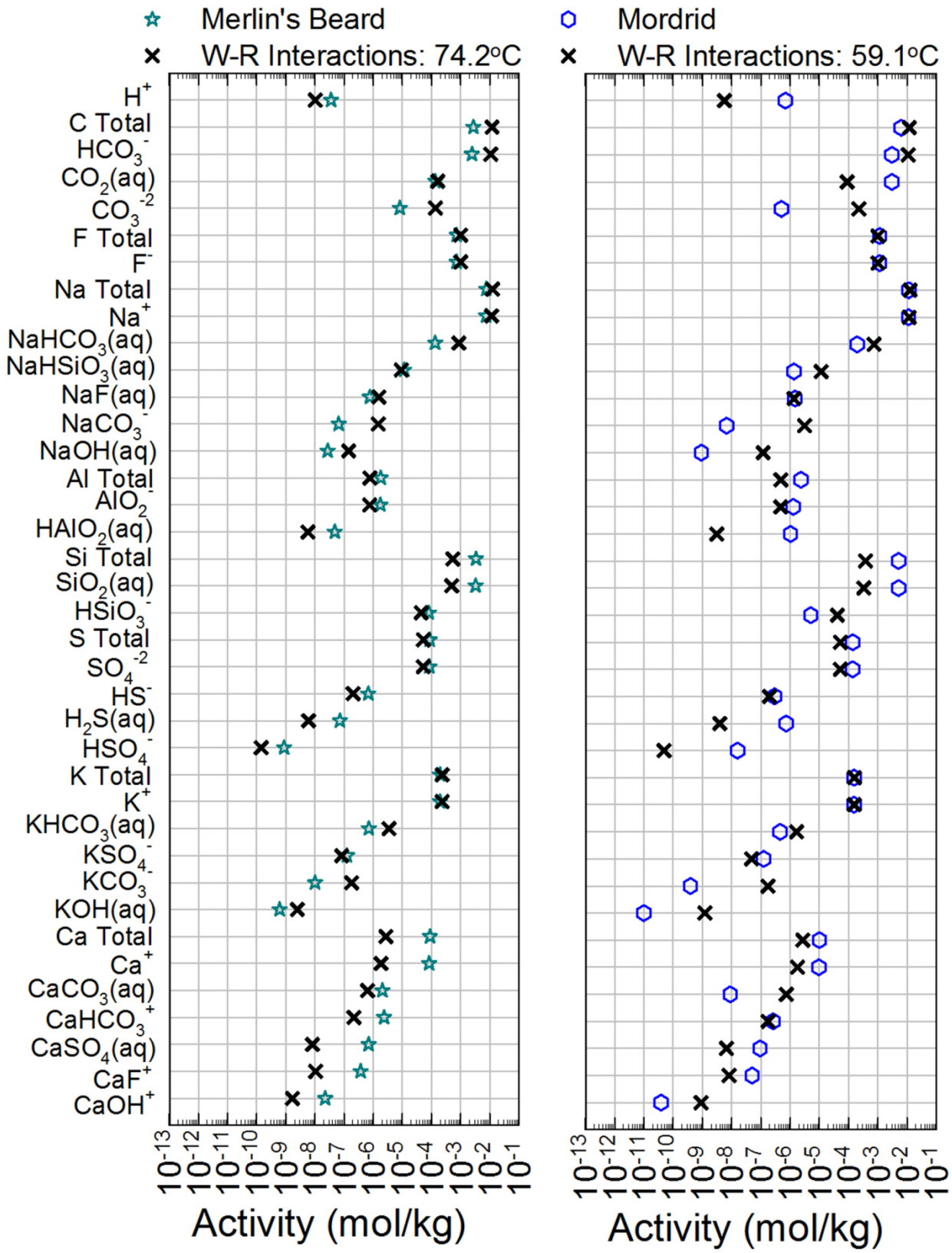

Figure 18: EQ3/6 predictions (water-rock reactions) and EQ3 speciation of Merlin's Beard and Mordrid.

When the calibrated EQ3/6 model was attempted to be cooled to 17.3°C, the model encountered error and self-terminated prematurely. This is why there is not a prediction for the chemical speciation at 17.3°C plotted against the EQ3 speciation of Grizzly Pool (Fig. 19). A comparison of the EQ3 speciation of all of the Y-5 features shows that Grizzly Pool had the lowest activity of H^+, total aluminum, total silicon, and total sulfur (Fig. 19). However, Grizzly Pool did have a similar order of magnitude of total carbon, total fluorine, total sodium, and total potassium as the other features (Fig. 19). The total calcium values and the activities of calcium species varied more between all features than for other elements, and the Grizzly Pool calcium species fit in the range defined by the other features (Fig. 19).

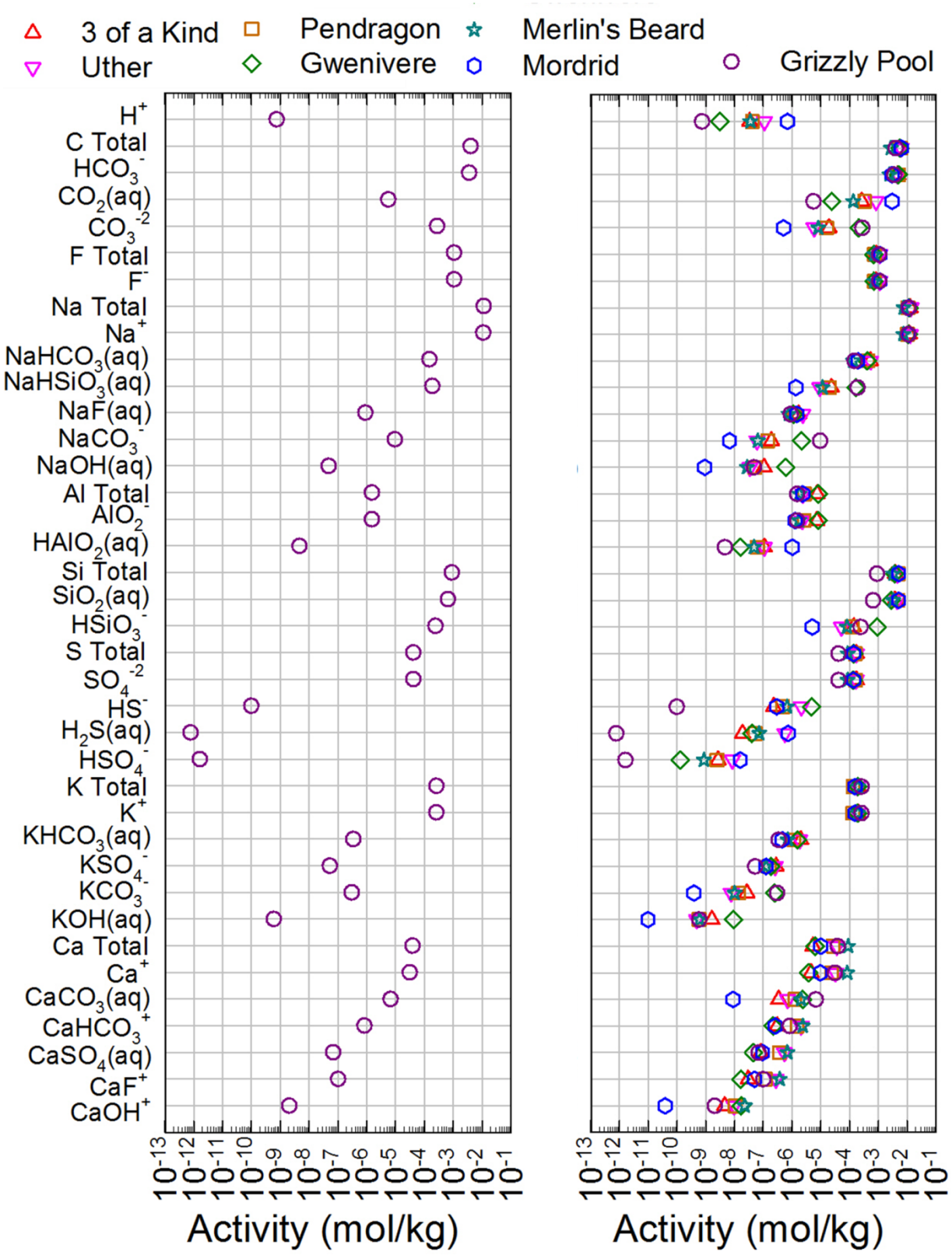

Figure 19: EQ3 speciation of Grizzly Pool and composite EQ3 speciation of all springs.

It is worth noting that many of the differences between the EQ3 speciations of the thermal features and the cooled EQ3/6 predictions were pH dependent. The activities of H^+ from the EQ3 speciations were different from the activities of H^+ from both field measurements and the EQ3/6 predictions (Table IV).

Table IV: pH values (field, EQ3, and EQ3/6) for Y-5 thermal features.

Spring	field pH	EQ3 pH	EQ3/6 pH
3 of a kind	7.756	7.471	7.719
Uther	7.459	6.959	7.719
Pendragon	7.483	7.375	7.838
Gwenivere	8.593	8.504	7.899
Merlin's Beard	6.502	7.446	7.987
Mordrid	8.117	6.157	8.245
Grizzly Pool	9.598	9.121	NA

NA = not applicable

Other EQ3 outputs of relevance include total dissolved solids (TDS) and ionic strength (Fig. 20). Both TDS and ionic strength generally increased with increasing conductivity for all thermal features except Grizzly Pool (Fig. 20).

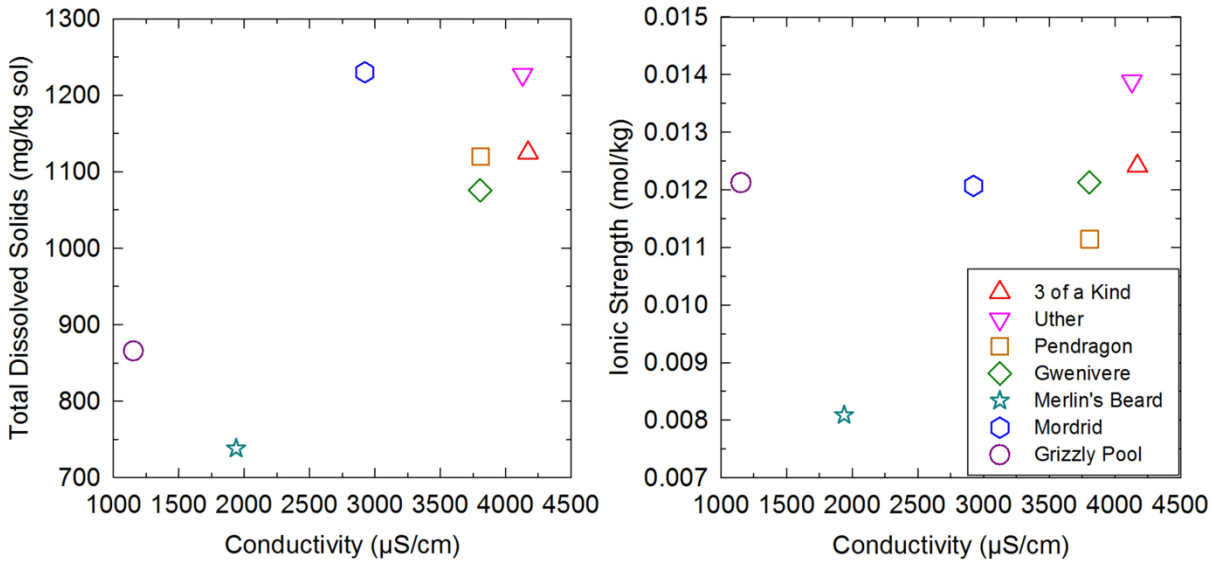

Figure 20: Total dissolved solids and ionic strength from EQ3 vs. field conductivity for Y-5 features. Error for conductivity is within symbol size.

The EQ3 and EQ3/6 outputs also noted minerals that were saturated or supersaturated. Minerals that were saturated in the EQ3/6 predictions at all temperatures were bornite, muscovite, quartz, sphalerite, and microcline (Or_{82}). There were no supersaturated minerals in the EQ3/6 predictions due to the use of partial equilibrium backward rate laws.

Supersaturated minerals from the EQ3 speciations of Y-5 thermal features are summarized in Tables V-VII. Most silica solids (except for β-cristobalite and amorphous silica) and all of the feldspars that were supersaturated were consistently supersaturated in all of the features (Table V). The aluminum-rich supersaturated minerals were only supersaturated for Mordrid, although gibbsite was also supersaturated in a few other features (Table V).

Table V: Supersaturated silica solids, feldspars, and aluminum-rich minerals in EQ3 speciation of Y-5 features.

Mineral	Stoichiometry	3 of a Kind	Uther	Pend.	Gwen.	Merlin's Beard	Mord.	Grizzly Pool
quartz	SiO_2	X	X	X	X	X	X	X
chalcedony	SiO_2	X	X	X	X	X	X	X
coesite	SiO_2	X	X	X	X	X	X	X
cristobalite	SiO_2	X	X	X	X	X	X	X
α-cristobalite	SiO_2	X	X	X	X	X	X	X
β-cristobalite	SiO_2		X	X		X	X	
amorphous Si	Si						X	
albite	$NaAlSi_3O_8$	X	X	X	X	X	X	X
albite, high	$NaAlSi_3O_8$	X	X	X	X	X	X	X
albite, low	$NaAlSi_3O_8$	X	X	X	X	X	X	X
K-feldspar	$KAlSi_3O_8$	X	X	X	X	X	X	X
microcline	$KAlSi_3O_8$	X	X	X	X	X	X	X
sanidine, high	$KAlSi_3O_8$	X	X	X	X	X	X	X
andalusite	Al_2SiO_5						X	
kyanite	Al_2SiO_5						X	
sillimanite	Al_2SiO_5						X	
boehmite	AlO(OH)						X	
gibbsite	$Al(OH)_3$	X	X			X	X	X
diaspore	AlO(OH)						X	

There was a great diversity of supersaturated minerals with "messy" stoichiometries represented by minerals from the zeolite, phyllosilicate, and sorosilicate groups (Table VI). The two supersaturated zeolites, laumontite and analcime, as well as the abundance of supersaturated phyllosilicates, have much simpler stoichiometries than the known zeolites and phyllosilicates in the Y-5 subsurface (mordonite, erionite, clinoptilolite, and montmorillonite) (Tables I, VI). The exception was illite, which was present in the rocks but has a similar stoichiometry to muscovite (see section 3.1.3). Muscovite was supersaturated in all EQ3 and EQ3/6 models (Tables VI).

Table VI: Supersaturated zeolites, phyllosilicates, and sorosilicates in EQ3 speciation of Y-5 features.

Mineral	Stoichiometry	3 of a Kind	Uther	Pend.	Gwen.	Merlin's Beard	Mord.	Grizzly Pool
laumontite	$CaAl_2Si_4O_{12}\cdot 4H_2O$	X	X	X	X	X	X	X
analcime	$NaAlSi_2O_6\cdot H_2O$	X	X	X	X	X	X	X
prehnite	$Ca_2Al_2Si_3O_{10}(OH)_2$						X	
margarite	$CaAl_4Si_2O_{10}(OH)_2$					X		
paragonite	$NaAl_3Si_3O_{10}(OH)_2$	X	X	X	X	X	X	X
muscovite	$KAl_3Si_3O_{10}(OH)_2$	X	X	X	X	X	X	X
phlogopite	$KAlMg_3Si_3O_{10}(OH)_2$	X		X	X	X		X
pyrophyllite	$Al_2Si_4O_{10}(OH)_2$	X	X	X	X	X	X	X
kaolinite	$Al_2Si_2O_5(OH)_4$		X	X	X	X	X	X
amesite	$Mg_2Al(AlSiO_5)(OH)_4$	X	X	X	X	X	X	X
antigorite	$Mg_{48}Si_{34}O_{85}(OH)_{62}$				X			X
chrysotile	$Mg_3Si_2O_5(OH)_4$				X			X
talc	$Mg_3Si_4O_{10}(OH)_2$	X		X	X	X		X
sepiolite	$Mg_4Si_6O_{15}(OH)_2\cdot 6H_2O$				X			X
clinochlore,14A	$Mg_5Al_2Si_3O_{10}(OH)_8$	X			X			X
clinochlore,7A	$Mg_5Al_2Si_3O_{10}(OH)_8$				X			X
epidote	$Ca_2FeAl_2Si_3O_{12}OH$	X	X	X	X	X	X	X
epidote, ord	$FeCa_2Al_2(OH)(SiO_4)_3$	X	X	X	X	X	X	X
lawsonite	$CaAl_2Si_2O_7(OH)_2\cdot H_2O$					X		X

Table VII summarizes the other silicate minerals (nesosilicate and inosilicates) that were supersaturated in the springs. The nesosilicate, andradite, was supersaturated in most springs, whereas the inosilicates (jadeite, diopside, anthophyllite, tremolite) were not as commonly

supersaturated (Table VII). The main iron minerals – goethite, pyrite, and hematite – were supersaturated in all springs in addition to being found in the Y-5 subsurface (Table I). A few copper-bearing and zinc bearing minerals were predicted as supersaturated in all of the Y-5 features, but carbonates were only supersaturated in Gwenivere and Grizzly Pool (Table VII).

Table VII: Other supersaturated silicate minerals and supersaturated minerals bearing iron, copper, zinc, or carbonate in EQ3 speciation of Y-5 features.

Mineral	Stoichiometry	3 of a Kind	Uther	Pend.	Gwen.	Merlin's Beard	Mord.	Grizzly Pool
andradite	$Ca_3Fe_2(SiO_4)_3$	X	X	X	X	X		X
jadeite	$NaAlSi_2O_6$						X	X
diopside	$CaMgSi_2O_6$				X			
anthophyllite	$Mg_7Si_8O_{22}(OH)_2$				X			
tremolite	$Ca_2Mg_5Si_8O_{22}(OH)_2$			X			X	
goethite	FeOOH	X	X	X	X	X	X	X
pyrite	FeS_2	X	X	X	X	X	X	X
hematite	Fe_2O_3	X	X	X	X	X	X	X
chalcopyrite	$CuFeS_2$	X	X	X	X	X	X	X
bornite	Cu_5FeS_4	X	X	X	X	X	X	
covellite	CuS	X	X	X	X	X	X	X
tenorite	CuO	X	X	X	X			
chalcocite	Cu_2S	X	X	X	X			
wurtzite	ZnS	X	X	X	X	X	X	X
sphalerite	ZnS	X	X	X	X	X	X	X
calcite	$CaCO_3$							X
dolomite	$(Ca,Mg)(CO_3)_2$				X			X
dolomite, ord	$(Ca,Mg)(CO_3)_2$				X			X

Even though the halogens were poorly represented in the EQ3/6 model outputs, it was important to consider the halogens in the EQ3 speciation of the thermal features (Fig. 21). Each of the halogens measured in the Y-5 features speciated with a variety of cations, which were all either alkali metals or alkaline earth metals except for one transition metal, zinc (Fig. 21). Chlorine speciated with the most cations, and bromine speciated with the least cations (Fig. 21). Between features, the speciation of bromine was closely aligned whereas the speciation of chlorine and especially fluorine were less aligned (Fig. 21).

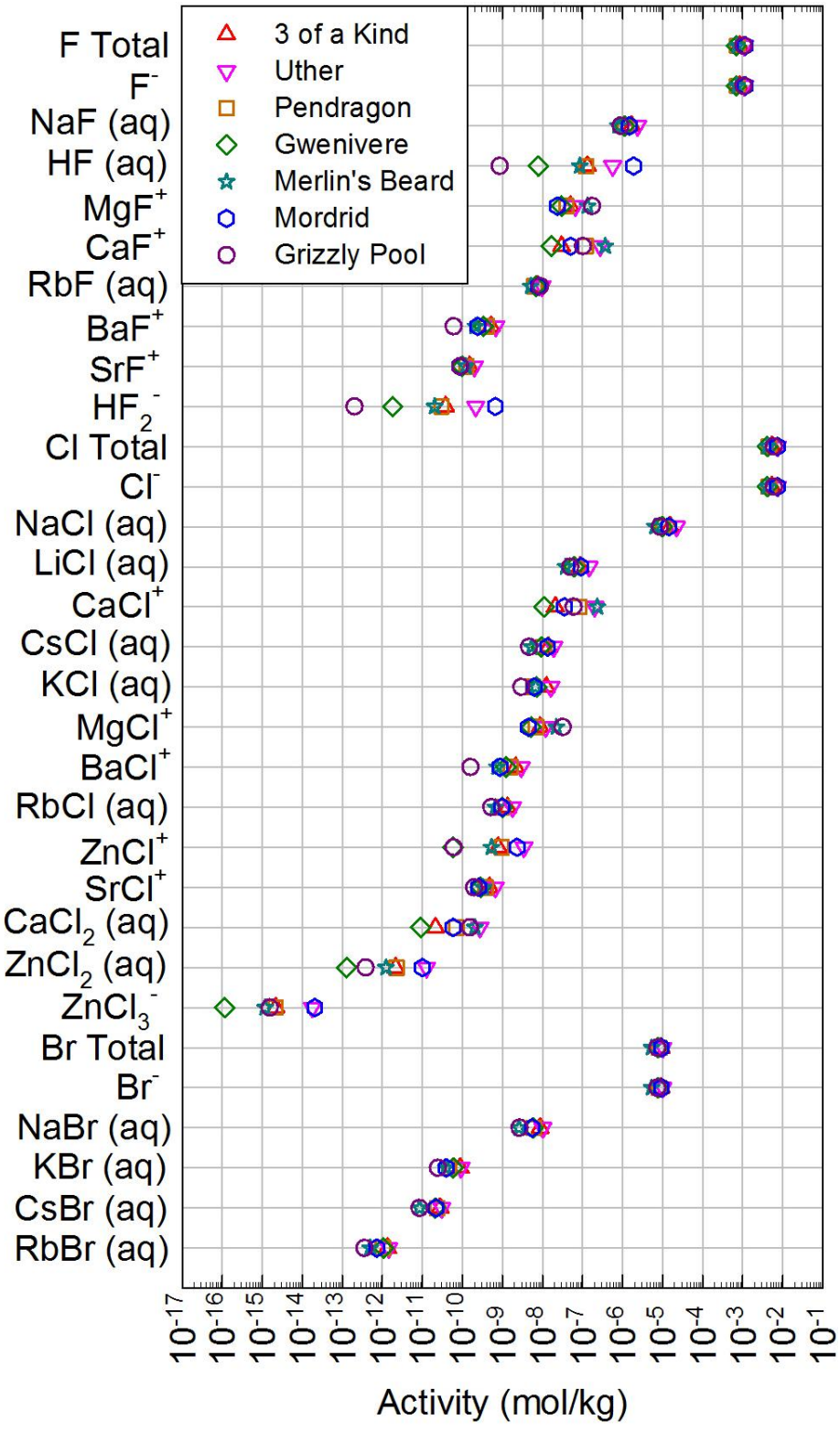

Figure 21: Halogen speciation (EQ3) in Y-5 thermal features.
Only species greater than 10^{-17} mol/kg for all features were displayed.

Despite the variety of species for all three halogens, the speciation of each halogen was dominated by one ion (comprising 99% or more): fluoride, chloride, or bromide (Fig. 21, 22). The same remained true in the EQ3/6 outputs at each temperature (Appendix H), even though chlorine and bromine were not able to be calibrated in the EQ3/6 outputs due to their lack of stoichiometric inclusion in rock forming minerals. Fluorine was attempted to be calibrated in the EQ3/6 outputs, but was only present in the rock as secondary fluorite. Attempting to put fluoride into solution only from fluorite led to an overabundance of calcium in solution, especially because calcium was present in other minerals like plagioclase. In order to calibrate the masses of both fluorine and calcium, the starting amount of fluorite had to be decreased and concentration of fluoride in the initial water had to be increased (Fig. 15; Appendix H).

All of the Y-5 features had similar activities of fluoride (although Uther, Mordrid, and Grizzly Pool had greater fluoride than the other springs), which made it easier to calibrate fluoride at all temperatures in the EQ3/6 outputs (Fig. 21, 22). Chloride was nearly half an order of magnitude greater than fluoride in all springs, and the same three springs had distinctly higher fluoride and chloride than the rest of the features (Fig. 21, 22). Bromide was a relatively minor constituent of each feature with the greatest activity in any one feature being only ~10 μmol/kg (Fig. 21, 23). Although Uther and Mordrid had the two largest activities of bromide, 3 of a Kind had the third largest bromide activity, and there was more variation in the other springs for bromide than for the other halogens (Fig. 21, 22).

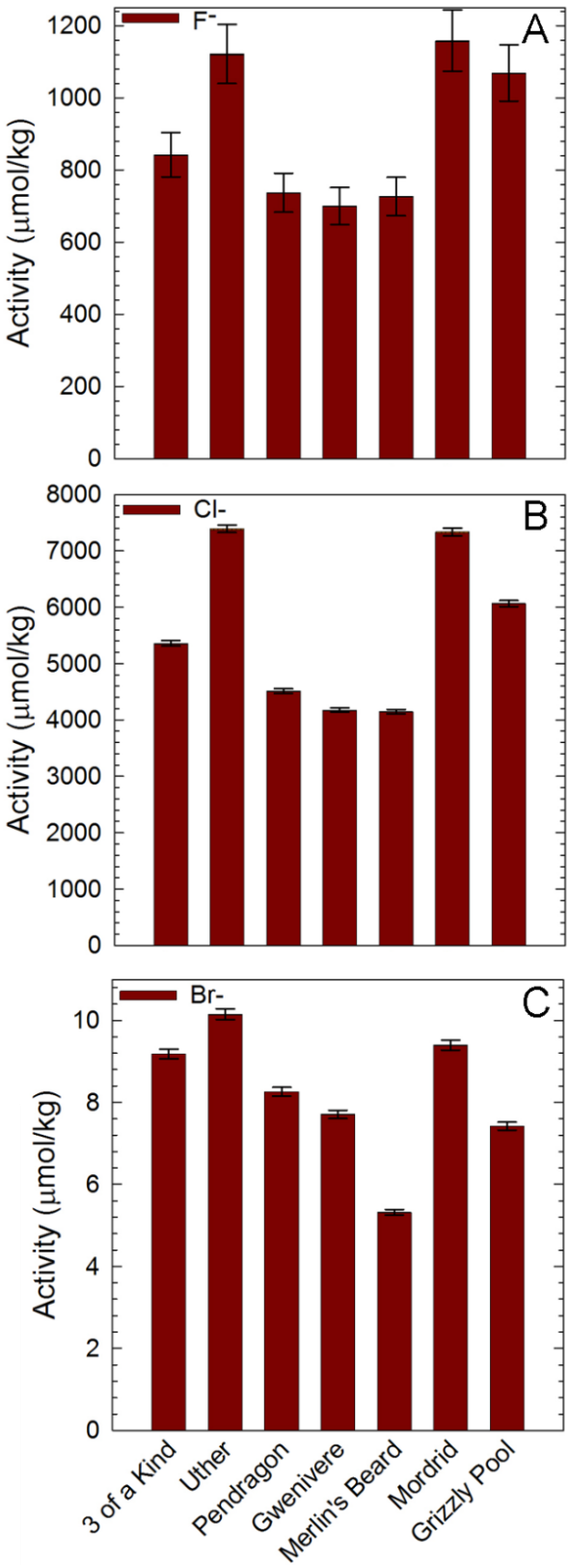

Figure 22: Halogen speciation (99% or more for each halogen) (EQ3) in the Y-5 thermal features. Error bars show instrumental error on the total F, Cl, and Br used as EQ3 inputs.

Boron and lithium were other important elements that could not be included in the calibrated EQ3/6 models due to their lack of stoichiometric inclusion in rock forming minerals. Total lithium and total boron increased in a roughly linear trend in the Y-5 thermal features (Fig. 23A), but multiple species of both lithium and boron existed in the features (Fig. 23B).

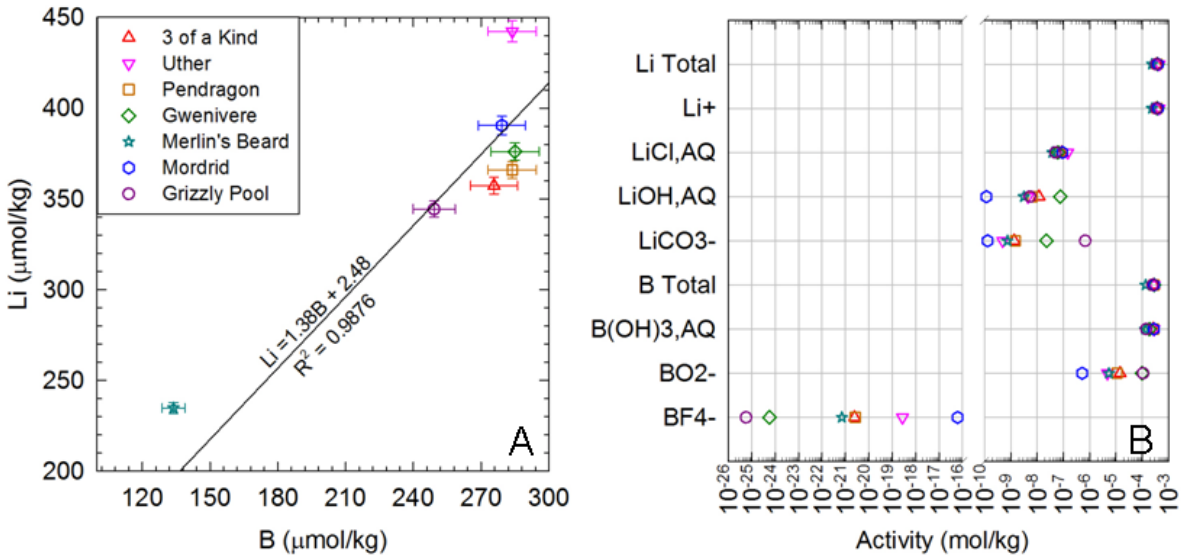

Figure 23: Lithium and boron in Y-5 thermal features.
(A) Li vs B gives a trend line of Li = 1.38B + 2.48. (B) Lithium and boron speciation (EQ3) for Y-5 thermal features. Error bars are within symbol size.

Despite the variety of lithium species in the system (Fig. 23 B), greater than 99% of the lithium speciated as Li^+ in all of the Y-5 thermal features (Fig. 23 B, 24 A). Most of the features had similar Li^+ activities, but Uther had the greatest Li^+ activity and Merlin's Beard had the lowest (Fig. 24 A). Two main species of boron were present in the features, although $B(OH)_3$ (aq) was the dominant boron species over BO_2^- in all of the features (Fig. 24 B). BO_2^- comprised just under half of the boron in Gwenivere and Grizzly Pool, the two springs most alkaline in their EQ3 speciations (Table IV). All of the features had similar total boron, except for Merlin's Beard, which had only about half as much boron as the other features (Fig. 24 B).

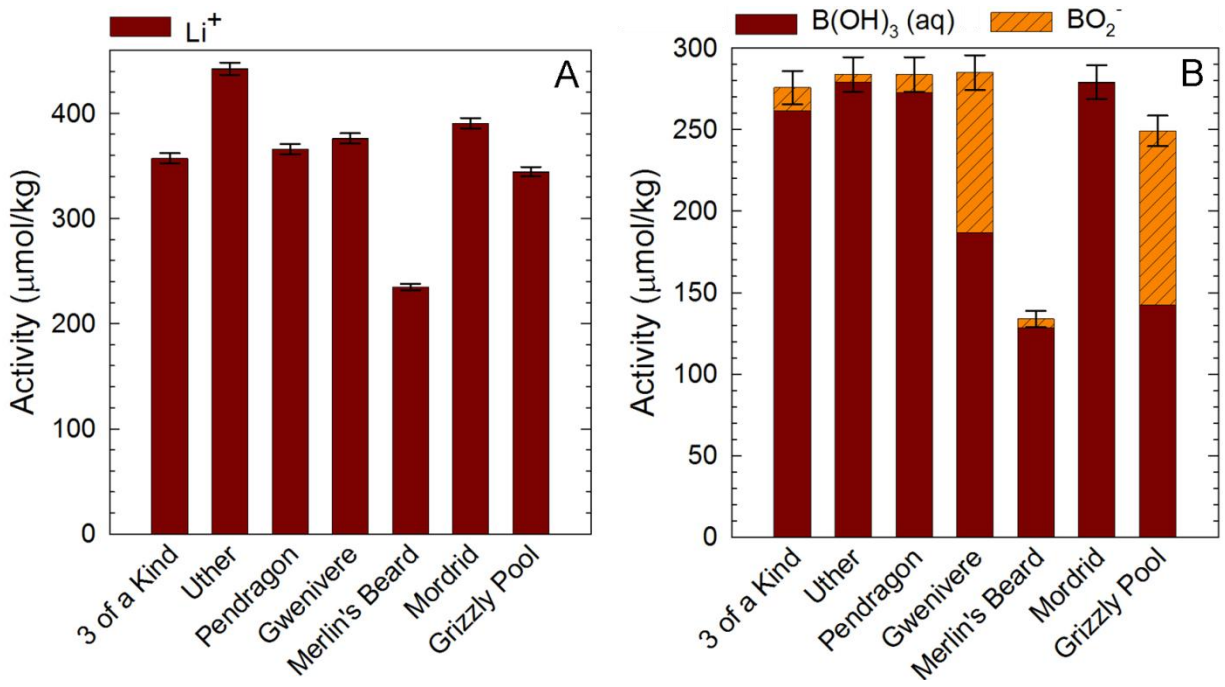

Figure 24: Lithium (A) and boron (B) speciation (99% or more) (EQ3) in Y-5 thermal features. Error bars show instrumental error on the total Li and B used as EQ3 inputs.

The quantitative results of lithium and boron speciation from the EQ3/6 models were meaningless because those elements were not calibrated. However, the lithium and boron species in the EQ3/6 results were analyzed by looking at the relative abundance of the species for each element. In the EQ3/6 outputs, at all analyzed temperatures, Li^+ encompassed greater than 99% of all lithium (Appendix H). A comparison of the relative abundance of boron species in both the EQ3 and EQ3/6 outputs revealed that the two boron species $B(OH)_3$ (aq) and BO_2^- remained the most abundant (Fig. 25). Greater than 50% of the boron existed as $B(OH)_3$ (aq) in the EQ3/6 outputs, and the proportions of boron species between the EQ3/6 and EQ3 outputs were generally similar (Fig. 25). An exception was that BO_2^- was predicted to encompass 18.5% of the boron in Mordrid as opposed to less than 1% expected from the EQ3 speciation (Fig. 25).

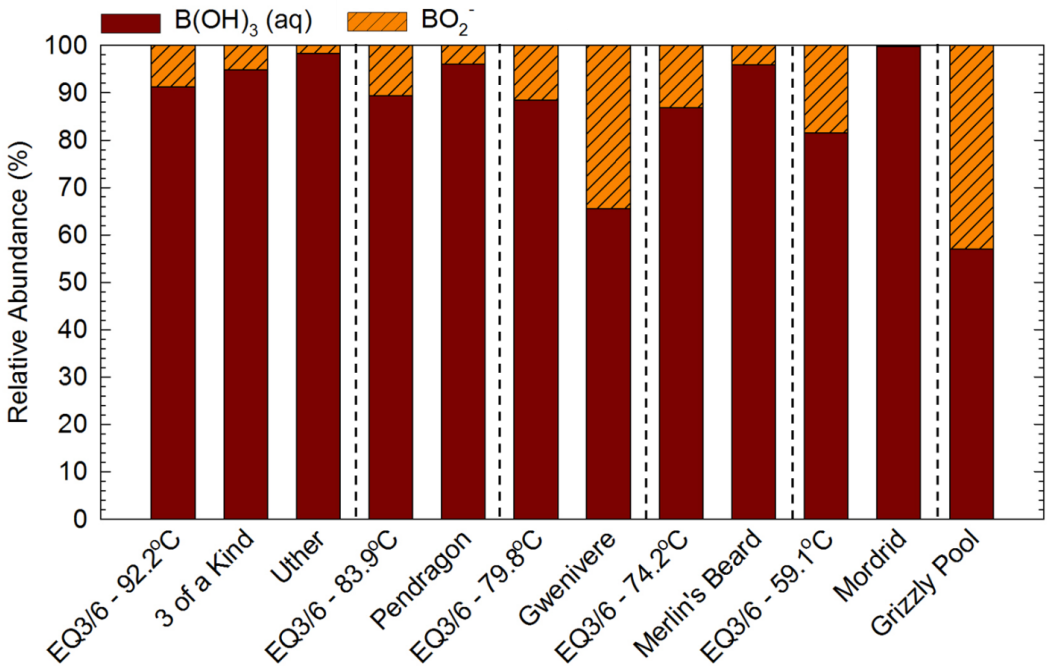

Figure 25: Relative abundances of boron species from EQ3 and EQ3/6.

3.3.2. Trace Elements

Other than lithium and boron, only six trace elements (As, Rb, Mo, Sb, Cs, and W) were consistently measured above the lower detection limit in all of the Y-5 features. In the EQ3 speciations of the Y-5 thermal features, the two dominant species for arsenic were $HAsO_4^{-2}$ and $H_2AsO_4^-$, but there was one dominant species for each of the other five elements summarized here (Fig. 26). For rubidium, Rb^+ was the dominant species, although there was a tiny amount of RbF (aq) that also showed up for all features except Merlin's Beard (at the scale of Fig. 26 B). Nearly all of the molybdenum speciated as MoO_4^{-2} in all of the features, but $HMoO_4^-$ was low yet noticeable in Mordrid (Fig. 26 C). For all features, $HSbO_2$ (aq) was the dominant species of antimony, but Gwenivere had more SbO_2^- than the other features (Fig. 26 D). A small portion of CsCl (aq) was in Uther, but essentially all of the cesium was speciated as Cs^+ in all of the features (Fig. 26 E). For tungsten, WO_4^{-2} was the main species for all of the features (Fig. 26 F).

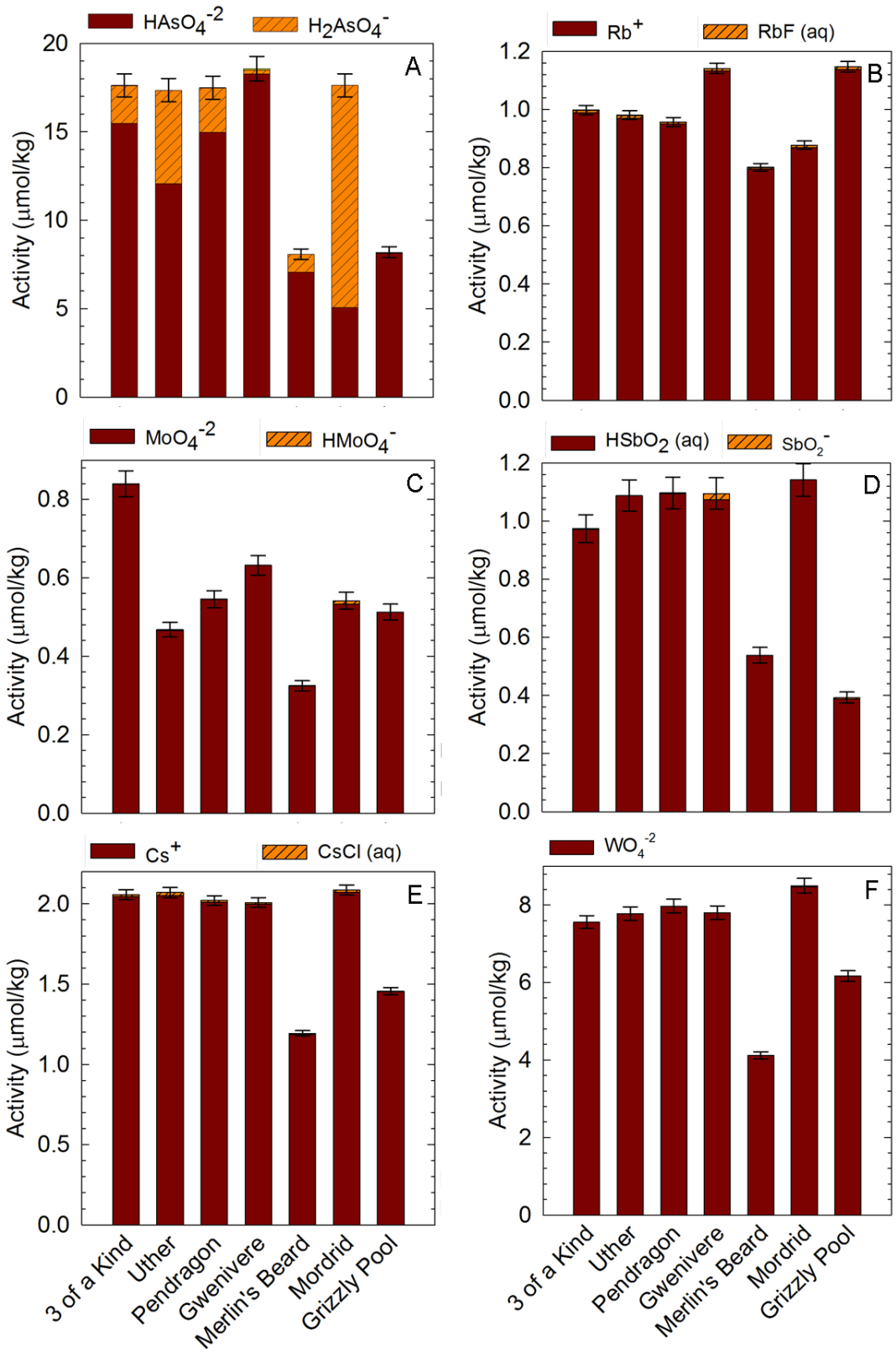

Figure 26: EQ3 speciation of trace elements (99% or more) above detection limit for all Y-5 features. (A) arsenic, (B) rubidium, (C) molybdenum, (D) antimony, (E) cesium, and (F) tungsten. Keys are above each graph. Error bars show instrumental error on the total elemental concentrations used as EQ3 inputs.

The total arsenic was equivalent (within error) in all springs except Merlin's Beard and Grizzly Pool, which had the lowest total arsenic (Fig. 26 A). The same was true for antimony, cesium, and tungsten: Merlin's Beard and Grizzly Pool had less of those trace elements than the other features, which all otherwise had similar total amounts (Fig. 26 D, E, F). This trend was nearly reversed for rubidium, which was similar in most features but higher in Gwenivere and Grizzly Pool (Fig. 26 B). There was no clear trend for molybdenum between the springs, but 3 of a Kind had the greatest total molybdenum and Merlin's Beard had the lowest (Fig. 26 C).

In the EQ3/6 predictions, at each analyzed temperature, the dominant species (greater than 99%) of rubidium, molybdenum, antimony, cesium, and tungsten were the same as the dominant species seen in the EQ3 outputs (Appendix H; Fig. 26). The same was not true for arsenic (Fig. 27). EQ3/6 outputs produced dominantly arsenites ($HAsO_2$ (aq), $H_2AsO_3^-$, and AsO_2^-), whereas the dominant species in the EQ3 outputs were arsenates (Fig. 27).

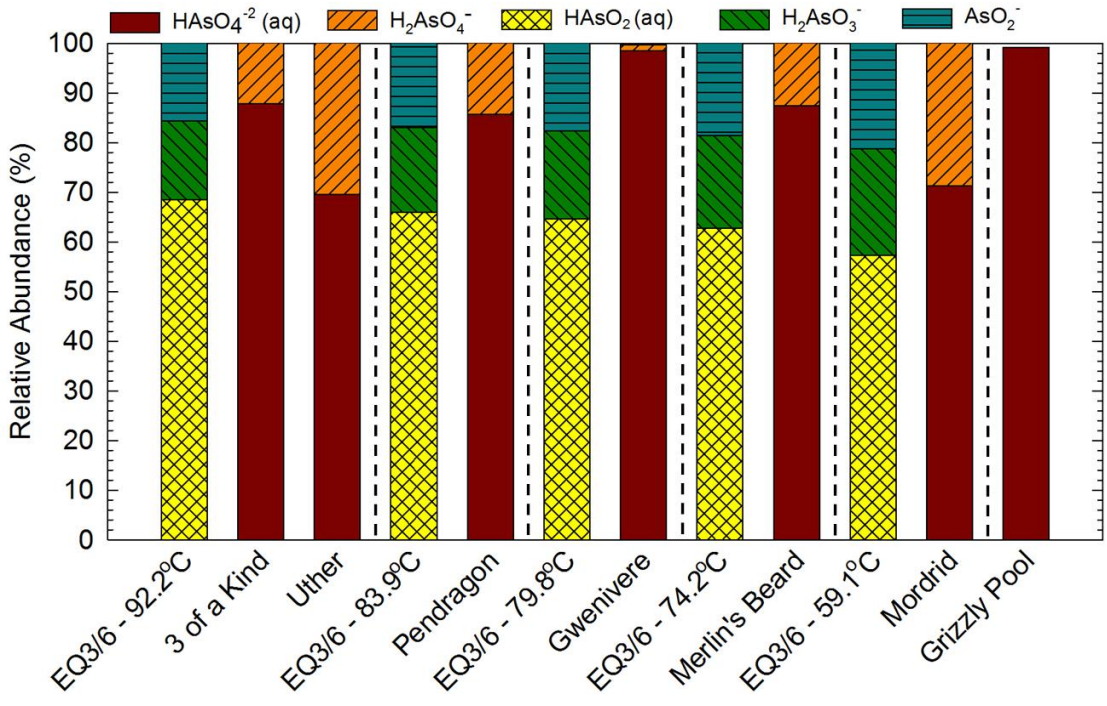

Figure 27: Relative abundances of arsenic species from EQ3 and EQ3/6.

The dominant arsenite species in the EQ3/6 outputs were present in the EQ3 speciation of the measured thermal feature data, but in almost negligible quantities (Fig. 28). In the EQ3/6 outputs, the relative abundance of $HAsO_2$ (aq) decreased with temperature while the relative abundances of $H_2AsO_3^-$ and AsO_2^- increased with temperature, which was not seen as consistently with the distribution of the arsenites in the EQ3 outputs (Fig. 27, 28).

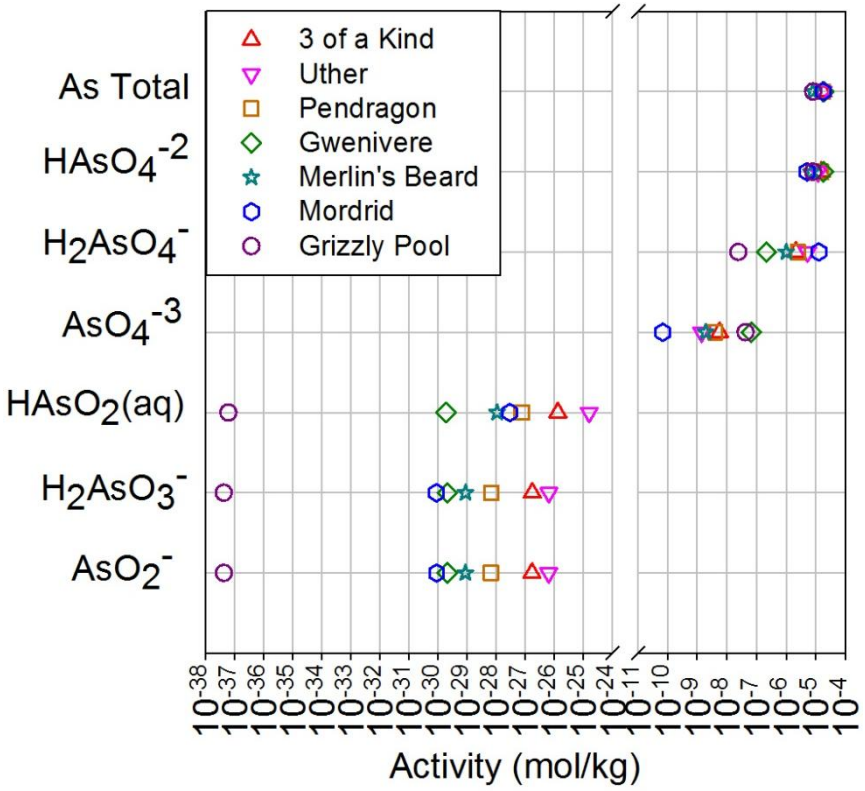

Figure 28: Arsenic speciation (EQ3) in Y-5 thermal features.
Error bars are within symbol size.

3.3.3. Nutrients (C, N, P, S)

Four major nutrients are considered here: carbon, nitrogen, phosphorus, and sulfur. In all features, more than 99% of the total carbon was encompassed by HCO_3^-, $NaHCO_3$ (aq), CO_2 (aq), and CO_3^{-2}, which were all calibrated in EQ3/6 (Fig. 29 A, C). More than 99% of the total nitrogen was comprised of NH_3 (aq), NH_4^+, and NO_3^- in the EQ3 speciations, but of NH_3 (aq), NH_4^+, and N_2 (aq) in the EQ3/6 outputs (Fig 30 B, D). Nitrogen was not calibrated in EQ3/6.

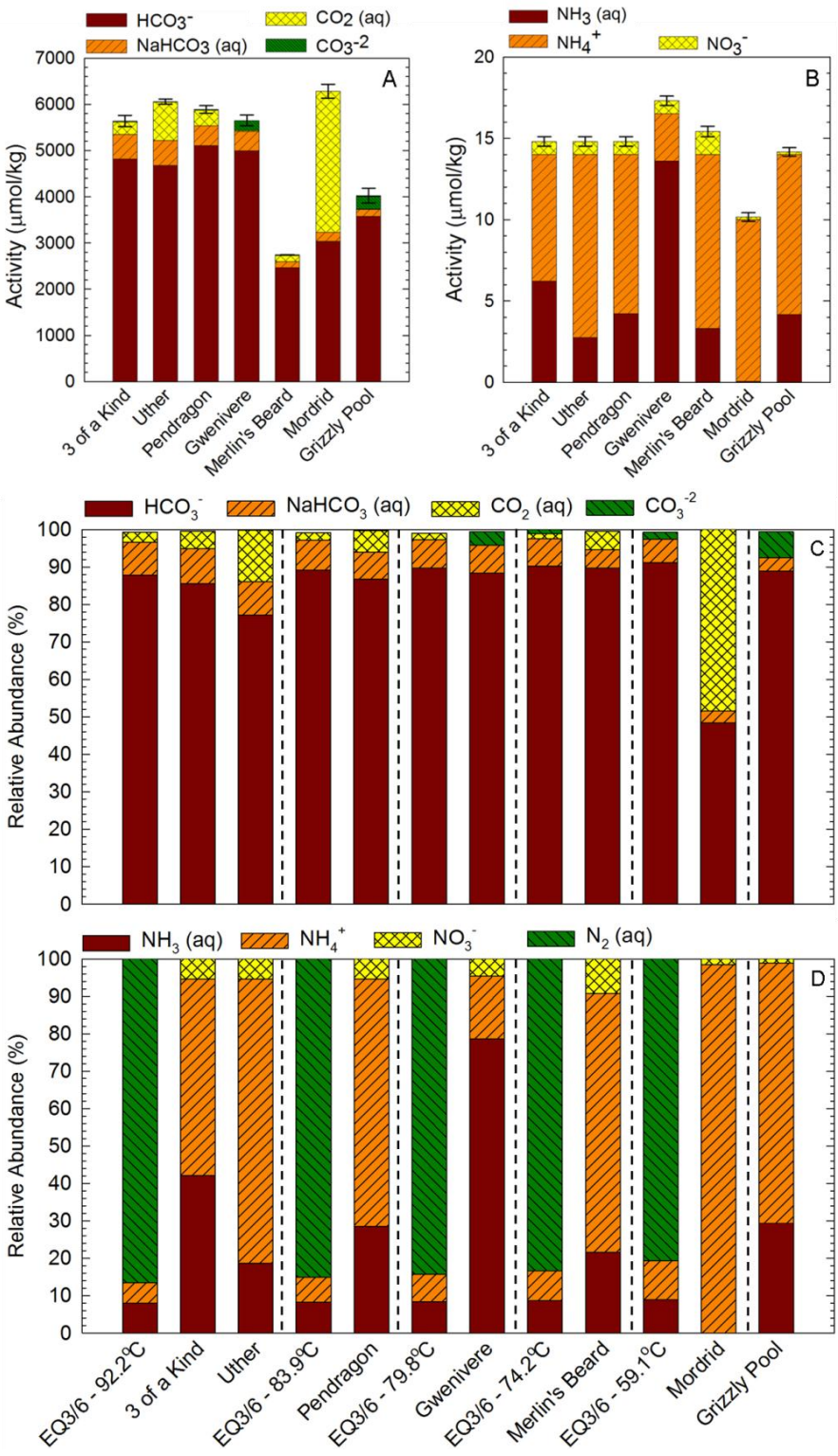

Figure 29: Carbon and nitrogen: EQ3 speciation and EQ3/6 relative abundances. (A) EQ3 speciation of carbon totaling 99% or more. (B) EQ3 speciation of nitrogen totaling 99% or more. (C) Relative abundances of carbon species from EQ3 and EQ3/6. (D) Relative abundances of nitrogen species from EQ3 and EQ3/6. Keys are above each graph. Error bars show instrumental error on the total elemental concentrations used as EQ3 inputs.

Even though Merlin's Beard and Grizzly Pool had less total carbon than the other features, carbon remained one of the most abundant elements in all Y-5 features (Fig. 29 A, Fig. 16-19). The EQ3/6 predictions for the carbon species were overall similar to what was expected based on EQ3 speciation of the thermal features, with minor variation (see section 3.3.1).

The total EQ3 nitrogen values were combinations of cited ammonia values and measured nitrate values (which were all below the lower detection limit, except for Merlin's Beard) (Table III; Appendix E). Because nitrate was measured below the lower detection limit for most springs, the amount of nitrate used in the EQ3 inputs was frequently the value of the lower detection limit and thus were maximum values. The cited ammonia values were nonetheless larger than the values used for nitrate, so the dominant species in the Y-5 thermal features was mostly NH_3 (aq) and NH_4^+ (Fig. 29 B, D). The EQ3/6 outputs predicted a distinct lack of nitrate (Fig. 29 D).

Phosphorus was measured as phosphate at the lower detection limit for all Y-5 features except 3 of a Kind, and over 99% of the total phosphorus existed as HPO_4^{-2} and $H_2PO_4^-$ in the Y-5 features (Fig. 30 A, C). There were different lower detection limits for the Y-5 features based on different dilution factors used during sample analysis. The lower detection limits were used as total values for the EQ3 inputs, which were maximum values for the features. Greater than 50% of the phosphorus was expected to be speciated as HPO_4^{-2} in all of the features (except Uther) for both the EQ3 speciations and EQ3/6 predictions (Fig. 30 C).

The dominant sulfur species was sulfate in all EQ3 and EQ3/6 outputs (Fig. 30 B, D). There were minor amounts of HS^- seen in the EQ3 speciation of Uther, Gwenivere, and Mordrid, but greater than 95% of the sulfur in all features was still sulfate (Fig. 30 D). Sulfur was calibrated in EQ3/6 although phosphorus was not.

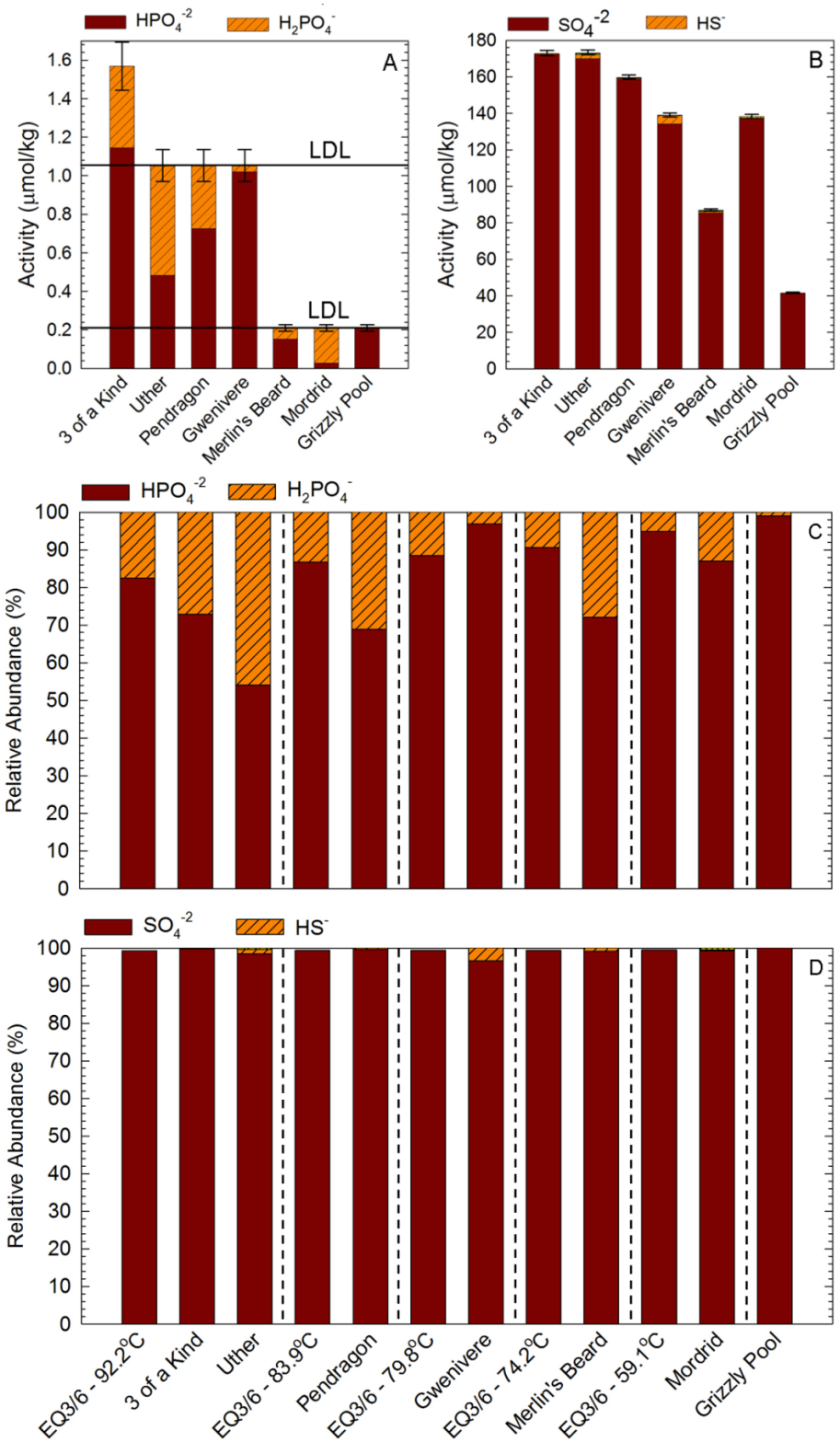

Figure 30: Phosphorus and sulfur: EQ3 speciation and EQ3/6 relative abundances. (A) EQ3 speciation of phosphorus totaling 99% or more. LDL = lower detection limit at 0.21 µmol/kg and 1.1 µmol/kg. (B) EQ3 speciation of sulfur totaling 99% or more. (C) Relative abundances of phosphorus species from EQ3 and EQ3/6. (D) Relative abundances of sulfur species from EQ3 and EQ3/6. Keys are above each graph. Error bars show instrumental error on the total elemental concentrations used as EQ3 inputs.

Although there were only a few dominant species for each nutrient, there were a myriad of minor species for each nutrient (Fig. 31; Appendix H). Many minor species of nitrogen and phosphorus had essentially negligible activities, but some minor species of carbon and sulfur were present in activities similar to trace element activities (Fig. 26, 31; Appendix H).

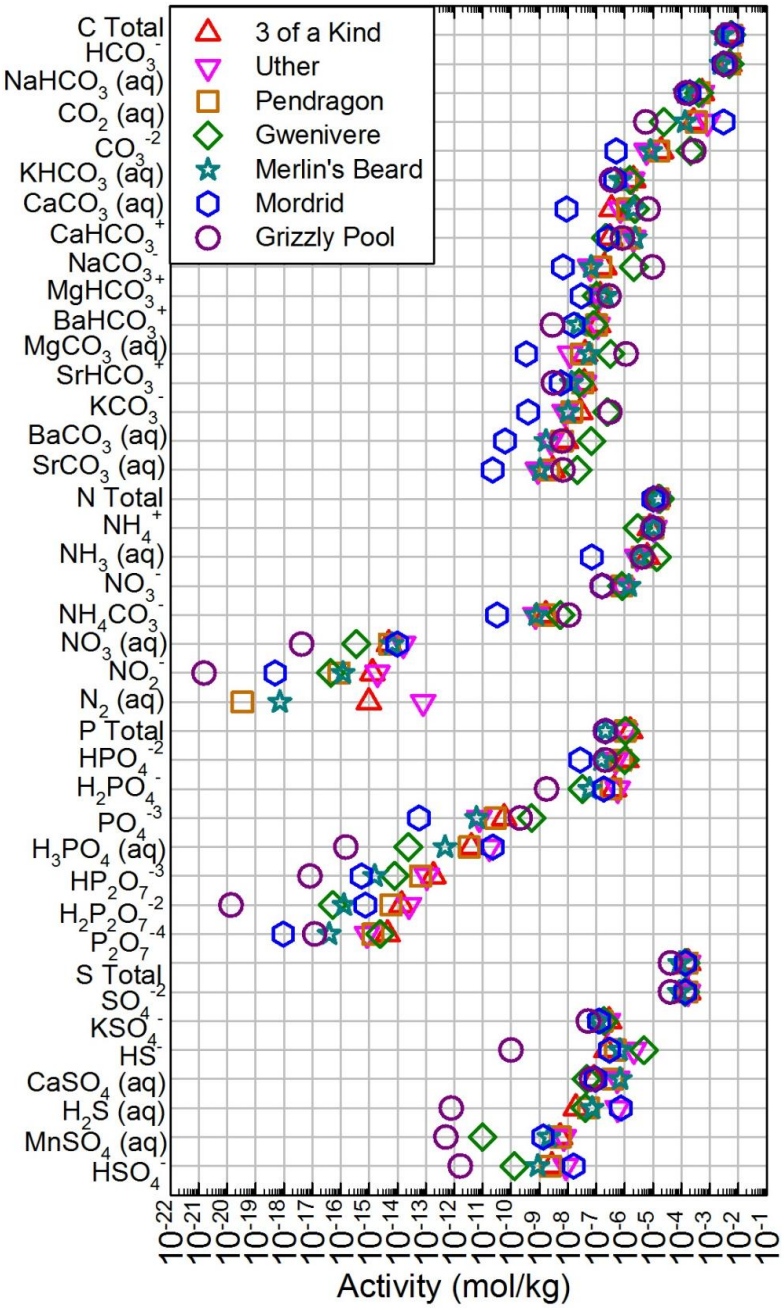

Figure 31: C, N, P, and S speciation (EQ3) in Y-5 thermal features. Only species greater than 10^{-22} mol/kg are shown.

3.4. Microbial Diversity of 3 of a Kind Sediment

Archaea and bacteria were found in 3 of a Kind sediment (Fig. 32, Tables VIII-IX). There was a greater diversity of bacteria at all levels of classification than of archaea. Only selected phyla, genera, and species are displayed here for convenience (Fig. 32, Tables VIII-IX).

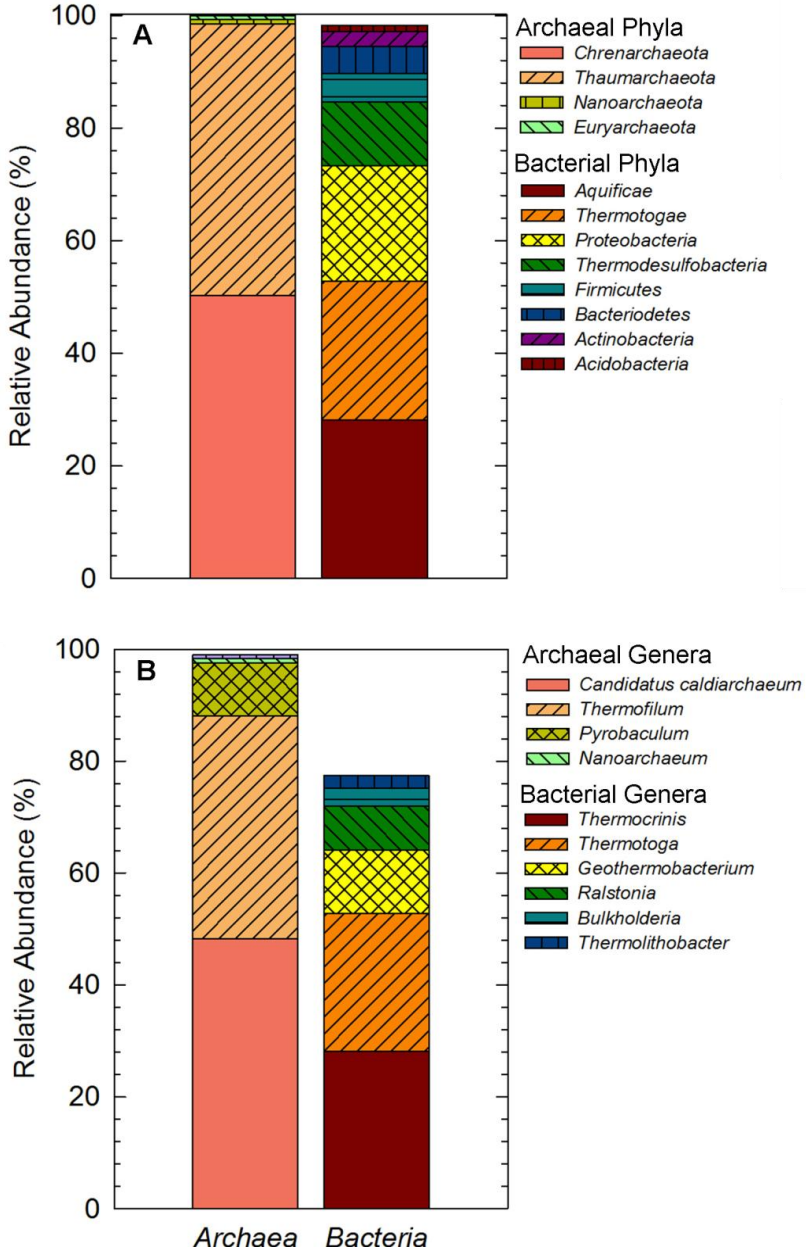

Figure 32: Relative abundances of Archaeal and Bacterial phyla and genera. (A) 100% of Archaeal phyla are represented. Bacterial phyla above 1% are represented, totaling 98.19%. (B) Archaeal general above 0.5% are represented, totaling 98.95%. Bacterial genera above 2% are represented, totaling 77.38%.

Table VIII: Archaeal species (in genera above 0.5%) in 3 of a Kind sediment.

Archaeal Species (in genera above 0.5%)	Counts	Relative Abundance (%)
Candidatus Caldiarchaeum subterraneum	41,833	48.20%
Thermofilum sp.	34,625	39.90%
Pyrobaculum sp.	7,075	8.15%
Pyrobaculum Thermoproteus neutrophilus	890	1.00%
Pyrobaculum calidifontis	144	0.20%
Pyrobaculum islandicum	48	0.06%
Pyrobaculum arsenaticum	10	0.01%
Nanoarchaeum equitans	703	0.80%
Methanocaldococcus infernus	546	0.63%
Total	85,874	98.95%

Table IX: Bacterial species (above 2% in genera above 2%) in 3 of a Kind sediment.

Bacterial Species (above 2% in genera above 2%)	Counts	Relative Abundance (%)
Thermocrinis ruber	30,421	28.06%
Thermotoga petrophila	24,513	22.61%
Geothermobacterium spp.	12,374	11.41%
Ralstonia sp.	5,018	4.63%
Ralstonia spp.	3,437	3.17%
Burkholderia sp.	2,788	2.57%
Burkholderia ferrariae	508	0.47%
Burkholderia sacchari	118	0.11%
Burkholderia spp.	8	0.01%
Thermolithobacter ferrireducens	2,465	2.27%
Total	81,650	75.31%

4. Discussion

4.1. Water-Rock Interactions

4.1.1. Supersaturated EQ3 Minerals

Many of the minerals that were supersaturated in the Y-5 thermal features based on EQ3 speciation were more than likely not actually present in the features. EQ3 and EQ3/6 are better at predicting the classes of minerals that precipitated rather than specific minerals that precipitated (ex: the models might predict correctly that silica-rich zeolites precipitated, but not whether mordonite or heulandite precipitated) (Bruton, 1995). This is sometimes due to an over or under estimate of the thermodynamic stability of minerals in the database, or due to a lack of kinetic consideration of the mineral formation (Bruton, 1995). However, some improbable minerals were also calculated to be supersaturated in the Y-5 features because (1) there was too much input of elements that were actually measured below the lower detection limit and/or (2) because more realistic minerals were not available in the thermodynamic database to instead precipitate.

The silica solids and feldspars were perhaps the most likely to precipitate in the Y-5 thermal features. These were the major constituents of the Y-5 drill core (Fig 4; Tables I, II; Appendix B), and both secondary silica and secondary K-feldspar were found in the Y-5 subsurface via both visual inspection (Fig. 6) and EQ3/6 predictions at all temperatures. However, it is clear that not all of the supersaturated Al_2SiO_5 polymorphs could have formed in Mordrid (Table V). Andalusite, kyanite, and sillimanite are well studied metamorphic indicator minerals that exist in well defined, separate temperature-pressure regimes (Miyashiro, 1961; Althaus, 1967). The only of these polymorphs that could form at surficial pressures would be andalusite (Althaus, 1967), although andalusite would still be extremely unlikely to form in a

spring setting. It is nonetheless relevant to note that Mordrid would precipitate aluminum-rich minerals before the other springs.

All of the Y-5 features had multiple supersaturated phyllosilicates, which is realistic (Tables I, VI). However, the serpentine minerals (antigorite and chrysotile), are common alteration minerals of mafic systems and are unlikely to have formed in the Y-5 features, which are hosted in a felsic system. The other magnesium-rich phyllosilicates (Table VI) were also unlikely to have formed because magnesium was actually measured below the lower detection limit for all features except Merlin's Beard and Grizzly Pool (Appendix E). For the features where magnesium was below the lower detection limit, the starting concentrations of magnesium in the EQ3 inputs were the lower detection limits and thus maximum values (Appendix E). It is unsurprising that the magnesium-rich phyllosilicates were predicted mostly in the two features with the most basic pH, Gwenivere and Grizzly Pool, because those minerals are more common in mafic systems, which often produce basic hydrothermal fluid. This provides some credibility to the possibility of the magnesium-rich phyllosilicates in Grizzly Pool, which had measurable magnesium, but not for Gwenivere, where magnesium was measured below the lower detection limit (Appendix E). The undetectable magnesium concentrations in the water *could* be due to magnesium minerals precipitating and pulling magnesium out of the water, but this is unlikely because there was little magnesium in the Y-5 drill core (Fig. 8; Keith *et al.*, 1968-78, Beeson and Bargar, 1984). Muscovite and kaolinite are the most probable phyllosilicates to have actually formed, although illite would likely form instead of muscovite based on its detection in the Y-5 drill core (Table I). An important phyllosilicate not in the database that might have been able to form is lepidolite, a lithium-rich phyllosilicate known to have formed in the very shallow

subsurface of drill core Y-3, which was also removed from the Lower Geyser Basin (Bargar *et al.*, 1973).

The presence of the zeolites laumontite and analcime (Table VI) were important in that they represent the correct prediction of zeolites precipitation, although laumontite and analcime were not specifically identified in the Y-5 core. Analcime has been found with lepidolite and other alteration minerals in drill core Y-3 (Bargar *et al.*, 1973), and laumontite is not an unreasonable part of this suite of minerals (Barnes *et al.*, 1978). However, it has already been noted that the few zeolites that were positively identified in the Y-5 subsurface (mordonite, erionite, and clinoptilolite) were not in the EQ3/6 database (Table I,II). Many of the above mentioned minerals (including both phyllosilicates and zeolites) were calculated as supersaturated at least in part because realistic felsic alteration minerals for the Y-5 area, like the zeolites and phyllosilicates in the Y-5 core that had "messier" cation and aluminum ratios (Table I), were not options in the thermodynamic database.

It is doubtful that any of the supersaturated sorosilicates, nesosilicate, or inosilicates in the Y-5 thermal features actually formed (Table VI). There was possibly not enough iron to form either variety of epidote because, similar to magnesium, iron inputs to the EQ3 models were maximum values due to iron being measured below the lower detection limit for all thermal features (except for Grizzly Pool). Unlike for magnesium, iron was definitely present in the Y-5 drill core, so iron could be reaching the surficial thermal features and then precipitating out of solution as minerals (Fig. 8; Keith *et al.*, 1968-78, Beeson and Bargar, 1984). However, even though iron minerals (hematite, goethite, pyrite, magnetite) and iron stained chalcedony were present in the Y-5 drill core, no epidote was detected in the drill core, and a surficial spring setting is more unlikely to host epidote than the subsurface (Keith and Muffler, 1978; Keith *et*

al., 1968-78). The other supersaturated sorosilicate, lawsonite, is a high pressure metamorphic mineral characteristic of blueschist and doubtful to form at the surficial spring pressures (Schmidt and Poli, 1994; Okamoto and Maruyama, 1999). Most of the other supersaturated silicate minerals (nesosilicate and inosilicates) are commonly found in skarn deposits (andradite, diopside, anthophyllite, and tremolite) and require magnesium and/or iron (Table VI), which have already been noted as being overrepresented in EQ3 inputs for most samples. Jadeite is the exception (Table VI), although this high pressure pyroxene often forms from the feldspathoid nepheline (Newton and Kennedy, 1968; Green *et al.*, 2007). Due to lack of nepheline or high pressure in the Y-5 springs, jadeite would not have formed. It is expected that the supersaturation of these minerals was again likely due to the lack of more suitable secondary minerals (i.e. the zeolites and phyllosilicates found in the Y-5 drill core) that could accommodate extra silica, aluminum, calcium, and other cations in the specific ratios seen in the true alteration minerals (Table I).

The copper minerals were likely supersaturated in most Y-5 features because they were overrepresented in the EQ3 inputs due to being measured below the detection limit in most springs (Table VIII, Appendix E). Copper was only measured above the detection limit for 3 of a Kind, but it was only 2×10^{9} mol/kg more than the detection limit (Appendix E). It is unlikely that copper was almost nearly undetectable in the thermal feature waters due to mineral precipitation because, like magnesium, there was barely any copper in the Y-5 drill core (Fig. 7; Keith *et al.*, 1968-78, Beeson and Bargar, 1984). It is tempting to say the same for zinc, which was only measured above the detection limit for Merlin's Beard (4.08×10^{-7} mol/kg) (Appendix E). All the zinc values for the thermal feature waters were corrected for the blank, which had zinc measured at the same order of magnitude as the samples (2.11×10^{-7} mol/kg) (Appendix E).

After the blank correction, the zinc concentration in Merlin's Beard (1.97×10^{-7} mol/kg) was also essentially the same as the blank (Appendix E). However, while zinc, like copper, was only detected as a trace element in the Y-5 rocks and not as a stoichiometric constituent of a mineral, there was an order of magnitude more zinc than copper in the drill core (Fig. 7; Beeson and Bargar, 1984). It is then more likely for the zinc minerals than copper minerals to be present in the surficial springs, although, if so, the zinc minerals would be in negligible quantities.

The iron minerals predicted to be supersaturated by EQ3 are much more likely to exist than zinc minerals in the Y-5 thermal features due to the elevated iron in the Y-5 drill core compared to zinc (Fig. 7, 8; Keith *et al.*, 1968-78, Beeson and Bargar, 1984). Even so, the iron minerals – particularly the oxidized minerals (goethite and hematite) – are obvious and visibly orange when present. Both Grizzly Pool and Mordrid looked orange (Fig. 3), possibly indicative of oxidized iron, but more likely of photosynthetic pigments in microbial mats. Detected iron in the water of Grizzly Pool (4.81×10^{-7} mol/kg) was still less than the lower detection limit for iron for the other Y-5 features (9.76×10^{-7} mol/kg), all measured below the lower detection limit (Appendix E). This evidence, combined with visual observations, suggests that Grizzly Pool contained some oxidized iron solids, Mordrid was orange due to a photosynthetic microbial mat (Fig. 3), and none of the other features likely had any iron-bearing minerals precipitating.

4.1.2. Silica Supersaturation and Decompressional Boiling

One of the most difficult elements to calibrate in the EQ3/6 predictions was one of the most abundant: silicon (Fig. 16-18). During calibration, the final concentration of the dominant silicon species, SiO_2 (aq), remained fixed at 7.25×10^{-4} mol/kg (Appendix H), despite variations in initial temperature, time length, starting concentration of silica in the meteoric water, silica mineral proportions, and forward rate law constants for silica minerals. This was most likely due

to the EQ3/6 model being saturated in quartz. Other silicon-bearing minerals were also saturated, including microcline (Or_{82}) and muscovite. However, a mass imbalance of -3.11×10^{-3} mol/kg total Si was present in the final calibrated EQ3/6 model at 92.2°C (Appendix H). The simultaneous saturation of quartz and deficiency of total dissolved Si implies that the system was supersaturated in silica. There were similar silica deficiencies seen between the EQ3/6 predictions and EQ3 speciations for all temperatures analyzed (Fig. 16-18).

In the EQ3/6 models, the backward rate laws were set to be in partial equilibrium with the system, which allowed minerals to precipitate as necessary to prevent supersaturation of dissolved components. However, there were dozens of supersaturated minerals expected in the Y-5 features based on the EQ3 models, including five polymorphs of silica that were predicted as supersaturated in all Y-5 features (Table V-VII). Thus, preventing supersaturation in the EQ3/6 model (i.e. setting the backward rate laws to be in partial equilibrium) was unrealistic. Instead, the backward rate laws should have been adjusted to allow for dissolved silica to be in partial equilibrium with a higher polymorph of silica, perhaps α-cristobalite.

Supersaturation of silica can be achieved in hydrothermal water in more than one way. One scenario to account for silica supersaturation is as new subsurface fractures open, fresh rock is exposed, allowing for silica dissolution (and rapid ^{18}O exchange between the water and the minerals) (Sturchio *et al.*, 1990). This process could account for the silica supersaturation (and the ^{18}O enrichment noted in the Y-5 hydrothermal silica minerals from Sturchio *et al.* (1990)) (Sturchio *et al.*, 1990). Alternatively, if water is already quartz-saturated but amorphous silica or metastable silica minerals are absent, then conductive cooling can relatively inefficiently lead to silica supersaturation (Sturchio *et al.*, 1990). However, the third scenario leading to silica supersaturation is when: (1) water that is already quartz-saturated is present, (2)

obsidian/amorphous silica or metastable silica minerals are present, and (3) ^{18}O exchange occurs isothermally between the water and the rock (Sturchio *et al.*, 1990). For example, quartz-saturated water at 200°C in contact with amorphous silica (i.e. obsidian) or metastable silica minerals (ex: α-cristobalite formed via devitrification) can be enriched in silica respectively up to 944 mg/L SiO_2 (1.57 x 10^{-2} mol/kg SiO_2) or 464 mg/L SiO_2 (7.72 x 10^{-3} mol/kg SiO_2) (Sturchio *et al.*, 1990). While all three of these scenarios can lead to silica supersaturation in hydrothermal fluid, not all are likely to be responsible at once (Sturchio *et al.*, 1990).

There is evidence for silica supersaturation in the Y-5 area thermal water due to the third scenario outlined above (specific to the abundance of α-cristobalite). Y-5 contains both obsidian and α-cristobalite, but α-cristobalite is abundant throughout the rhyolitic tuff that comprises most of the core whereas obsidian only exists abundantly in the youngest, unconsolidated deposits (Fig. 4; Appendix B) (Keith and Muffler, 1978). The Y-5 area subsurface also would have had temperatures reasonably close to 200°C (maximum modern measured Y-5 borehole temperature of 167.8°C (White, 1975) and Y-5 fluorite fluid inclusion homogenization temperatures 131°C to 275°C (Bargar and Fournier, 1988)). Sturchio *et al.* (1990) reached a similar conclusion, which also accounts for the ^{18}O enrichment they found in the Y-5 hydrothermal chalcedony. The 92.2°C EQ3/6 predicted concentration of silica (7.75 x 10^{-4} mol/kg SiO_2) is almost exactly an order of magnitude less than the upper limit of silica enrichment from α-cristobalite at 200°C (7.72 x 10^{-3} mol/kg SiO_2). This is unsurprising due to the difference in temperature.

However, Sturchio *et al.* (1990) also proposes a second process – decompressional boiling – that likely contributes to both silica supersaturation and ^{18}O enrichment, which, as previously stated, have been observed respectively in the Y-5 hydrothermal water and rock. Keith and Muffler (1978) additionally thought that decompressional boiling has influenced the

Y-5 subsurface based on the presence of the "vapor-saturated zone" tuff (Fig. 4), small-scale subsurface breccias (Fig. 5), and seemingly contemporaneous fracture formation and fracture fill (lithic fragments locally sourced, layered chalcedony that does not span large areas) (Fig. 5) (Keith and Muffler, 1978). This evidence, along with a lack of evidence for tectonic faulting or a hydrothermal explosion after the retreat of the Pinedale Glaciation, indicated to Keith and Muffler (1978) that the process that caused the decompressional boiling was likely tensional fracturing resulting from the resurgence of the Mallard Lake dome (Keith and Muffler, 1978). Decompressional boiling will most likely continue to occur periodically in the Y-5 subsurface because the area is still active due to the Mallard Lake dome, as is evidenced by continual GPS measurements, recent earthquake activity (Chang *et al.*, 2007, 2010), and the occasional eruption of the nearby Till Geyser.

Comparison of δD and chloride data for the Y-5 thermal features after Truesdell *et al.* (1977) (Fig. 33) are consistent with the existence of decompressional boiling in the Y-5 area. Truesdell *et al.* (1977) plotted δD versus chloride concentration for hydrothermal fluid from multiple geyser basins in YNP and developed curves indicative of fluid compositions and processes (see Fig. 33). On Fig. 33, lines C and D respectively represent single-stage or continuous steam separation (Truesdell *et al.*, 1977). Single-stage steam separation is when the vapor phase separates from the liquid stage at one temperature during decompressional boiling (Truesdell *et al.*, 1977). Continuous steam separation is when the vapor phase separates from the liquid phase as the temperature changes during decompressional boiling (Truesdell *et al.*, 1977).

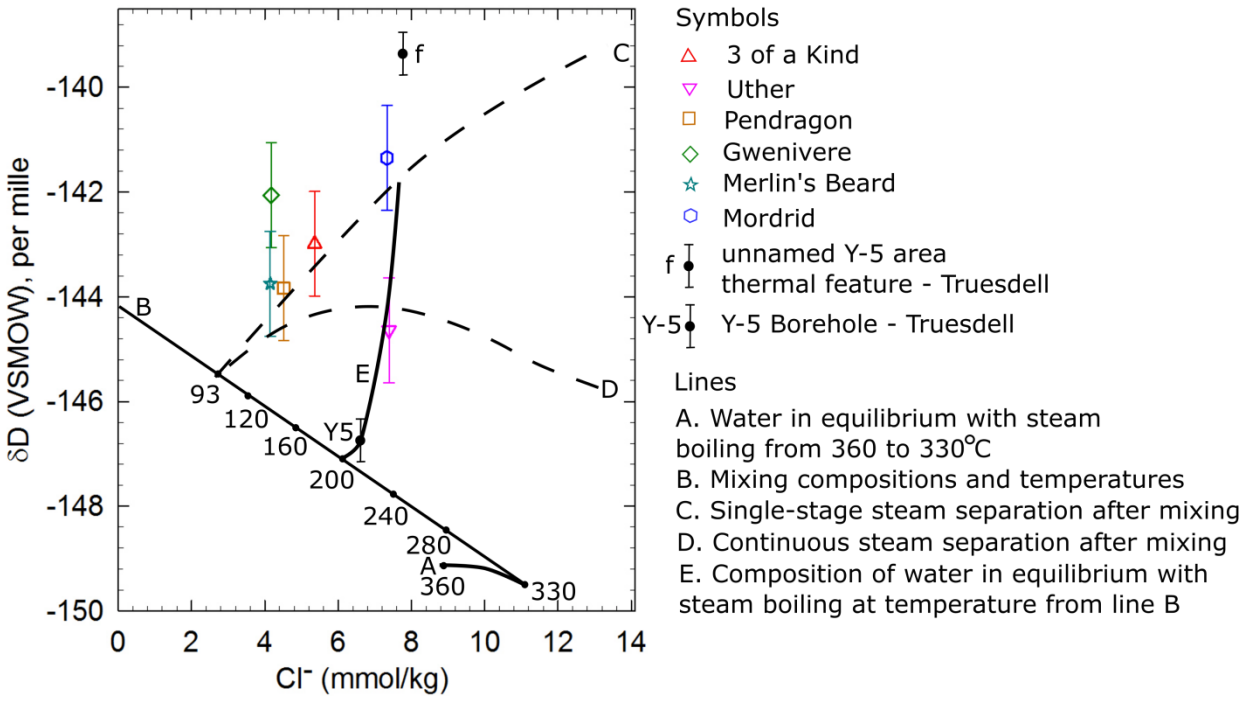

Figure 33: δD vs. chloride for the Y-5 thermal features.
Data is plotted on Fig. 9 from Truesdell *et al.*, 1977. δD error bars represent instrumental error (± 1‰).
Chloride error bars fall within symbol size.

Most of the Y-5 thermal features fall just above or on line C (single stage steam separation) within error, but Uther falls on line D (continuous steam separation) within error and Merlin's Beard and Pendragon fall on either line within error (Fig. 33). The steam forms from decompressional boiling of a mixture of deeply circulated water and shallow meteoric water defined at different temperatures (line B) (Truesdell *et al.*, 1977). It appears that all springs had single-stage steam separation except Uther, which had continuous steam separation (Fig. 33).

However, Uther and Mordrid seem to be connected because they had reversed stable water isotope values throughout the course of the sampling day (Fig. 11, 34). This was surprising because, in the field, the water levels in Uther and Pendragon were observed to change inversely occasionally throughout the day whereas the water level in Mordrid (and all the other thermal features) had appeared to be static. Although the later Pendragon sample overlaps with the earliest Uther sample for $\delta^{18}O \pm 0.1‰$, there is no other apparent relationship between the

water isotopes of Uther and Pendragon (Fig. 11, 34). Yet, in the field, Uther is positioned between Mordrid and Pendragon (Fig. 2, 3), so it is not unlikely that they are also related in the subsurface somehow.

If one assumes that the same source hydrothermal fluid feeds all of the Y-5 thermal features due to their proximity to each other, which is an assumption relied on for the modeling in this thesis, then the water isotopes from the different thermal features in the Y-5 area could be thought of as being representative of the source Y-5 hydrothermal fluid as it changed over the course of the sampling day. Using this assumption, there does seem to be a possible trend between time and $\delta^{18}O$ from the hydrothermal features in the Y-5 area (Fig. 34). What is most interesting about Fig. 34 is that at 10:24, the nearby Till Geyser erupted (which presumably is also fed by the same hydrothermal fluid as the Y-5 features analyzed in this thesis). The geyser eruption occurred right before a rise, drop, and subsequent rise in $\delta^{18}O$ in the general Y-5 area (Fig. 34). This is also around the same time that the inverse change in water level was observed between Uther and Pendragon (Fig. 34). There were no other observed eruptions of Till Geyser that day, but all field samplers were out of sight of the geyser for most of the afternoon, especially after 14:21, in order to collect full water samples of some of the southern features (Uther, Mordrid, and Pendragon). It appears that δD followed a nearly identical trend to $\delta^{18}O$ with time, although the "trend" with δD is much less pronounced when considering instrumental error (Fig. 34).

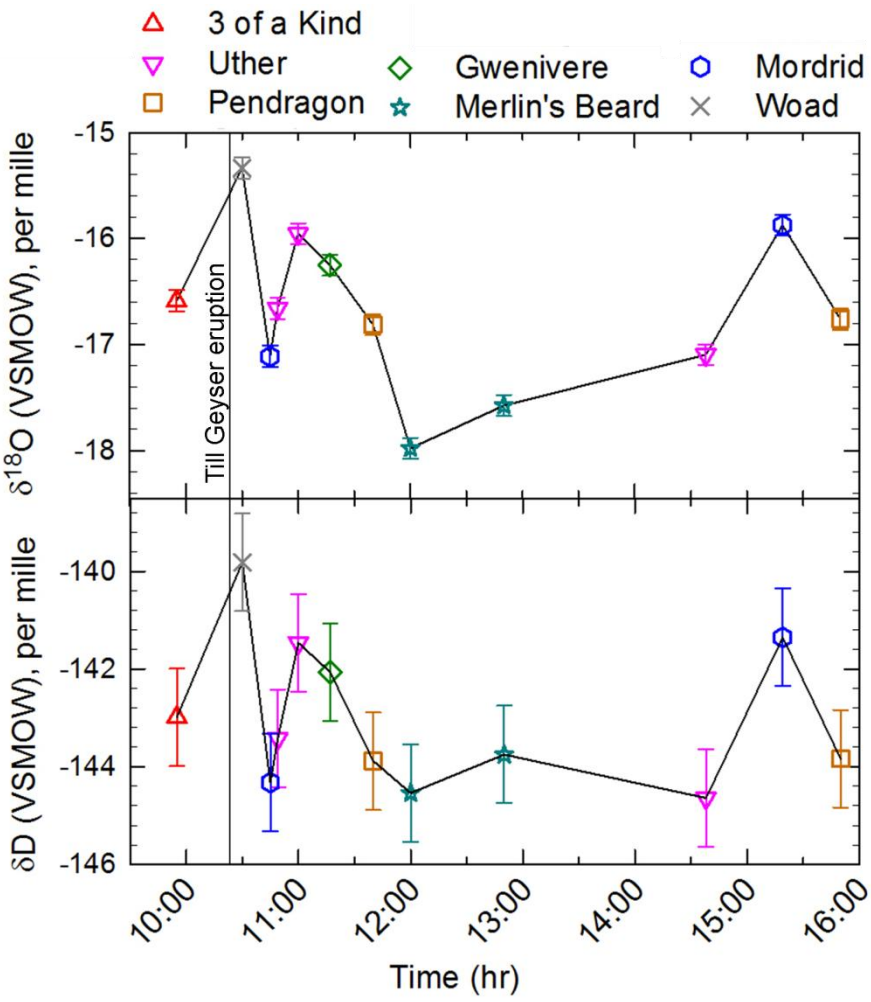

Figure 34: δD and $\delta^{18}O$ vs. time for Y-5 thermal features.
Error bars represent instrumental error (δD ± 1‰, δ18O ± 0.1‰). Eruption of Till Geyser noted.

If the chloride concentrations of Uther and Mordrid remain constant throughout the day (unknown), then the reversal in their isotope values (Fig. 11, 34) would indicate that the opposite of what we see in Figure 33 was true during the half hour after the observed eruption of Till Geyser (Fig. 34): Uther would have had single-stage steam separation whereas Mordrid would have had continuous steam separation.

It seems likely that, in general, the hydrothermal fluid feeding the Y-5 features commonly experiences single-stage steam separation with occasional continuous steam separation. It is possible that the mechanism which causes the eruptions of Till Geyser also

causes periodic continuous steam separation and heavier stable water isotopes (as seen in Woad directly after the geyser eruption) in the Y-5 area (Fig. 34). The lightening of the stable water isotopes in Mordrid and Uther after the geyser eruption could be due to a small lag in decompressional boiling, which could subsequently resume until another geyser eruption. If more thermal features were sampled for stable water isotopes around the time of the geyser eruption, this trend would likely be seen in all thermal features. It is possible that Till Geyser erupted unnoticed at some point between 14:30 and 15:30 during the sampling day, causing a similar spike and drop seen in the stable water isotopes collected later that afternoon (Fig. 34). This is highly hypothetical given the small number of data points for stable water isotopes in the Y-5 area and lack of consistent observation of Till Geyser (Fig. 11). The collection of more stable water isotope data points would be necessary to elucidate these interpretations, and could quickly support or refute this hypothesis. However, this preliminary hypothesis fits some of the field data and would account for some of the otherwise puzzling trends.

Mordrid and Uther also have the highest chloride concentrations of the analyzed Y-5 features, suggesting that Uther and Mordrid have the greatest proportion of deeply circulated water and are the least mixed with shallower meteoric water (Fig. 33). These springs also fall on line E, which represents the composition of water in equilibrium with steam boiling, which was drawn by Truesdell *et al.* (1977) through the data point for fluid measured from the Y-5 borehole. This would seem to indicate that Uther and Mordrid represent fluid that is most similar to the fluid originally analyzed from the Y-5 borehole (White, 1975), and that the other Y-5 thermal features analyzed in this document, including 3 of a Kind, would represent diluted versions of that water. However, this hypothesis is inconsistent with other data. How would the hottest and second coldest features (Uther at 92.2°C and Mordrid at 59.1°C) be less mixed than

all of the features with intermediate temperatures? How could 3 of a Kind be more dilute than Uther when the activities of most total constituents are almost the same (except for Ca, S^{-2}, and Al) (Fig. 16)?

Halides in YNP thermal features are generally interpreted as originating from and representing contribution from deeply circulated fluid (Truesdell *et al.*, 1977). Uther and Mordrid have the highest activities of not just chloride, but of the major species of each halide (F^-, Cl^-, and Br^-) (Fig. 22). Uther and Mordrid also have the highest predicted total dissolved solids (Fig. 20), and Uther has the highest ionic strength (Fig. 20), which are indicative of more dominant water-rock reactions. But, Uther and Mordrid are also the only two fully analyzed Y-5 thermal features without outflow channels (excluding the anomalous Grizzly Pool) (Fig. 3), which could lead to a greater accumulation of hydrothermally sourced components due to evaporation (especially considering that Uther is near boiling). It is thus more likely that concentration due to evaporation and boiling has led to the differences in halide concentrations for these features. Woad also does not have an outflow channel, and, if it were to be analyzed further, might also have higher concentrations of hydrothermally sourced inputs than otherwise might be expected.

4.1.3. Aluminum

As the EQ3/6 deficiencies in silica were likely due to silica saturation not being represented in the models, the deficiencies of dissolved aluminum in the EQ3/6 predictions were likely due to aluminum supersaturation not being represented in the models. Total dissolved aluminum was frequently too low in the EQ3/6 predictions to account for the total dissolved aluminum expected in the Y-5 thermal features based on EQ3 speciation (Fig. 16-18). This is most likely because the backward rate laws allowed for a few aluminum-bearing minerals

(muscovite and microcline) to be saturated and precipitating in the EQ3/6 predictions at all temperatures, which would pull aluminum out of solution. While these are known or similar to known secondary minerals found in the Y-5 drill core (Table I), these minerals could form even if dissolved aluminum was supersaturated. The EQ3 speciations of the Y-5 thermal features revealed that there were several supersaturated aluminum-bearing minerals (feldspars, phyllosilicates, and zeolites) present in the Y-5 features in various probabilities (see section 4.1.1). Aluminum supersaturation in the Y-5 thermal features could also be partly due to evaporative loss and solute concentration at the surface.

4.1.4. Sulfur

Sulfur was probably not supersaturated in the Y-5 thermal features, even though EQ3/6 predictions frequently contained a simultaneous deficiency of total sulfur and precipitation of sulfide minerals (sphalerite and bornite) at all temperatures (Fig. 16-18). The sulfides that were saturated in EQ3/6 predictions, sphalerite and bornite, were also supersaturated in all EQ3 speciations of Y-5 thermal features - but have already been discussed as being unlikely to form (see section 4.1.1).

The deficiency of total sulfur in the EQ3/6 predictions is partially due to the unrealistic precipitation of sulfide minerals due to over-estimation of copper and zinc inputs. There could additionally be a lack of sulfur input to the system. The only sulfur inputs to the EQ3/6 models were a negligible amount in the meteoric water and a minor amount of pyrite in the drill core. It is probable that H_2S (g) was an input to the system, even though there was not a characteristic sulfurous smell from any of the Y-5 thermal features. Measured concentrations of total dissolved sulfide from Y-5 features (2.49×10^{-7} mol/kg to 2.68×10^{-6} mol/kg) could have been greater in the subsurface due to possible H_2S (g) before oxidizing and/or degassing surficially in the

springs (Appendix E). It is also possible that microbes oxidize H_2S (g) in the system, skewing the sulfide measurements and resulting in too low of an input to the models (see section 4.2).

4.1.5. Sodium, Potassium, and Calcium

While total sodium and total potassium activities were well predicted by EQ3/6 at all temperatures, total calcium predictions were generally under-predicted by EQ3/6 (Fig. 16-18). In all features, the EQ3 models of the Y-5 thermal features noted supersaturated feldspars containing sodium and potassium but not calcium (Table V). This indicates that the thermal features were generally saturated in sodium and potassium but not in calcium.

This is unsurprising because felsic rocks, like the Y-5 drill core, often are sodium and potassium rich with lesser amounts of calcium. The variation in calcium seen in the Y-5 thermal features (Fig. 19, Appendix E) was probably due to differences in feldspar proportions in the rock of the Y-5 area. The anorthite content of the plagioclase feldspar in the core was variable: average An_{18-24} above 61 m, average An_{20-30} below 61m, and average $An_{23\pm5}$ overall (Keith *et al.*, 1968-78). This was also reflected in the distribution of values seen in the modified alkali-lime index (MALI) for the Y-5 core at multiple depths (Fig. 8 D). The MALI showed that, in general, the deepest rocks contained the least silica and calcium and the most sodium and potassium (Fig. 8 D).Throughout the Y-5 drill core, the rocks ranged between alkali-calcic, calc-alkaline, and calcic (Fig. 8 D). Considering that the Y-5 drill core is one representative slice of the Y-5 subsurface, it can be expected that there is just as much if not more variation in the calcium in the general Y-5 area subsurface as is represented by the MALI for the drill core. The total calcium activities of each thermal feature likely could have been more closely predicted by EQ3/6 if the plagioclase feldspar proportions and forward rate law constants were calibrated for each feature.

4.1.6. Iron

Even though the Y-5 rocks are ferroan (Fig. 8C), there was not necessarily an abundance of iron in the system. Because the iron index is a ratio, it means that there is more iron than magnesium in the system. Both iron and magnesium are dominant cations in mafic systems, and unsurprisingly neither iron nor magnesium was common in the Y-5 area (Appendix D, E). The iron probably originated from the unstable clinopyroxenes that were completely altered in the Y-5 drill core, and this iron seems to have broadly precipitated out of solution as fracture fill in the Y-5 subsurface (Fig. 5, 6). Based on measured dissolved iron in the Y-5 thermal features, not much iron remained in solution, which is unsurprising considering the pH of the thermal features (Appendix E). For these reasons, iron was not calibrated in EQ3/6.

4.1.7. Boron and Lithium

Of the trace elements in the Y-5 thermal features, boron and lithium were consistently present in the greatest concentrations (Fig. 7, Appendix C). Compared to the boron and lithium in the Y-5 drill core, boron was only slightly more concentrated in the rocks than the thermal features and lithium was much more concentrated in the rocks than in the thermal features (Fig. 7, Appendix C). In the Y-5 rocks, the average concentration of boron was 3.3 ppm whereas the average concentration of lithium was 70.3 ppm (Appendix C), which were consistent with values for altered rhyolitic YNP rocks (Shaw and Sturchio, 1992). This was also consistent with the expectation that, during the alteration of rhyolitic rocks, boron decreases in the rocks while lithium increases in the rocks. However, because of this, thermal waters generally contain much less total dissolved lithium than total dissolved boron (B/Li ≈ 3) (Shaw and Sturchio, 1992), which was not true for the Y-5 thermal features (B/Li ≈ 0.7) (Fig. 23). The Y-5 thermal features actually contained more dissolved total lithium (1.6 to 2.5 ppm; 2.3×10^{-4} to 4.4×10^{-4} mol/kg)

than dissolved total boron (1.4 to 2.4 ppm; 2.3 x 10^{-4} to 2.9 x 10^{-4} mol/kg), indicating that perhaps there are mechanisms removing boron from the thermal waters of the Y-5 area and/or preventing removal of lithium from the thermal waters. The removal of lithium from thermal waters has been specifically linked to illitic alteration (Shaw and Sturchio, 1992), which is present but not abundant in the Y-5 drill core and could be related to the elevated total dissolved lithium in the Y-5 thermal features (Fig 6, Table I).

4.1.8. pH Discrepancies

The chemical speciations of most elements were misaligned between EQ3 speciations and EQ3/6 predictions mostly due to pH variations (Fig. 16-18). During the calibration of the 92.2°C EQ3/6 prediction to the EQ3 speciation of 3 of a Kind, it was observed that the pH of the EQ3/6 prediction was controlled dominantly by the CO_2 (g) in the EQ6 inputs. Carbon dioxide gas in thermal features of the Midway Geyser Basin is generally not lost due to a steam phase in the subsurface (Fournier, 1989). Nonetheless, earlier, it was hypothesized that steam separation occasionally occurs continuously in the subsurface instead of as a single-stage separation at the surface in the Y-5 area (see section 4.1.2). This indicates that the pH of the thermal features may fluctuate along with changes in steam separation, CO_2 degassing, and stable water isotope values on a timescale observable within a day.

The potential for pH fluctuations within the course of a day in the Y-5 thermal features poses a problem because Uther, Pendragon, Mordrid, and Grizzly Pool had their *in situ* meter measurements, including pH, taken several hours before the full water samples were collected (Appendix E). Samples for stable water isotope analysis were collected with both the full water samples and the *in situ* meter measurements (except for Grizzly Pool). Although the stable water isotope values were essentially the same for Pendragon, the stable water isotope values were

different for the duplicate samples of Uther and Mordrid (Fig. 11). There were duplicate water isotope samples analyzed for Merlin's Beard as well, and even these were different (at least for $\delta^{18}O \pm 0.1‰$) despite those samples being collected within less than an hour of each other (Fig. 11). This could explain why, for Uther, Merlin's Beard, and Mordrid, their pH values in the EQ3 speciations were more different from their field pH values than for other springs (Table IV). As such, the pH dependent speciation of these springs could be misaligned due to daily fluctuations in the processes controlling CO_2 (g) in the thermal features. Despite the abiotic control on CO_2 (g) and pH of the Y-5 thermal features, Merlin's Beard and Mordrid had much larger pH discrepancies between field pH and EQ3 pH than Uther (Table IV).

There were also discrepancies between the pH of the temperature specific EQ3/6 predictions and both the pH values from the field and the pH values from EQ3 speciations (Table IV). The pH of the EQ3/6 predictions became more basic with decreasing temperature, assuming that none of the proportions of inputs changed. It has already been established here that it appears the proportion of CO_2 (g) changes in the thermal features throughout the timescale of one day, suggesting that varying the starting amount of CO_2 (g) in the EQ3/6 models could help align the pH dependent speciation of the EQ3 and EQ3/6 models at each temperature.

4.2. Microbial Impact

Overall, it appears that the mass imbalances and discrepancies in the chemical speciation between the EQ3 and EQ3/6 models at each temperature can be abiotically explained. However, it is expected that there were microbial influences in each thermal feature to different extents. Even in one of the hottest features, 3 of a Kind, low extracted DNA totaled ~5 ng DNA/g wet sediment. The diversity of microbes in the 3 of a Kind sediment gave an idea of the metabolisms that might occur in the other Y-5 thermal features. It is well known that microbes can exist at all

the temperatures of all of the Y-5 thermal features and likely influence the aqueous hydrothermal chemistries of these features, even though the dominant control on the aqueous chemistries of the Y-5 thermal features indeed seems to be hydrothermal water-rock reactions at depth.

4.2.1. Archaea in 3 of a Kind Sediment

A single species, *Candidatus caldiarchaeum subterraneum*, comprises nearly half of the archaea identified in the 3 of a Kind sediment (48.2%). It has been determined that this species is capable of metabolizing central carbohydrates, and can live aerobically and heterotrophically (Takami *et al.*, 2015). The genus *Thermofilum* (39.9%), which was not identified at the species level, is the next most abundant archaea. In general, *Thermofilum* produce H_2S (g) and are anaerobic chemoorganoheterotrophs (Stetter *et al.*, 1990; Wagner and Wiegel, 2008). Together, *C. caldiarchaeum subterraneum* and *Thermofilum sp.* comprise 88.1% of the archaea in the 3 of a Kind sediment.

There are multiple identified species of the genus *Pyrobaculum* (9.4%), most of which notably produce H_2S (g). *P. Thermoproteus neutrophilus* (1.0%) is an anaerobic, facultative chemolithoautotroph that produces H_2S (g) and was reclassified under the genus *Pyrobaculum* (Wagner and Wiegel, 2008; Chan *et al.*, 2013). *P. calidifontis* (0.2%) is a facultative aerobic, chemoorganoheterotroph that is generally similar to other *Pyrobaculum* species, except that it uses nitrate as a final electron acceptor instead of nitrite or compounds containing sulfur (Amo *et al.*, 2002; Wagner and Wiegel, 2008). *P. islandicum* (0.06%) is an anaerobic, facultative chemolithoautotroph that produces H_2S (g) by using sulfur, thiosulfate, or sulfite as electron acceptors (Stetter *et al.*, 1990; Wagner and Wiegel, 2008), and can reduce Fe(III) from magnetite but not hematite or goethite (Kashefi and Lovley, 2000). Other metals that can be reduced by *P. islandicum* include U(VI), Tc(VII), Cr(VI), Co(III), and Mn(IV), none of which were abundant

trace metals in the Y-5 drill core or the Y-5 thermal waters (Fig. 7; Appendix C, E) (Kashefi and Lovley, 2000). *P. arsenaticum* (0.01%) is an anaerobic, facultative chemolithoautotroph that produces arsenite and H_2S (g) by respectively using arsenate and either sulfur or thiosulfate as electron acceptors (Huber *et al.*, 2000; Wagner and Wiegel, 2008).

Nanoarchaeum equitans (0.8%) has been called both a symbiont and a parasite (Das *et al.*, 2006; Jahn *et al.*, 2008). *N. equitans* is dependent on the Archaeal host *Ignicoccus hospitalis* (Jahn *et al.*, 2008), which was not found in the 3 of a Kind sediment. It has previously been observed that when *I. hospitalis* expels H_2S (g), *N. equitans* cells can also be released from the host *I. hospitalis* cells (Jahn *et al.*, 2008). It is hypothesized here that the minor counts of *N. equitans* (703) combined with no counts of *I. hospitalis* in the surficial hot spring sediment could indicate the existence of *I. hospitalis* in the shallow subsurface, where H_2S (g) and *N. equitans* could be expelled by *I. hospitalis* before being carried to the surface by rising hydrothermal fluids. Several other H_2S (g) producing microbes were found in the 3 of a Kind sediment (ex: *Thermofilum, Pyrobaculum*), so it is not unreasonable that *I. hospitalis* could be present in the overall 3 of a Kind hydrothermal system despite not being found in the hot spring sediment.

4.2.2. Bacteria in 3 of a Kind sediment

Although there were over 250 bacterial species identified in 3 of a Kind sediment, about half (50.7%) of the bacterial community is comprised of two species: *Thermocrinis ruber* (28.1%) and *Thermotoga petrophila* (22.6%). *Thermocrinis ruber* is a chemolithoautotroph that anaerobically uses hydrogen, thiosulfate, and/or elemental sulfur to reduce oxygen (Huber *et al.*, 1998). It has been hypothesized that the seemingly widespread existence of *T. ruber* in YNP hot springs indicates that hydrogen oxidation is the primary production in many hot spring environments (Blank *et al.*, 2002). *T. ruber* has also been shown to produce arsenate even when

arsenite is the only present electron donor (Härtig *et al.*, 2014). *Thermotoga petrophila* is an obligate anaerobe that can heterotrophically reduce sulfur, although often with the tradeoff of lower growth rates (Takahata *et al.*, 2001).

The next most abundant genus is *Geothermobacterium* (11.4%), which was not identified to the species level in this study. However, a hyperthermophilic species of *Geothermobacterium* was previously found in YNP hot springs and has optimal growth in circumneutral pH values: *G. ferrireducens*, which is anaerobic, hyperthermophilic, and reduces iron (Kashefi *et al.*, 2002; Meyer-Dombard *et al.*, 2005). Another notable iron reducing bacteria identified in 3 of a Kind is *Thermolithobacter ferrireducens* (2.3%), which is similarly an anaerobic chemolithoautotroph (Sokolova *et al.*, 2007).

The genus *Ralstonia* (7.8%) was also not identified to the species level in this study, but contains microbes that can reduce nitrate and oxidize arsenite (Saltikov, 2011). Other arsenite-oxidizing nitrate-reducing genera identified in this study include *Burkholderia* (3.2%), *Halomonas* (1.0%), and *Pseudomonas* (0.6%) (Saltikov, 2011).

4.2.3. Nutrients and Arsenic in Thermal Features

The Y-5 features contained considerable carbon, nitrogen, and sulfur (Fig. 29-31). Carbon was the most abundant nutrient in the Y-5 features, and was dominantly speciated as bicarbonate in both the EQ3 speciations and EQ3/6 predictions (Fig. 29 A, C). Carbonate and bicarbonate speciated with a myriad of alkali earth and alkaline earth metals (Fig. 31). These carbon-bearing species were on the same order of magnitude as many calibrated species, but comprised a relatively small amount of the total carbon in the system (Fig. 16-18, 31). Carbon was predominantly removed abiotically from the Y-5 thermal features by degassing CO_2, not as precipitating carbonate minerals (Tables V-VII). Total DOC was only measurable in Grizzly

Pool and Mordrid (Fig. 14), which also had the lowest total dissolved inorganic carbon activities, suggesting greater microbial presence in these features.

Sulfur was present dominantly as sulfate in all EQ3 speciations and EQ3/6 predictions with low (< 5%) to negligible bisulfide in the features (Fig. 30 D). In the 3 of a Kind sediment, there were both archaeal and bacterial genera that produce H_2S (g) or just generally reduce sulfur (*Thermofilum, Pyrobaculum, Thermotoga*), but the sulfur oxidizing bacteria *Thermocrinis ruber* was much more abundant (Tables VIII - IX). This is consistent with the expectation that the vast majority of sulfur is speciated as sulfate (Fig. 30 B, D; 31). EQ3 speciations showed that reduced sulfur was present in the Y-5 thermal features as HS^- and H_2S (aq) with activities on the order of about $<10^{-6}$ mol/kg and $<10^{-8}$ mol/kg, respectively (Fig. 31). While these concentrations were greater than those of some trace elements (Fig. 26; Appendix E), the majority (more than 99%) of the total sulfur was accounted for by sulfate (Fig. 30 B, 31). There was a general decrease in total sulfur and sulfate with decreasing temperature, although Merlin's Beard and Grizzly Pool once again contained the least total sulfur (Fig. 30 B).

The dominant nitrogen species in the EQ3 speciations was NH_4^+, whereas the dominant nitrogen species in the EQ3/6 predictions was N_2 (aq) (Fig. 29 B, D). It is unsurprising that there was a disagreement between nitrogen speciation because (1) EQ3 nitrate inputs were frequently valued at the lower detection limit, which likely were overestimates, (2) EQ3 ammonia inputs were cited from literature and the true values were not known, and (3) the abundance of N_2 (aq) predicted by EQ3/6 would most likely have degassed or oxidized once reaching the surface, which would not be well represented in the EQ3 or EQ3/6 outputs. Bacteria genera present in 3 of a Kind sediment that reduce nitrate (to produce nitrite) include *Ralstonia, Burkholderia*, *Halomonas,* and *Pseudomonas* (see section 4.2.2). Although EQ3 speciations indicate that there

was nitrite present in all of the Y-5 thermal features, nitrate activities were $<10^{-15}$ mol/kg. This seems to indicate that any nitrate reducing bacteria do not have an appreciable impact on the aqueous hydrothermal chemistry of the thermal features.

Phosphorus was measured below the lower detection limit in all Y-5 thermal features except 3 of a Kind (Fig. 30 A). The lack of measureable phosphorus in most features could mean that (1) phosphorus was used up by whatever microbes are present, (2) there was negligible phosphorus input to the system, or (3) a combination of both (1) and (2), which is most probable. Measureable phosphorus in 3 of a Kind means that there was unsurprisingly at least one input of phosphorus to the system. There was minor phosphorus detected in the Y-5 drill core (Appendix D), which implies that there were accessory igneous phosphates, like apatite, in the Y-5 drill core even though none were specifically identified (Table I). The speciation of phosphorus is complex in the thermal features (Fig. 31), but the most common species, HPO_4^{-2}, is generally bioavailable to microbes.

The ratio of the nutrients in an environmental system is often analyzed using the Redfield ratio (C:N:P) (Redfield, 1934). The Redfield ratio, which is generally 106:16:1 for marine phytoplankton (Redfield, 1934), was indeterminable for Uther, Pendragon, Gwenivere, Mordrid, and Grizzly Pool due to both nitrate and phosphorus being measured below the lower detection limits in these features (Fig. 29-30, Appendix E). However, Redfield ratios were approximated for 3 of a Kind (3,675:9:1), which had measurable phosphorus, and Merlin's Beard (23,333:73:1), which had measurable nitrate. These Redfield ratios seem to suggest that high temperature neutral chloride YNP springs (< 90°C) are more likely to be limited in nitrogen whereas lower temperature neutral chloride YNP springs (~74°C) are more likely to be limited in phosphorus.

Arsenic was the most elevated trace element in all Y-5 features (excluding boron and lithium), and is a toxin to most organisms. However, bacteria identified in the 3 of a Kind sediment can oxidize arsenite to arsenate (*T. ruber, Ralstonia, Burkholderia*) (Tables VIII - IX). The presence of microbes that use arsenite as an electron donor means that the elevated "toxin" does not preclude the possibility of a microbial community. However, that does not mean that those genera are present in the other Y-5 features. At all temperatures, EQ3 speciations show that arsenic is dominantly speciated as arsenates, but the EQ3/6 predictions show that greater than 99% of the arsenic is speciated as arsenites as it reaches the springs at the surface (Fig. 27). The EQ3/6 prediction of arsenite species might just be due to the EQ3/6 models not being as oxidized as the surface of the thermal features. Nevertheless, the initial influx of arsenite to the surface provides opportunity for biological oxidation of the arsenite to arsenate, which most likely occurs to some extent along with abiotic oxidation in the thermal features.

4.2.4. Merlin's Beard, Mordrid, and Grizzly Pool

Merlin's Beard (74.2°C) and Grizzly Pool (17.3°C) have more evidence for microbial influence than the other thermal features. These two features contained less dissolved components than the other features, which were reflected in lower ionic strengths and conductivities (Fig. 20). Of the thermal features, Merlin's Beard had the lowest ionic strength, lowest total dissolved solids, the second lowest conductivity, the lowest activities of H^+, Li^+, total B, F^- (along with 3 of a Kind, Gwenivere, and Pendragon), Cl^- (along with Gwenivere), Br^-, MoO_4^{-2}, Cs^+, Rb^+, and WO_4^{-2}, and the second lowest activities of total silica, $HSbO_2$ (aq), and SO_4^{-2} (Fig. 12-14, 20-24, 26, 28-31) – all indicating less influence from water-rock interactions. The stable water isotopes for Merlin's Beard were similar to the values of the other Y-5 features, but were closer to the global meteoric water line and Yellowstone meteoric water line than the

other Y-5 features (Fig. 9). This indicates that Merlin's Beard had a greater contribution from shallow meteoric water than the other Y-5 features, which would account for the lower dissolved components. Merlin's Beard also had the lowest total P (along with Mordrid and Grizzly Pool) and lowest total C (Fig. 30-31), which could be due to microbial metabolisms or to dilution. Merlin's Beard was the only feature with orders of magnitude less dissolved oxygen than was expected for saturation at its temperature (Fig. 12), which could be indicative of aerobic microbial metabolisms. Merlin's Beard had negligible DOC (Fig. 14), contrary to the idea of a larger microbial community, unless microbes used so much DOC that there was not any left to measure. Also, Merlin's Beard had the highest Ca^{+2} (Fig. 18-19, 26), contrary to less water-rock reactions. Overall, Merlin's Beard was anomalous from expectations.

Grizzly Pool was more similar to Merlin's Beard than the other thermal features, but actually contained more dissolved components than Merlin's Beard. Of the Y-5 thermal features, Grizzly Pool contained: the second lowest total dissolved solids and ionic strength, second lowest activities of Li^{+}, total B, total As, Cs^{+}, WO_4^{-2}, and SO_4^{-2}, the lowest conductivity, and the lowest activities of total silica and $HSbO_2$ (aq) (Fig. 20-24, 26, 28, 30-31). Grizzly Pool had the lowest total phosphorus (like Merlin's Beard and Mordrid) (Fig. 30 A), the second lowest inorganic carbon (Fig. 29 A), and the highest DOC (Fig. 14), which could all be the result of microbial metabolisms. Grizzly Pool was saturated with dissolved oxygen (Fig. 12), which could be due to its low temperature, large surface area, and/or indicate a lack of quick recharge (hydrothermal or meteoric). Of the Y-5 thermal features, Grizzly Pool had the heaviest stable water isotopes, indicating greater evaporation, which again was probably due to its large surface area (Fig. 3, 8). The stable water isotope values were between the Yellowstone thermal water lines and the meteoric water lines, suggesting there were both meteoric and hydrothermal input

(Fig. 9). Although it does not seem as though Grizzly Pool has a direct hydrothermal input from the subsurface (despite the central hole seen in aerial imagery (Fig. 2, 3)), based on its geochemistry there does appear to be hydrothermal input to Grizzly Pool, most likely from the outflows of Pendragon and Merlin's Beard (Fig. 2, 3). Although Uther, Mordrid, Woad, or Grizzly Pool do not currently have outflow channels, they might have all had north flowing outflows in the past, which seems to have been noted on older topographic maps of the area (Ball *et al.*, 2010). In the field, Grizzly Pool seemingly hosted macrophytes, which were alive. This, combined with the above outlined data, indicates that the aqueous chemistry of Grizzly Pool represents the greatest influence from life (both macroscopic and most likely microscopic).

Mordrid was the coolest spring (59.1°C) and the second coolest feature (besides Grizzly Pool) analyzed. It would be expected to have the most microbial impact of the springs, and it does have the second highest DOC of the Y-5 features (Fig. 14). It also has the most discrepancies between its EQ3 speciation and the 59.1°C EQ3/6 predictions, but it also had the largest pH change between field pH and EQ3 pH (Table IV). The discrepancy in field pH and EQ3 pH indicates disequilibrium, but this is likely influenced by the change in stable water isotopes and decompressional boiling throughout the sampling day (Fig. 11, 34) (see section 4.1.2). The EQ3/6 predicted pH (8.245) is actually more similar to the field pH (8.117) than the EQ3 pH (6.157). Although the discrepancies between the EQ3 prediction and EQ3/6 speciation are great, they are probably smaller than they seem – the EQ3/6 prediction might align more closely if Mordrid had been sampled simultaneously in all regards. Even so, Mordrid had a lower temperature, higher amount of available dissolved oxygen, second highest DOC, and lowest total nitrogen and phosphorus, which could indicate that it is a more suitable habitat for microbes than other thermal features with similarly high dissolved components (3 of a Kind, Uther, Pendragon,

or Gwenivere). The orange coloration of Mordrid, which was not seen in any other Y-5 feature except for the largely un-sampled Woad, was visually similar to a photosynthetic microbial mat (Fig. 3), lending credibility to the assumption that Mordrid had greater microbial influence than many of the hotter thermal features.

5. Conclusions

Comparisons between the EQ3 speciation of Y-5 area thermal features and EQ3/6 water-rock reaction predictions at the temperature of each feature revealed greater discrepancies at cooler temperatures. There were, however, mass imbalances in total silicon, aluminum, sulfur, calcium, and hydrogen ions at all temperatures. Much of the modeled mass imbalances and variation between the Y-5 thermal features can be explained abiotically. Silica and aluminum were supersaturated in the thermal features, which was not represented in the EQ3/6 predictions. There likely would have been a small but important input of H_2S (g) from the subsurface, which was not part of the EQ3/6 models but would introduce more sulfur to the system. Variations in total dissolved calcium in the Y-5 thermal features probably reflected variations in plagioclase feldspar in the general Y-5 area subsurface. pH was controlled by CO_2 (g), which likely varied throughout the day as steam separation occasionally changed from single-stage to continuous. Changes in steam separation in the Y-5 thermal features were reflected by stable water isotopes, and were likely influenced by the same mechanism(s) responsible for the daily eruption of the nearby Till Geyser. Merlin's Beard and Grizzly Pool generally contained less dissolved components than the other Y-5 features, indicating that they had more dilution from shallower meteoric water than the other features. Grizzly Pool also contained more dissolved components than expected and, similar to Uther and Mordrid (which often contained slightly greater dissolved components than the other features), could be due to its lack of outflow channel.

Even though the variability in the Y-5 area is well explained abiotically, microbial communities should inhabit each thermal feature. One of the hottest features, 3 of a Kind, was shown to have low extracted DNA yields (~5 ng DNA/g wet sediment). The microbial community in the 3 of a Kind sediment included archaea and bacteria, and overall contained

nitrate reducers, arsenite oxidizers, H_2S producers, sulfur oxidizers, iron reducers, hydrogen oxidizers, and microbes that can metabolize carbon. The diversity of microbes represented in 3 of a Kind are not necessarily in the other Y-5 area thermal features, but the other Y-5 area thermal features most likely contain similarly identifiable microbial communities. Whatever communities are present in the other features, they do not seem to make much of an impact on the aqueous hydrothermal chemistries of 3 of a Kind, Uther, Pendragon, or Gwenivere. The exception is in regards to sulfur, which is frequently under-predicted for these features probably in part due to microbial activity. Merlin's Beard, Mordrid, and Grizzly Pool seem to have greater impact from microbes than the other features, but the dominant controls on their aqueous hydrothermal chemistries are abiotic factors including subsurface hydrothermal water-rock reactions and surficial dilution.

6. Future Research

As is often the case with research, this study opened up as many new questions as it answered, leaving room for further researchers to expand upon this work. Perhaps the most obvious avenue to pursue would be to extract DNA from sediment of all the thermal features, not just 3 of a Kind. This would clearly show which microbes inhabit the different features and would allow for direct correlations to be made between model discrepancies and *in situ* microbial communities. Along the same lines, microbial protein could also be extracted from the sediment of each thermal feature. Whereas DNA shows what is living in a system, proteins demonstrate which microbial metabolisms are actively occurring in a system. Such approaches would quickly help validate or refute hypotheses formed in this thesis to describe the EQ3 and EQ3/6 aqueous hydrothermal chemistry discrepancies.

In order to explicitly investigate the impact that microbes might have on the sulfur in the thermal waters, stable sulfur isotopes from sulfate and sulfide (if possible) could be analyzed. Stable oxygen isotopes from sulfate could be additionally measured. This isotope work could clearly demonstrate the extent of abiotic or biotic influence on the dissolved sulfur.

Another exciting topic that would greatly benefit from further work is the hypothesis that eruptions of the nearby Till Geyser represent changes from single-stage to continuous steam separation in the hydrothermal fluid feeding the overall Y-5 area. Continual temperature measurements using thermistors in different Y-5 thermal features over the course of a 12 or 24 hour field day could be coupled with frequent collection of stable water isotope samples (maybe four times an hour for 8 hours). This would allow researchers to monitor changes in the area through different thermal features and understand if the Y-5 thermal features are as closely related as preliminary evidence presented in this thesis starts to suggest.

There is also always room for continual improvement in modeling techniques. As previously mentioned, the backward rate laws should be adjusted to allow for dissolved silica to be in equilibrium with α-cristobalite instead of quartz. Also, further work should be done on the reduction-oxidation constraints on the EQ3/6 models to allow for further oxidation once the fluid reaches the surface. Some of the elements that were measured frequently below the lower detection limit in the features but were included anyway could be omitted for clarity. One final overall improvement to the model would be the ability to model the trace elements as being sourced non-stoichiometrically from the rocks, if at all possible.

7. References Cited

Alsop, E.B., Boyd, E.S., Raymond, J., 2014. Merging metagenomics and geochemistry reveals environmental controls on biological diversity and evolution. BMC Ecol. 14, 16.

Althaus, E., 1967. The triple point andalusite—sillimanite—kyanite. Contrib. Mineral. Petrol. 16, 29–44.

Amo, T., Paje, M.L.F., Inagaki, A., Ezaki, S., Atomi, H., Imanaka, T., 2002. Pyrobaculum calidifontis sp. nov., a novel hyperthermophilic archaeon that grows in atmospheric air. Archaea 1, 113–121.

Ball, J.W., McMleskey, R.B., Nordstrom, D.K., 2010. Water-chemistry data for selected springs, geysers, and streams in Yellowstone National Park, Wyoming, 2006-2008 (USGS Numbered Series No. 2010–1192), Open-File Report. U.S. Geological Survey.

Bargar, K.E., Beeson, M.H., 1985. Hydrothermal alteration in research drill hole Y-3, Lower Geyser Basin, Yellowstone National Park, Wyoming. USGPO, Distribution Branch, Text Products Section, US Geological Survey.

Bargar, K.E., Beeson, M.H., 1984. Hydrothermal alteration in research drill hole Y-6, Upper Firehole River, Yellowstone National Park, Wyoming. USGPO, Distribution Branch, Text Products Section, US Geological Survey.

Bargar, K.E., Beeson, M.H., 1981. Hydrothermal alteration in research drill hole Y-2, Lower Geyser Basin, Yellowstone National Park, Wyoming. Am. Mineral. 66, 473–490.

Bargar, K.E., Beeson, M.H., Fournier, R.O., Muffler, L.J.P., 1973. Present-day deposition of lepidolite from thermal waters in Yellowstone National Parkl. Am. Mineral. 58, 901–904.

Bargar, K.E., Fournier, R.O., 1988. Effects of glacial ice on subsurface temperatures of hydrothermal systems in Yellowstone National Park, Wyoming: Fluid-inclusion evidence. Geology 16, 1077–1080.

Bargar, K.E., Muffler, L.P., 1982. Hydrothermal alteration in research drill hole Y-11 from a vapor-dominated geothermal system at Mud Volcano, Yellowstone National Park, Wyoming. US Geological Survey.

Barnes, I., Downes, C.J., Hulston, J.R., 1978. Warm springs, South Island, New Zealand, and their potentials to yield laumontite. Am. J. Sci. 278, 1412–1427.

Beeson, M.H., Bargar, K.E., 1984. Major and trace element analyses of drill cores from thermal areas in Yellowstone National Park, Wyoming. US Geological Survey.

Blank, C.E., Cady, S.L., Pace, N.R., 2002. Microbial composition of near-boiling silica-depositing thermal springs throughout Yellowstone National Park. Appl. Environ. Microbiol. 68, 5123–5135.

Boyd, E.S., Hamilton, T.L., Spear, J.R., Lavin, M., Peters, J.W., 2010. [FeFe]-hydrogenase in Yellowstone National Park: evidence for dispersal limitation and phylogenetic niche conservatism. ISME J. 4, 1485.

Boyd, E.S., Jackson, R.A., Encarnacion, G., Zahn, J.A., Beard, T., Leavitt, W.D., Pi, Y., Zhang, C.L., Pearson, A., Geesey, G.G., 2007. Isolation, characterization, and ecology of sulfur-respiring crenarchaea inhabiting acid-sulfate-chloride-containing geothermal springs in Yellowstone National Park. Appl. Environ. Microbiol. 73, 6669–6677.

Brock, T.D., 2012. Thermophilic microorganisms and life at high temperatures. Springer Science & Business Media.

Brock, T.D., 1967. Micro-organisms adapted to high temperatures. Nature 214, 882.

Bruton, C.J., 1995. Testing EQ3/6 and GEMBOCHS using fluid-mineral equilibria in the wairakei geothermal system. Lawrence Livermore National Lab., CA (United States).
Chan, P.P., Cozen, A.E., Lowe, T.M., 2013. Reclassification of Thermoproteus neutrophilus Stetter and Zillig 1989 as Pyrobaculum neutrophilum comb. nov. based on phylogenetic analysis. Int. J. Syst. Evol. Microbiol. 63, 751–754.
Chang, W.-L., Smith, R.B., Farrell, J., Puskas, C.M., 2010. An extraordinary episode of Yellowstone caldera uplift, 2004–2010, from GPS and InSAR observations. Geophys. Res. Lett. 37.
Chang, W.-L., Smith, R.B., Wicks, C., Farrell, J.M., Puskas, C.M., 2007. Accelerated uplift and magmatic intrusion of the Yellowstone caldera, 2004 to 2006. Science 318, 952–956.
Christiansen, R.L., 2001. The Quaternary and pliocene Yellowstone plateau volcanic field of Wyoming, Idaho, and Montana.
Christiansen, R.L., Blank Jr., H.R., 1972. Volcanic Stratigraphy of the Quaternary Rhyolite Plateau in Yellowstone National Park (USGS Numbered Series No. 729- B), Professional Paper. U.S. Geological Survey.
Christiansen, R.L., Foulger, G.R., Evans, J.R., 2002. Upper-mantle origin of the Yellowstone hotspot. Geol. Soc. Am. Bull. 114, 1245–1256.
Clark, J.F., Turekian, K.K., 1990. Time scale of hydrothermal water-rock reactions in Yellowstone National Park based on radium isotopes and radon. J. Volcanol. Geotherm. Res. 40, 169–180.
Cline, J.D., 1969. Spectrophotometric determination of hydrogen sulfide in natural waters. Limnol. Oceanogr. 14, 454–458.
Cox, A., Shock, E.L., Havig, J.R., 2011. The transition to microbial photosynthesis in hot spring ecosystems. Chem. Geol. 280, 344–351.
Craig, H., 1961. Isotopic variations in meteoric waters. Science 133, 1702–1703.
Dahlquist, G., 2017. Foundations for a Geobiochemical Characterization of Mudpots in Yellowstone National Park (M.S.). Montana Tech of The University of Montana, United States -- Montana.
Das, S., Paul, S., Bag, S.K., Dutta, C., 2006. Analysis of Nanoarchaeum equitans genome and proteome composition: indications for hyperthermophilic and parasitic adaptation. BMC Genomics 7, 186.
Dick, J.M., 2016. An introduction to CHNOSZ.
Dick, J.M., 2008. Calculation of the relative metastabilities of proteins using the CHNOSZ software package. Geochem. Trans. 9, 10.
Dobson, P.F., Kneafsey, T.J., Hulen, J., Simmons, A., 2003. Porosity, permeability, and fluid flow in the Yellowstone geothermal system, Wyoming. J. Volcanol. Geotherm. Res. 123, 313–324.
Dobson, P.F., Salah, S., Spycher, N., Sonnenthal, E.L., 2004. Simulation of water–rock interaction in the Yellowstone geothermal system using TOUGHREACT. Sel. Pap. TOUGH Symp. 2003 33, 493–502.
Eby, N. G. 2004. Principles of Environmental Geochemistry. Belmont: Brooks/Cole Cengage Learning. 67-69.
Farrell, J., Smith, R.B., Taira, T., Chang, W., Puskas, C.M., 2010. Dynamics and rapid migration of the energetic 2008–2009 Yellowstone Lake earthquake swarm. Geophys. Res. Lett. 37.
Fenner, C.N., 1936. Bore-hole investigations in Yellowstone Park. J. Geol. 44, 225–315.

Fernández-Prini, R., Alvarez, J.L., Harvey, A.H., 2003. Henry's constants and vapor–liquid distribution constants for gaseous solutes in H 2 O and D 2 O at high temperatures. J. Phys. Chem. Ref. Data 32, 903–916.

Fournier, R.O., 1989. Geochemistry and dynamics of the Yellowstone National Park hydrothermal system. Annu. Rev. Earth Planet. Sci. 17, 13–53.

Frost, B.R., Frost, C.D., 2008. A geochemical classification for feldspathic igneous rocks. J. Petrol. 49, 1955–1969.

Green, E., Holland, T., Powell, R., 2007. An order-disorder model for omphacitic pyroxenes in the system jadeite-diopside-hedenbergite-acmite, with applications to eclogitic rocks. Am. Mineral. 92, 1181–1189.

Härtig, C., Lohmayer, R., Kolb, S., Horn, M.A., Inskeep, W.P., Planer-Friedrich, B., 2014. Chemolithotrophic growth of the aerobic hyperthermophilic bacterium Thermocrinis ruber OC 14/7/2 on monothioarsenate and arsenite. FEMS Microbiol. Ecol. 90, 747–760.

Hedenquist, J.W., Henley, R.W., 1985. Hydrothermal eruptions in the Waiotapu geothermal system, New Zealand; their origin, associated breccias, and relation to precious metal mineralization. Econ. Geol. 80, 1640–1668.

Helgeson, H.C., Brown, T.H., Nigrini, A., Jones, T.A., 1970. Calculation of mass transfer in geochemical processes involving aqueous solutions. Geochim. Cosmochim. Acta 34, 569–592.

Holloway, J.M., Nordstrom, D.K., Böhlke, J.K., McCleskey, R.B., Ball, J.W., 2011. Ammonium in thermal waters of Yellowstone National Park: processes affecting speciation and isotope fractionation. Geochim. Cosmochim. Acta 75, 4611–4636.

Honda, S., Muffler, L.J.P., 1970. Hydrothermal alteration in core from research drill hole Y-1, Upper Geyser Basin, Yellowstone National Park, Wyoming. Am. Mineral. 55, 1714.

Huber, R., Eder, W., Heldwein, S., Wanner, G., Huber, H., Rachel, R., Stetter, K.O., 1998. Thermocrinis ruber gen. nov., sp. nov., a pink-filament-forming hyperthermophilic bacterium isolated from Yellowstone National Park. Appl. Environ. Microbiol. 64, 3576–3583.

Huber, R., Sacher, M., Vollmann, A., Huber, H., Rose, D., 2000. Respiration of arsenate and selenate by hyperthermophilic archaea. Syst. Appl. Microbiol. 23, 305–314.

Hurwitz, S., Lowenstern, J.B., 2014. Dynamics of the Yellowstone hydrothermal system. Rev. Geophys. 52, 375–411.

Inskeep, W.P., Jay, Z.J., Tringe, S.G., Herrgard, M., Rusch, D.B., 2013. The YNP metagenome project: environmental parameters responsible for microbial distribution in the Yellowstone geothermal ecosystem. Front. Microbiol. 4, 67.

Jahn, U., Gallenberger, M., Junglas, B., Eisenreich, W., Stetter, K.O., Rachel, R., Huber, H., 2008. Nanoarchaeum equitans and Ignicoccus hospitalis: new insights into a unique, intimate association of two archaea. J. Bacteriol. 190, 1743–1750.

Johnson, J.W., Oelkers, E.H., Helgeson, H.C., 1992. SUPCRT92: A software package for calculating the standard molal thermodynamic properties of minerals, gases, aqueous species, and reactions from 1 to 5000 bar and 0 to 1000 C. Comput. Geosci. 18, 899–947.

Kashefi, K., Holmes, D.E., Reysenbach, A.-L., Lovley, D.R., 2002. Use of Fe (III) as an electron acceptor to recover previously uncultured hyperthermophiles: isolation and characterization of Geothermobacterium ferrireducens gen. nov., sp. nov. Appl. Environ. Microbiol. 68, 1735–1742.

Kashefi, K., Lovley, D.R., 2000. Reduction of Fe (III), Mn (IV), and toxic metals at 100 C by Pyrobaculum islandicum. Appl. Environ. Microbiol. 66, 1050–1056.

Keith, T.E.C., Muffler, L.J.P., and Bargar, C.N., 1968-78. Unpublished Y-5 Core Logs. USGS Core Research Center.

Keith, T.E., White, D.E., Beeson, M.H., 1978. Hydrothermal alteration and self-sealing in Y-7 and Y-8 drill holes in northern part of Upper Geyser Basin, Yellowstone National Park, Wyoming. US Govt. Print. Off.,.

Keith, T.E.C., Muffler, L.J.P., 1978. Minerals produced during cooling and hydrothermal alteration of ash flow tuff from Yellowstone drill hole Y-5. J. Volcanol. Geotherm. Res. 3, 373–402.

Kell, G.S., 1975. Density, thermal expansivity, and compressibility of liquid water from 0. deg. to 150. deg.. Correlations and tables for atmospheric pressure and saturation reviewed and expressed on 1968 temperature scale. J. Chem. Eng. Data 20, 97–105.

Kharaka, Y.K., Thordsen, J.J., White, L.D., 2002. Isotope and chemical compositions of meteoric and thermal waters and snow from the greater Yellowstone National Park region. Geological Survey Menlo Park, CA.

King, J.M., Hurwitz, S., Lowenstern, J.B., Nordstrom, D.K., McCleskey, R.B., 2016. Multireaction equilibrium geothermometry: A sensitivity analysis using data from the Lower Geyser Basin, Yellowstone National Park, USA. J. Volcanol. Geotherm. Res. 328, 105–114.

Lanphere, M.A., Champion, D.E., Christiansen, R.L., Izett, G.A., Obradovich, J.D., 2002. Revised ages for tuffs of the Yellowstone Plateau volcanic field: Assignment of the Huckleberry Ridge Tuff to a new geomagnetic polarity event. GSA Bull. 114, 559–568.

Lowenstern, J.B., Hurwitz, S., McGeehin, J.P., 2016. Radiocarbon dating of silica sinter deposits in shallow drill cores from the Upper Geyser Basin, Yellowstone National Park. J. Volcanol. Geotherm. Res. 310, 132–136.

Meyer-Dombard, D.R., Shock, E.L., Amend, J.P., 2005. Archaeal and bacterial communities in geochemically diverse hot springs of Yellowstone National Park, USA. Geobiology 3, 211–227.

Miyashiro, A., 1961. Evolution of metamorphic belts. J. Petrol. 2, 277–311.

Moloney, T.P., Sims, K.W., Kaszuba, J.P., 2011. Uranium and Thorium Decay Series Isotopic Contraints on the Source and Residence Time of Solutes in the Yellowstone Hydrothermal System. Univ. Wyo. Natl. Park Serv. Res. Cent. Annu. Rep. 33, 187–207.

Newton, M.S., Kennedy, G.C., 1968. Jadeite, analcite, nepheline, and albite at high temperatures and pressures. Am. J. Sci. 266, 728–735.

Okamoto, K., Maruyama, S., 1999. The high-pressure synthesis of lawsonite in the MORB+ H2O system. Am. Mineral. 84, 362–373.

Pierce, K.L., Morgan, L.A., Link, P.K., 1992. The track of the Yellowstone hot spot: Volcanism, faulting, and uplift. Reg. Geol. East. Ida. West. Wyo. Geol. Soc. Am. Mem. 179, 1–53.

Redfield, A.C., 1934. On the proportions of organic derivatives in sea water and their relation to the composition of plankton. James Johnstone Meml. Vol. 176–192.

Reysenbach, A.-L., Ehringer, M., Hershberger, K., 2000. Microbial diversity at 83°C in Calcite Springs, Yellowstone National Park: another environment where the Aquificales and "Korarchaeota" coexist. Extremophiles 4, 61–67.

Saltikov, C.W., 2011. Regulation of arsenic metabolic pathways in prokaryotes, in: Microbial Metal and Metalloid Metabolism. American Society of Microbiology, pp. 195–210.

Schmidt, M.W., Poli, S., 1994. The stability of lawsonite and zoisite at high pressures: Experiments in CASH to 92 kbar and implications for the presence of hydrous phases in subducted lithosphere. Earth Planet. Sci. Lett. 124, 105–118.

Schmidt, R., 2017. Biogeochemical Interactions in Flooded Underground Mines (M.S.). Montana Tech of The University of Montana, United States -- Montana.

Shaw, D.M., Sturchio, N.C., 1992. Boron-Lithium relationships in rhyolites and associated thermal waters of young silicic calderas, with comments on incompatible element behaviour. Geochim. Cosmochim. Acta 56, 3723–3731.

Shelly, D.R., Hill, D.P., Massin, F., Farrell, J., Smith, R.B., Taira, T., 2013. A fluid-driven earthquake swarm on the margin of the Yellowstone caldera. J. Geophys. Res. Solid Earth 118, 4872–4886.

Shock, E.L., Holland, M., Amend, J.P., Osburn, G.R., Fischer, T.P., 2010. Quantifying inorganic sources of geochemical energy in hydrothermal ecosystems, Yellowstone National Park, USA. Geochim. Cosmochim. Acta 74, 4005–4043.

Smith, R.B., Jordan, M., Steinberger, B., Puskas, C.M., Farrell, J., Waite, G.P., Husen, S., Chang, W.-L., O'Connell, R., 2009. Geodynamics of the Yellowstone hotspot and mantle plume: Seismic and GPS imaging, kinematics, and mantle flow. J. Volcanol. Geotherm. Res. 188, 26–56.

Sokolova, T., Hanel, J., Onyenwoke, R.U., Reysenbach, A.-L., Banta, A., Geyer, R., González, J.M., Whitman, W.B., Wiegel, J., 2007. Novel chemolithotrophic, thermophilic, anaerobic bacteria Thermolithobacter ferrireducens gen. nov., sp. nov. and Thermolithobacter carboxydivorans sp. nov. Extremophiles 11, 145–157.

St. Clair, B., 2017. Kinetics, Thermodynamics and Habitability of Microbial Iron Redox Cycling (PhD Thesis). Arizona State University.

Stetter, K.O., Fiala, G., Huber, G., Huber, R., Segerer, A., 1990. Hyperthermophilic microorganisms. FEMS Microbiol. Lett. 75, 117–124.

Sturchio, N.C., Chan, L.-H., 2003. Lithium isotope geochemistry of the Yellowstone hydrothermal system. Spec. Publ.-Soc. Econ. Geol. 10, 171–180.

Sturchio, N.C., Keith, T.E.C., Muehlenbachs, K., 1990. Oxygen and carbon isotope ratios of hydrothermal minerals from Yellowstone drill cores. J. Volcanol. Geotherm. Res. 40, 23–37.

Sturchio, N.C., Pierce, K.L., Murrell, M.T., Sorey, M.L., 1994. Uranium-series ages of travertines and timing of the last glaciation in the northern Yellowstone area, Wyoming-Montana. Quat. Res. 41, 265–277.

Takahata, Y., Nishijima, M., Hoaki, T., Maruyama, T., 2001. Thermotoga petrophila sp. nov. and Thermotoga naphthophila sp. nov., two hyperthermophilic bacteria from the Kubiki oil reservoir in Niigata, Japan. Int. J. Syst. Evol. Microbiol. 51, 1901–1909.

Takami, H., Arai, W., Takemoto, K., Uchiyama, I., Taniguchi, T., 2015. Functional classification of uncultured "Candidatus Caldiarchaeum subterraneum" using the MAPLE system. PloS One 10, e0132994.

Truesdell, A.H., Nathenson, M., Rye, R.O., 1977. The effects of subsurface boiling and dilution on the isotopic compositions of Yellowstone thermal waters. J. Geophys. Res. 82, 3694–3704.

Wagner, I.D., Wiegel, J., 2008. Diversity of thermophilic anaerobes. Ann. N. Y. Acad. Sci. 1125, 1–43.

Wagner, W., Pruss, A., 1993. International Equations for the Saturation Properties of Ordinary Water Substance. Revised According to the International Temperature Scale of 1990. Addendum to J. Phys. Chem. Ref. Data 16, 893 (1987). J Phys Chem Ref Data 22.

White, D.E., 1978. Conductive heat flows in research drill holes in thermal areas of Yellowstone National Park, Wyoming. US Geol Surv. Jour Res. 6, 765–774.

White, D.E., 1975. Physical results of research drilling in thermal areas of Yellowstone National Park, Wyoming. US Government Printing Office.

Wolery, T.J., 2010. EQ3/6 A Software Package for Geochemical Modeling. Lawrence Livermore National Lab.(LLNL), Livermore, CA (United States).

Wolery, T.W., Jarek, R.L., 2003. Software user's manual. EQ36 Version 8, 376.

8. Appendix A: DIC Speciation Calculations

Total inorganic carbon was speciated as H_2CO_3 (assumed to all decompose to CO_2 (aq)), HCO_3^-, and CO_3^{-2} using the following equations from Eby, 2004:

$$\gamma_{H_2CO_3}[H_2CO_3] = \frac{C_T}{\propto_H} \tag{6}$$

$$\gamma_{HCO_3^-}[HCO_3^-] = \frac{C_T K_{a1}}{\{H^+\} \propto_H} \tag{7}$$

$$\gamma_{CO_3^{-2}}[CO_3^{-2}] = \frac{C_T K_{a1} K_{a2}}{\{H^+\}^2 \propto_H} \tag{8}$$

where [ ] denotes the concentration of the interior species in mol/kg, γ denotes the activity coefficient for the subscripted chemical species (assumed to be one for simplification); { } denotes the activity of the interior species in mol/kg; C_T is the total dissolved inorganic carbon (DIC) in mol/kg; K_{a1} is the first acid dissociation constant of carbonic acid; K_{a2} is the second acid dissociation constant of carbonic acid, and $\propto_H$ is the relationship:

$$\propto_H = \left(1 + \frac{K_{a1}}{\{H^+\}} + \frac{K_{a1}K_{a2}}{\{H^+\}^2}\right) \tag{9}$$

Equations 6 – 9 were derived through rearrangements and substitutions of the equilibrium equations for the deprotonation of carbonic acid and the mass balance of carbon species in a system. See pages 68 – 69 of Eby (2004) for the full details on these equations.

Values of $\log K_{a1}$ and $\log K_{a2}$ were determined at the field temperature of each sample using the program CHNOSZ, which is a package for the R software environment that can be used to model the relative stabilities of aqueous species, minerals, and even proteins (Dick, 2008, 2016). CHNOSZ utilizes a database called OBIGT ("OrganoBioGeoTherm") that is internally consistent, drawing predominantly on the thermodynamic database (and subsequent updates to

that database) produced by Harold C. Helgeson and his colleagues at the Laboratory of Theoretical Geochemistry and Biogeochemistry at the University of California Berkeley (Dick, 2008, 2016). The main line of code used to find $\log K_{a1}$ is:

> subcrt(c("H+","HCO3-","CO2","H2O"),c(1,1,-1,-1),c("aq","aq","aq","liq"),T=92.2)

and the main line of code used to find values of $\log K_{a2}$ is:

> subcrt(c("H+","CO3-2","HCO3-"),c(1,1,-1),c("aq","aq","aq"),T=92.2)

The temperature was varied in these lines of code for each sample. Table X summarizes the logKa1 and logKa2 values found through CHNOSZ.

Table X: Carbonic acid dissociation constants from CHNOSZ at sample temperatures.

Sample	T (^{0}C)	$\log K_{a1}$	K_{a1}	$\log K_{a2}$	K_{a2}
3 of a Kind	92.2	-6.33	4.63E-07	-10.08	8.29E-11
Uther	92.2	-6.33	4.63E-07	-10.08	8.29E-11
Pendragon	83.9	-6.30	4.95E-07	-10.08	8.23E-11
Gwenivere	79.8	-6.29	5.09E-07	-10.09	8.16E-11
Merlin's Beard	74.2	-6.28	5.25E-07	-10.10	8.02E-11
Mordrid	59.1	-6.26	5.48E-07	-10.13	7.36E-11
Grizzly Pool	17.3	-6.40	4.02E-07	-10.40	3.96E-11

For each sample, two measurements were needed as inputs to equations 1 – 4: $\{H^+\}$ and C_T. C_T is DIC value measured on the Aurora 1030W Total Carbon Analyzer, and the following equation was used to convert *in situ* pH measurement of each sample to $\{H^+\}$:

$$\{H^+\} = 10^{-pH} \tag{10}$$

Table XI summarizes the lower, middle, and upper values for these values, taking error into consideration for both types of data.

Table XI: H^+ and DIC for Y-5 thermal features.

Sample Name	H+ (mol/kg)			DIC (mol/kg)		
	Low	Middle	High	Low	Middle	High
3 of a Kind	1.73E-08	1.75E-08	1.77E-08	5.75E-03	5.88E-03	6.01E-03
Uther	3.40E-08	3.48E-08	3.56E-08	6.46E-03	6.53E-03	6.59E-03
Pendragon	3.14E-08	3.29E-08	3.44E-08	6.19E-03	6.30E-03	6.40E-03
Gwenivere	2.38E-09	2.55E-09	2.74E-09	5.75E-03	5.86E-03	5.97E-03
Merlin's Beard	3.11E-07	3.15E-07	3.18E-07	4.38E-03	4.39E-03	4.41E-03
Mordrid	7.46E-09	7.64E-09	7.82E-09	6.28E-03	6.43E-03	6.59E-03
Grizzly Pool	2.52E-10	2.52E-10	2.53E-10	4.48E-03	4.66E-03	4.84E-03

The final lower, middle, and upper values for the calculated carbon species (CO_2 (aq), HCO_3^-, and CO_3^{-2}) for each sample are summarized in Tables XII - XIII.

Table XII: Speciated H_2CO_3 as CO_2 (aq) for Y-5 thermal features.

Sample Name	CO_2 (aq) (mol/kg)		
	Low	Middle	High
3 of a Kind	2.06E-04	2.13E-04	2.21E-04
Merlin's Beard	4.40E-04	4.55E-04	4.69E-04
Grizzly Pool	3.68E-04	3.91E-04	4.15E-04
Uther	2.59E-05	2.83E-05	3.10E-05
Pendragon	1.63E-03	1.64E-03	1.66E-03
Mordrid	8.35E-05	8.76E-05	9.18E-05
Gwenivere	2.42E-06	2.53E-06	2.63E-06

Table XIII: Speciated HCO_3^- and CO_3^{-2} for Y-5 thermal features.

Sample Name	HCO_3^- (mol/kg)			CO_3^{2-} (mol/kg)		
	Low	Middle	High	Low	Middle	High
3 of a Kind	5.52E-03	5.64E-03	5.76E-03	2.64E-05	2.67E-05	2.69E-05
Merlin's Beard	6.01E-03	6.06E-03	6.11E-03	1.47E-05	1.45E-05	1.43E-05
Grizzly Pool	5.81E-03	5.89E-03	5.97E-03	1.52E-05	1.47E-05	1.43E-05
Uther	5.53E-03	5.65E-03	5.77E-03	1.90E-04	1.81E-04	1.72E-04
Pendragon	2.75E-03	2.75E-03	2.74E-03	7.08E-07	6.99E-07	6.90E-07
Mordrid	6.13E-03	6.28E-03	6.43E-03	6.04E-05	6.05E-05	6.06E-05
Gwenivere	3.87E-03	4.03E-03	4.18E-03	6.09E-04	6.32E-04	6.56E-04

9. Appendix B: Summarized Y-5 Core Log

The following is a synthesis of personal observations and the notes left by Keith *et al.*, 1968-78. Major core log divisions and mineral identifications are from Keith *et al.*, 1968-78; the bulk of the summarized core log is original divisions based on personal observations.

General Notes:

- 52 boxes of core: 37 bulk core and 15 skeleton core
- 1 original thin section remains, along with numerous containers of powdered core
- Italicized notes represent subsections of larger sections of the core
- "White inclusions" means some combination of quartz ± k-feldspar ± pumice
- The handwritten laboratory logs by T.E.C. Keith, L.P. Muffler, and C. N. Bargar (1968-78) provided the following details:
    - Specific mineralogies
    - Depth of vapor-saturated zone
    - Distribution of lithic fragments between zones
    - Pink tuff has dominant quartz and subordinate α–cristobalite
    - Grey tuff has dominant α–cristobalite and subordinate quartz
    - Average plagioclase feldspar composition: $An_{23\pm5}$ (calcic oligoclase)
        - $An_{18\text{-}24}$ above 200 ft
        - $An_{20\text{-}30}$ below 200ft

List of minerals identified by Keith et al., 1968-67:

- α–cristobalite
- β–cristobalite
- quartz
- chalcedony
- obsidian
- opal
- tridymite
- sanidine
- k-feldspar
- plagioclase
- alkali feldspar
- goethite
- magnetite
- hematite
- pyrite
- mordonite
- erionite
- clinoptilolite
- calcite
- fluorite
- zircon
- pyrolusite
- hollandite
- montmorillonite
- illite

CORE LOG OVERVIEW

0.3 – 11.9 m	"Messy" deposits
11.9 – 34.9 m	"Vapor-saturated zone" tuff (Keith *et al.*, 1968-78)
~34.9 – ~99.1 m	Densely welded crystal-rich ash flow tuff (Keith *et al.*, 1968-78)
~99.1 – ~118.9 m	Densely welded lithic-rich ash flow tuff (Keith *et al.*, 1968-78)
~118.9 – 164.0 m	Densely welded crystal-rich ash flow tuff (Keith *et al.*, 1968-78)

SUMMARIZED CORE LOG

Depth (m)	Description
0.3 - 3	- No core material left.
3 – 4.6	- Bag of 1-3” specimens of pink rhyolite with quartz phenocrysts. - A few rhyolite cobbles with quartz ± k-feldspar phenocrysts (streaky to rounded; yellow rimmed).
4.7	- A rhyolite cobble in contact with sandstone (clasts are dominantly rounded, glassy, black obsidian with opal cement).
4.7 – 7.1	- Pebble conglomerate.
7.1 – 9.7	- Volcanic breccias (green/pink, pyrolusite bearing).
10.4 – 11.9	- Minimal core material. Starts with white, soft pale pink tuff that becomes darker and denser with depth.
11.9 – 14.9	- Beginning of vapor-saturated zone. White to pink/reddish tuff that is fractured every few centimeters.
14.9 – 34.9	- End of vapor-saturated zone. Tuff becomes increasingly more welded.
35.2 – 36.0	- Grey densely welded tuff with abundant white inclusions.
36.0 – 39.1	- Pink densely welded tuff with abundant white inclusions.
39.1 – ~39.8	- Pink densely welded tuff with abundant white inclusions with heavy iron oxide staining.
39.8 – ~40.5	- Dark grey densely welded tuff with red veins surrounding and sometimes connecting white inclusions.
40.5 – 40.7	- Pink densely welded tuff with abundant white inclusions.
40.5 – 40.8	- Transition between pink and grey tuff.
41.0 – 42.8	- Grey welded tuff, more porous.
42.8 – 44.5	- Pink densely welded tuff with greyer sections and abundant white inclusions.
44.5 – 44.8	- Transition from pink to grey densely welded tuff.
44.8 – 50.2	- Grey densely welded tuff with white inclusions, pink splotches, and cavities (0.5 – 2.0”) filled with secondary minerals.
47.7 – 47.9	*- Grey tuff brecciated with red cement (chalcedony + goethite).*
50.2 – ~99.1	- Grey densely welded tuff with white inclusions, less pink, minimal cavities, and occasional infiltration of red veins and pumice fragments.
58.5 – 59.0	*- Soft tan conglomerate (mostly matrix with sand to pebble size clasts).*
~64.0	*- White inclusions gradually become larger and more dominant with more pink rings.*
~69.5	*- Orange/red (chalcedony + goethite) perpendicular to core becomes increasingly frequent (every ~0.5 m).*
72.8	*- Minimal pink is present.*
73.9 – 76.7	*- Abundant red/orange (chalcedony + goethite).*
76.8	*- Essentially no pink left in the tuff, and white inclusions are more abundant and squigglier.*
83.9	*- Grey tuff matrix becomes gently browner.*
90.7 – 96.1	*- White inclusions start to become frequently tinged with yellow.*

90.8 – 94.8 - *Grey densely welded tuff.*

91.3 – 92.5 - *Vertical clay (montmorillonite) vein approximately parallel to core axis with associated red veining (chalcedony + goethite).*

91.3 – 94.9 - *Red veining (chalcedony + goethite) becomes regular (every several centimeters).*

94.8 - *Grey tuff matrix becomes gently browner.*

97.1 - *White inclusions become less squiggly.*

~99.1 – 118.9 - Keith *et al.*, 1968-78 note lithic fragments dominant over phenocrysts in the tuff.

~103.6 - *Tuff is redder with lithic fragments obvious and occasional red (chalcedony + goethite) and clay (montmorillonite) veining.*

- *Tuff becomes redder and has larger lithic fragments with depth.*

110.3 - *Tuff begins gradually becoming more porous and less densely welded.*

116.4 - *Tuff begins gradually becoming more densely welded, and is densely welded by this depth.*

~112.5 – 113.4 - *Dominantly red iron stained (Keith and Muffler think might be sediment).*

118.4-119.6 - Transition from lithic to crystal rich tuff.

119.8 – 164.0 - Densely welded brownish grey tuff with white inclusions.

119.8 – 121.3 - *Occasional red veins and yellow staining around non-smeared white inclusions.*

121.3 - *White inclusions are more smeared.*

~123.9 - *Tuff becomes more pink with occasional ~0.3 long sections of grey.*

137.2 - *After here, white clasts tend to be red stained in pink and pink-grey tuff and not red stained in grey tuff.*

141.8 - *Inclusions become rarely smeared.*

145.1 - *Black/dark grey veining becomes more frequent.*

147.1 – 150.3 - *Black/dark grey veins thicken.*

153.4 – 153.9 - *Tuff transitions from pink to grey.*

153.9 – 155.7 - *Grey tuff.*

155.7 – 156.8 - *Pink-grey tuff.*

156.8 – ~160.6 - *Grey tuff.*

~160.6 – 164.0 - *Pink-grey tuff.*

10. Appendix C: Trace Element Concentrations in Y-5 Rocks and Surrounding Thermal Features

Table XIV: Trace elements in Y-5 drill core and surrounding thermal features.

Element (ppm)	Y-5 Avg. (Bargar and Beeson, 1984)	170813CA	170813HA	170813JA	170813EA	170813FA	170813IA	170813GA	Percent Error*
		3 of a Kind	Uther	Pendragon	Gwenivere	Merlin's Beard	Mordrid	Grizzly Pool	
Li	70.3	2.480	3.070	2.540	2.610	1.630	2.710	2.390	1.3%
Be	2.3	< 0.0002	0.002	0.002	< 0.0002	0.002	0.001	< 0.001	6.3%
B	3.3	2.390	2.460	2.460	2.470	1.160	2.420	2.160	3.7%
V	3.3	< 0.005	< 0.005	< 0.005	< 0.005	< 0.001	< 0.003	0.002	5.2%
Cr	1.7	< 0.002	< 0.002	< 0.002	< 0.002	< 0.001	< 0.001	< 0.001	5.8%
Co	1.2	< 0.005	< 0.005	< 0.005	< 0.005	< 0.001	< 0.003	< 0.001	4.9%
Ni	< 4.6	< 0.005	< 0.005	< 0.005	< 0.005	< 0.001	< 0.003	< 0.001	4.4%
Cu	3.1	0.010	< 0.010	< 0.010	< 0.010	< 0.003	< 0.005	< 0.003	4.9%
Zn**	22.6	< 0.006	< 0.006	< 0.006	< 0.006	0.004	< 0.001	0.002	6.1%
Ga	20.9	0.007	< 0.005	< 0.005	0.006	0.002	0.005	< 0.001	2.6%
As	BDL	1.320	1.300	1.310	1.390	0.605	1.320	0.613	3.8%
Sr	27.0	< 0.010	< 0.010	< 0.010	< 0.010	0.009	< 0.005	0.008	4.4%
Zr	218.6	< 0.005	< 0.005	< 0.005	< 0.005	< 0.001	< 0.003	< 0.001	2.5%
Nb	11.6	0.006	< 0.005	< 0.005	< 0.005	< 0.001	0.004	< 0.001	2.6%
Mo	2.3	0.020	0.011	0.013	0.015	0.008	0.013	0.012	4.0%
Pd	BDL	< 0.005	< 0.005	< 0.005	< 0.005	< 0.001	< 0.003	< 0.001	2.8%
Ag	< 0.1	< 0.002	< 0.002	< 0.002	< 0.002	< 0.001	< 0.001	< 0.001	4.5%

BDL = below detection limit

*Percent error represents instrumental error calculated from replicates of the standards used for the analyses of the thermal feature water. No error was reported for trace elements in the Y-5 drill core (Beeson and Bargar, 1984).

**Zn values for thermal waters corrected for field blank (Zn = 0.0038 ppm).

Table XIV: Continued – trace elements in Y-5 drill core and surrounding thermal features.

Element (ppm)	Y-5 Avg. (Bargar and Beeson, 1984)	170813CA 3 of a Kind	170813HA Uther	170813JA Pendragon	170813EA Gwenivere	170813FA Merlin's Beard	170813IA Mordrid	170813GA Grizzly Pool	Percent Error*
Cd	BDL	< 0.002	< 0.002	< 0.002	< 0.002	< 0.001	< 0.001	< 0.001	5.3%
Sn	< 6.8	< 0.005	< 0.005	< 0.005	< 0.005	< 0.001	< 0.003	< 0.001	3.0%
Ba	661.4	< 0.010	< 0.010	< 0.010	< 0.010	0.005	< 0.005	0.002	4.3%
La	132.4	< 0.002	< 0.002	< 0.002	< 0.002	< 0.001	< 0.001	< 0.001	3.0%
Ce	228.6	< 0.002	< 0.002	< 0.002	< 0.002	< 0.001	< 0.001	< 0.001	2.8%
Pr	BDL	< 0.002	< 0.002	< 0.002	< 0.002	< 0.001	< 0.001	< 0.001	3.0%
Nd	133.7	< 0.002	< 0.002	< 0.002	< 0.002	< 0.001	< 0.001	< 0.001	2.6%
W	BDL	0.368	0.379	0.388	0.380	0.201	0.414	0.300	2.2%
Tl	BDL	< 0.002	< 0.002	< 0.002	< 0.002	< 0.001	< 0.001	< 0.001	3.6%
Pb	17.3	< 0.002	< 0.002	< 0.002	< 0.002	< 0.001	< 0.001	< 0.001	4.3%
Th	BDL	0.003	< 0.002	< 0.002	< 0.002	< 0.001	0.002	< 0.001	3.0%
U	BDL	< 0.002	< 0.002	< 0.002	< 0.002	0.0005	< 0.001	0.0005	3.0%

BDL = below detection limit

*Percent error represents instrumental error calculated from replicates of the standards used for the analyses of the thermal feature water. No error was reported for trace elements in the Y-5 drill core (Beeson and Bargar, 1984).

10. Appendix D: Numerical Values for Petrologic Investigation

Table XV: Weight percentages of major element oxides measured in Y-5 drill core (Beeson and Bargar, 1984).

Depth (m)	SiO_2	Al_2O_3	CaO	Na_2O	K_2O	P_2O_5	Fe_2O_3	FeO	MgO
24.8	75.70	12.50	0.30	2.60	5.30	0.04	1.70	0.04	0.03
35.2	79.30	10.90	0.34	2.50	4.40	0.05	1.60	0.04	0.02
36.5	75.70	12.60	0.31	2.90	5.10	0.06	2.00	0.04	0.01
36.9	74.30	13.00	0.34	3.20	5.30	0.07	2.20	0.04	0.05
42.4	76.70	11.60	0.28	2.50	4.90	0.05	1.80	0.04	0.05
80.9	73.80	13.00	0.39	3.10	5.10	0.04	2.00	0.16	0.05
160.2	74.30	13.90	0.59	3.40	5.50	0.06	0.94	0.12	0.05
Avg.	75.69	12.50	0.36	2.89	5.09	0.05	1.75	0.07	0.04

Table XVI: Calculations for petrologic analysis of Y-5 drill core.

Depth (m)	Al[a]	Ca[a]	Na[a]	K[a]	P[a]	ASI[b]	AI[c]	FeO_T[d]	Fe-index[e]	MALI[f]
24.8	0.245	0.005	0.084	0.113	0.001	1.221	0.050	1.57	0.981	7.600
35.2	0.214	0.006	0.081	0.093	0.001	1.195	0.040	1.48	0.987	6.560
36.5	0.247	0.006	0.094	0.108	0.001	1.200	0.050	1.84	0.995	7.690
36.9	0.255	0.006	0.103	0.113	0.001	1.158	0.040	2.02	0.976	8.160
42.4	0.228	0.005	0.081	0.104	0.001	1.207	0.040	1.66	0.971	7.120
80.9	0.255	0.007	0.100	0.108	0.001	1.190	0.050	1.96	0.975	7.810
160.2	0.273	0.011	0.110	0.117	0.001	1.157	0.050	0.97	0.951	8.310
Avg.	0.245	0.006	0.093	0.108	0.001	1.188	0.040	1.64	0.978	7.607

[a]Converted from weight percent (Table XV) of the element oxide to weight percent of the element using molecular masses.
[b]Aluminum-Saturation Index (ASI) = Al/(Ca-1.67P + Na + K) (Frost and Frost, 2008)
[c]Alkalinity Index (AI) = Al – (K + Na) (Frost and Frost, 2008)
[d]Total iron oxide (FeO_T) = FeO + 0.9*Fe_2O_3 (Frost and Frost, 2008)
[e]Fe-index = (FeO_T)/(FeO_T + MgO) (Frost and Frost, 2008)
[f]Modified Alkali-Lime Index (MALI) = Na_2O + K_2O – CaO (Frost and Frost, 2008)

11. Appendix E: Measured Aqueous Geochemistries of Y-5 Thermal Features

Table XVII: Sample collection times for Y-5 thermal features.

Sample ID	Sample Location	Time of Sample Collection	
		***In situ* Meters with Water Isotope Sample**	**Full Water Sample**
170813CA*	3 of a Kind	9:55	10:01
170813EA*	Gwenivere	11:17	11:25
170813FA	Merlin's Beard	--	12:50
170813GA	Grizzly Pool	--	13:38
170813HA	Uther	--	14:38
170813IA	Mordrid	--	15:19
170813JA	Pendragon	--	15:50
170813MR12MH*	Grizzly Pool	10:16	--
170813MR13MH	Woad	10:30	--
170813MR14MH	Mordrid	10:45	--
170813MR15MH	Uther	11:00	--
170813MR16MH	Pendragon	11:40	--
170813MR17MH	Merlin's Beard	12:00	--

*Water isotope samples were collected only with the full water sample for 3 of a Kind, Gwenivere, and Grizzly Pool.

Table XVIII: *In situ* meter data for Y-5 thermal features.

Sample ID	Sample Name	pH*	Conductivity (µS/cm)*	Specific Conductivity (µS/cm)*	Dissolved Oxygen (µmol/kg)*	Temperature (^{0}C)*
170813CA	3 of a Kind	7.756 ± 0.005	4171 ± 8	Lerr	< 0.30	92.2 ± 0.1
170813MR15MH	Uther	7.459 ± 0.010	4129 ± *8*	Lerr	< 0.13	92.2 ± 0.1
170813MR16MH	Pendragon	7.483 ± 0.020	3807 ± 8	Lerr	0.13 ± 0.63	83.9 ± 0.1
170813EA	Gwenivere	8.593 ± 0.030	3805 ± *8*	Lerr	23.8 ± 0.3	79.8 ± 0.2
170813MR17MH	Merlin's Beard	6.502 ± 0.005	1938 ± *4*	Lerr	3.38 ± 0.06	74.2 ± 0.2
170813MR14MH	Mordrid	8.117 ± 0.010	2920 ± 60	1796 ± *4*	119 ± 2	59.1 ± *0.1*
170813MR12MH	Grizzly Pool	9.598 ± *0.005*	1152 ± 2	1342 ± *3*	458 ± 6	17.3 ± *0.1*

Lerr = low error (temperature too high to convert to specific conductivity)

*Error is from fluctuation during field measurement. If field error < instrumental error, then the instrumental error is given in italics: pH ± 0.005; conductivity ± 0.2%; temperature ± 0.1^{o}C.

Table XIX: Field spectrophotometry data for Y-5 thermal features.

Sample ID	Sample Location	Fe^{+2} (µmol/kg) ± 0.36*	S^{-2} (µmol/kg) ± 0.001**	SiO_2 (mmol/kg) ± 0.12**
170813CA	3 of a Kind	< 0.36	0.249	3.90
170813HA	Uther	< 0.36	2.680	3.89
170813JA	Pendragon	< 0.36	0.530	3.35
170813EA	Gwenivere	< 0.36	4.830	1.09
170813FA	Merlin's Beard	< 0.36	0.748	4.59
170813IA	Mordrid	< 0.36	1.030	5.07
170813GA	Grizzly Pool	< 0.36	NaN	4.89

NaN = not a number

*The magnitude of the ferrous iron error is also the detection limit for the test.

**Error is reported as seven times the test sensitivity given in Hach methods to help account for non-ideal field conditions.

Table XX: δD and $\delta^{18}O$ for Y-5 area thermal features.

Sample ID	Sample Location	$\delta^{18}O$ (vs. VSMOW) (±0.1)	δD (vs. VSMOW) (±1)	Time of Sample
170813CA	3 of a kind	-16.6	-143	10:01
170813HA	Uther	-17.1	-145	14:38
170813MR15MH	Uther	-16.0	-141	11:00
170813-10:49	Uther	-16.7	-143	10:49
170813JA	Pendragon	-16.8	-144	15:50
170813MR16MH	Pendragon	-16.8	-144	11:40
170813EA	Gwenivere	-16.3	-142	11:25
170813FA	Merlin's Beard	-17.6	-144	12:50
170813MR17MH	Merlin's Beard	-18.0	-145	12:00
170813IA	Mordrid	-15.9	-141	15:19
170813MR14MH	Mordrid	-17.1	-144	10:45
170813MR13MH	Woad	-15.3	-140	10:30
170813GA	Grizzly Pool	-6.5	-93	13:38

Table XXI: δD and $\delta^{18}O$ for Rabbit Creek area snow.

Sample ID	Sample Location	$\delta^{18}O$ (vs. VSMOW) (±0.1)	δD (vs. VSMOW) (±1)
170426E	RCA Snow 1	-19.9	-164
170426F	RCA Snow 2	-20.3	-168

Table XXII: δD and $\delta^{18}O$ for Tomato Soup thermal features.

Sample ID	Sample Location	$\delta^{18}O$ (vs. VSMOW) (±0.1)	δD (vs. VSMOW) (±1)
170717B	Sundried Tomato	-5.7	-116
170717C	Pepper Spray	-5.7	-116
170717D	Sweet Relief	-8.9	-123
170717E	The Nozzle	-9.7	-127
326	The Loo	-7.4	-118
327	B+TSTL	-8.7	-118
328	Rrruffle	-10.0	-123
329	--	-15.9	-135
330	G	-10.9	-126
170807IB5	Pepper Spray Turbid	-6.1	-116
170807IB6	Pepper Spray Less Turbid 1	-7.0	-120
170807IB7	Pepper Spray Less Turbid 2	-5.0	-114
170807IB8	The Nozzle	-9.0	-123
170807IB9	"B" Tomato Soup	-7.6	-120
170807IB10	Sun Dried Tomato	-6.4	-118
170807IB11	The Loo	-8.4	-121
170807IB12	TBFP	-6.9	-118
170807IB13	Unnamed 3	-9.5	-125
170807IB14	Unnamed 4	-7.2	-118
170807IB15	Storm Cloud Green	-7.5	-119
170807IB16	Storm Cloud Beige	-7.5	-119
170807IB17	Unnamed 5	-12.8	-136
170807IB18	Unnamed 6	-9.4	-124
170807IB19	Unnamed 7	-6.9	-112
170807IB20	Unnamed 8	-5.6	-104

Table XXIII: δD and $\delta^{18}O$ for Rabbit Creek North and South thermal features.

Area	Sample ID	Sample Location	$\delta^{18}O$ (vs. VSMOW) (±0.1)	δD (vs. VSMOW) (±1)
Rabbit Creek North	170807P	RC Source	-16.4	-144
	170807R	Kiwi	-15.3	-140
	170807S	The Hammer	-13.1	-133
	170807IB1	The Hammer	-16.5	-144
	170807IB2	Unnamed 1	-16.2	-143
	170807IB3	Unnamed 2	-16.1	-143
	170807IB4	Rabbit's Nest (?)	-15.8	-142
	170807IB21	Unnamed 9	-11.1	-131
	170807IB22	Rum Runner (?)	-17.0	-142
	170807IB23	Small Spitting Thing	-15.7	-134
	170807IB24	Other Small Thing	-15.0	-137
	170807IB25	Unnamed 10	-16.2	-142
	170807IB26	Unnamed 11	-15.7	-142
Rabbit Creek South	170813FH	Shift hole	-8.0	-122
	170813FI	Rasputin	-12.9	-132
	170813FN	Spitting Cobra Source	-18.3	-143
	170813MR22MH	Titannia	-11.4	-125
	170813MR23MH	Oberon	-11.3	-132
	170813MR24MH	Arrakis	-14.4	-132
	170813MR25MH	Iron Fist	-13.8	-127
	170813MR26MH	Cliff?	-17.3	-141
	170813MR27MH	Arrogant Bastard	-18.9	-145
	170813MR28MH	School bus	-13.1	-130

Table XXIV: Dissolved organic carbon (DOC) in Y-5 thermal features.

DOC (mol/kg)	170813DA	170813CA	170813HA	170813JA	170813EA	170813FA	170813IA	170813GA	Standard Deviation**
	Field Blank	3 of a kind	Uther	Pendragon	Gwenivere	Merlin's Beard	Mordrid	Grizzly Pool	
DOC	2.46E-05	4.00E-05	2.05E-04	6.91E-05	5.06E-05	2.41E-05	6.88E-04	1.56E-03	1.85E-06
DOC*	---	1.54E-05	1.80E-04	4.45E-05	2.60E-05	-5.06E-07	6.64E-04	1.53E-03	1.85E-06

*DOC values corrected for DOC value in blank.

**The average standard deviation for all samples analyzed in the same run was used as instrumental error, except for Mordrid, whose standard deviation from its own three replicates exceeded the average.

Table XXV: Major dissolved cations and anions in the Y-5 thermal features.

Ion (mol/kg)	170813DA	170813CA	170813HA	170813JA	170813EA	170813FA	170813IA	170813GA	Percent Error*
	Field Blank	3 of a kind	Uther	Pendragon	Gwenivere	Merlin's Beard	Mordrid	Grizzly Pool	
Li^{+}	< 2.0E-06	3.6E-04	4.4E-04	3.7E-04	3.8E-04	2.3E-04	3.9E-04	3.4E-04	1.3%
NO_2^{-}	< 2.2E-07	< 1.1E-06	< 1.1E-06	< 1.1E-06	< 1.1E-06	< 2.2E-07	< 2.2E-07	< 2.2E-07	1.2%
NO_3^{-}	6.8E-07	< 8.1E-07	< 8.1E-07	< 8.1E-07	< 8.1E-07	1.4E-06	< 1.6E-07	< 1.6E-07	4.6%
F^{-}	< 5.3E-07	8.4E-04	1.1E-03	7.4E-04	7.0E-04	7.3E-04	1.2E-03	1.1E-03	7.3%
Na^{+}	< 5.2E-07	1.3E-02	1.3E-02	1.1E-02	1.2E-02	7.7E-03	1.1E-02	1.1E-02	3.2%
Mg^{+2}	< 2.2E-07	< 2.2E-06	< 2.2E-06	< 2.2E-06	< 2.2E-06	7.9E-06	< 1.1E-06	1.2E-05	1.1%
PO_4^{-3}	< 2.1E-07	1.6E-06	< 1.1E-06	< 1.1E-06	< 1.1E-06	< 2.1E-07	< 2.1E-07	< 2.1E-07	7.9%
SO_4^{-2}	< 5.2E-06	1.7E-04	1.7E-04	1.6E-04	1.3E-04	8.6E-05	1.4E-04	4.2E-05	0.8%
Cl^{-}	< 2.8E-07	5.4E-03	7.4E-03	4.5E-03	4.2E-03	4.1E-03	7.3E-03	6.1E-03	0.9%
K^{+}	< 9.6E-07	2.0E-04	1.9E-04	1.3E-04	2.0E-04	2.0E-04	1.5E-04	2.6E-04	1.0%
Ca^{+2}	< 7.1E-08	5.4E-06	3.6E-05	2.7E-05	6.5E-06	8.9E-05	1.0E-05	3.9E-05	1.4%
Br^{-}	< 1.3E-07	9.2E-06	1.0E-05	8.3E-06	7.7E-06	5.3E-06	9.4E-06	7.4E-06	1.3%

*Percent error represents instrumental error calculated from replicates of the standards used for the analyses of the samples.

Table XXVI: Dissolved trace elements in the Y-5 thermal features.

Element (mol/kg)	170813DA	170813CA	170813HA	170813JA	170813EA	170813FA	170813IA	170813GA	Percent Error*
	Field Blank	3 of a kind	Uther	Pendragon	Gwenivere	Merlin's Beard	Mordrid	Grizzly Pool	
Be	< 1.11E-11	< 2.22E-08	2.33E-07	2.41E-07	< 2.22E-08	2.30E-07	1.17E-07	< 5.55E-08	6.3%
B	1.99E-07	2.76E-04	2.84E-04	2.84E-04	2.85E-04	1.34E-04	2.79E-04	2.49E-04	3.7%
Al	9.84E-08	7.46E-06	2.37E-06	2.71E-06	8.19E-06	1.81E-06	2.34E-06	1.52E-06	7.9%
Ti	< 1.93E-07	< 1.93E-06	< 1.93E-06	< 1.93E-06	< 1.93E-06	< 4.83E-07	< 9.66E-07	8.04E-07	5.6%
V	< 9.84E-09	< 9.84E-08	< 9.84E-08	< 9.84E-08	< 9.84E-08	< 2.46E-08	< 4.92E-08	3.29E-08	5.2%
Cr	< 4.59E-09	< 4.59E-08	< 4.59E-08	< 4.59E-08	< 4.59E-08	< 1.15E-08	< 2.30E-08	< 1.15E-08	5.8%
Mn	< 3.64E-08	< 3.64E-07	5.11E-07	4.72E-07	< 3.64E-07	3.28E-07	< 1.82E-07	< 9.10E-08	5.7%
Fe	< 1.95E-12	< 9.76E-07	< 9.76E-07	< 9.76E-07	< 9.76E-07	< 2.44E-07	< 4.88E-07	4.81E-07	16.2%
Co	< 8.48E-09	< 8.48E-08	< 8.48E-08	< 8.48E-08	< 8.48E-08	< 2.12E-08	< 4.24E-08	< 2.12E-08	4.9%
Ni	< 3.25E-08	< 3.25E-07	< 3.25E-07	< 3.25E-07	< 3.25E-07	< 8.12E-08	< 1.62E-07	< 8.12E-08	4.4%
Cu	< 1.22E-08	2.29E-07	< 2.27E-07	< 2.27E-07	< 2.27E-07	< 5.69E-08	< 1.14E-07	< 5.69E-08	4.9%
Zn	2.11E-07	< 5.52E-07	< 5.52E-07	< 5.52E-07	< 5.52E-07	4.08E-07	< 2.76E-07	3.36E-07	6.1%
Zn**	---	< 3.40E-07	< 3.40E-07	< 3.40E-07	< 3.40E-07	1.97E-07	< 6.44E-08	1.25E-07	6.1%
Ga	< 1.80E-08	2.57E-07	< 1.80E-07	< 1.80E-07	2.20E-07	7.01E-08	1.88E-07	< 4.49E-08	2.6%
As	< 2.67E-09	1.76E-05	1.74E-05	1.75E-05	1.86E-05	8.07E-06	1.76E-05	8.18E-06	3.8%
Se	< 2.90E-08	< 2.90E-07	< 2.90E-07	< 2.90E-07	< 2.90E-07	3.63E-11	< 1.45E-07	2.31E-07	3.3%
Rb	< 8.11E-09	9.98E-07	9.81E-07	9.57E-07	1.14E-06	8.02E-07	8.78E-07	1.15E-06	1.6%
Sr	< 1.38E-08	< 1.38E-07	< 1.38E-07	< 1.38E-07	< 1.38E-07	1.23E-07	< 6.91E-08	1.04E-07	4.4%
Zr	< 1.07E-08	< 1.07E-07	< 1.07E-07	< 1.07E-07	< 1.07E-07	< 2.66E-08	< 5.33E-08	< 2.66E-08	2.5%

*Percent error represents instrumental error calculated from replicates of the standards used for the analyses of the samples.
**Zn values corrected for Zn value in blank.

Table XXVI: Continued – dissolved trace elements in the Y-5 thermal features.

Element (mol/kg)	170813DA Field Blank	170813CA 3 of a kind	170813HA Uther	170813JA Pendragon	170813EA Gwenivere	170813FA Merlin's Beard	170813IA Mordrid	170813GA Grizzly Pool	Percent Error*
Nb	< 5.38E-09	6.73E-08	< 5.38E-08	< 5.38E-08	< 5.38E-08	< 1.35E-08	4.43E-08	< 1.35E-08	2.6%
Mo	< 2.14E-08	8.40E-07	4.68E-07	5.46E-07	6.32E-07	3.25E-07	5.42E-07	5.13E-07	4.0%
Pd	< 2.10E-08	< 2.10E-07	< 2.10E-07	< 2.10E-07	< 2.10E-07	< 5.26E-08	< 1.05E-07	< 5.26E-08	2.8%
Ag	< 3.58E-09	< 3.58E-08	< 3.58E-08	< 3.58E-08	< 3.58E-08	< 8.94E-09	< 1.79E-08	< 8.94E-09	4.5%
Cd	< 1.39E-08	< 1.39E-07	< 1.39E-07	< 1.39E-07	< 1.39E-07	< 3.47E-08	< 6.95E-08	< 3.47E-08	5.3%
Sn	< 1.74E-08	< 1.74E-07	< 1.74E-07	< 1.74E-07	< 1.74E-07	< 4.35E-08	< 8.69E-08	< 4.35E-08	3.0%
Sb	< 2.87E-09	9.74E-07	1.09E-06	1.10E-06	1.09E-06	5.38E-07	1.14E-06	3.92E-07	4.9%
Cs	< 3.76E-09	2.06E-06	2.07E-06	2.02E-06	2.01E-06	1.19E-06	2.09E-06	1.46E-06	1.5%
Ba	< 6.48E-08	< 6.48E-07	< 6.48E-07	< 6.48E-07	< 6.48E-07	3.39E-07	< 3.24E-07	1.52E-07	4.3%
La	< 1.44E-09	< 1.44E-08	< 1.44E-08	< 1.44E-08	< 1.44E-08	< 3.60E-09	< 7.21E-09	< 3.60E-09	3.0%
Ce	< 1.61E-09	< 1.61E-08	< 1.61E-08	< 1.61E-08	< 1.61E-08	< 4.03E-09	< 8.07E-09	< 4.03E-09	2.8%
Pr	< 1.42E-09	< 1.42E-08	< 1.42E-08	< 1.42E-08	< 1.42E-08	< 3.55E-09	< 7.10E-09	< 3.55E-09	3.0%
Nd	< 8.07E-09	< 8.07E-08	< 8.07E-08	< 8.07E-08	< 8.07E-08	< 2.02E-08	< 4.03E-08	< 2.02E-08	2.6%
W	< 4.11E-09	7.56E-06	7.77E-06	7.97E-06	7.80E-06	4.12E-06	8.50E-06	6.17E-06	2.2%
Tl	< 3.32E-09	< 3.32E-08	< 3.32E-08	< 3.32E-08	< 3.32E-08	< 8.29E-09	< 1.66E-08	< 8.29E-09	3.6%
Pb	< 1.84E-09	< 1.84E-08	< 1.84E-08	< 1.84E-08	< 1.84E-08	< 4.61E-09	< 9.22E-09	< 4.61E-09	4.3%
Th	< 8.62E-10	1.41E-08	< 8.62E-09	< 8.62E-09	< 8.62E-09	< 2.15E-09	7.24E-09	< 2.15E-09	3.0%
U	< 8.46E-10	< 8.46E-09	< 8.46E-09	< 8.46E-09	< 8.46E-09	2.21E-09	< 4.23E-09	2.23E-09	3.0%

*Percent error represents instrumental error calculated from replicates of the standards used for the analyses of the samples.

12. Appendix F: Aqueous Chemistries of Rabbit Creek Area Snow & Calibrated EQ3 input for EQ3/6

Table XXVII: *In situ* meter readings for the Rabbit Creek area snow (melted, unfiltered).

Sample ID	Sample Name	pH*	Conductivity (µS/cm)*	Specific Conductivity (µS/cm)*	Temperature (^{0}C)*
170426E	RCA Snow 1	5.570 ± 0.020	55.10 ± *1.10*	91.00 ± *1.82*	4.4 ± 0.1
170426F	RCA Snow 2	5.533 ± *0.005*	54.50 ± *1.09*	89.90 ± *1.80*	4.3 ± 0.1
---	RCA Snow Avg.	5.552 ± 0.012	54.80 ± *1.10*	90.45 ± *1.81*	4.4 ± 0.1

*Error is from fluctuation during field measurement. If field error < instrumental error, then the instrumental error is given in italics: pH ± 0.005; conductivity ± 0.2%; temperature ± 0.1°C.
Reported temperature is from the conductivity meter.

Table XXVIII: Major dissolved cations and anions in Rabbit Creek area snow.

Ion (mol/kg)	170426D	170426E	170426F	---
	RCA Blank	RCA Snow 1	RCA Snow 2	RCA Snow Avg.
NO_2^-	< 2.17E-07	< 2.17E-07	< 2.17E-07	< 2.17E-07
NO_3^-	6.93E-07	9.68E-07	8.71E-07	9.19E-07
F^-	< 5.26E-07	< 5.26E-07	< 5.26E-07	< 5.26E-07
Na^+	1.57E-06	4.87E-07	5.05E-07	4.96E-07
Mg^{+2}	< 2.14E-07	< 2.14E-07	< 2.14E-07	< 2.14E-07
PO_4^{-3}	< 2.11E-06	< 2.11E-06	< 2.11E-06	< 2.11E-06
SO_4^{-2}	< 5.20E-06	< 5.20E-06	< 5.20E-06	< 5.20E-06
Cl^-	7.84E-06	7.93E-06	8.10E-06	8.01E-06
K^+	< 1.08E-06	< 1.08E-06	1.10E-06	1.09E-06
Ca^{+2}	< 9.13E-08	4.32E-07	5.82E-07	5.07E-07
Br^-	< 1.25E-07	< 1.25E-07	< 1.25E-07	< 1.25E-07

Table XXIX: Dissolved trace elements in Rabbit Creek area snow.

Element (mol/kg)	170426D	170426E	170426F	---
	RCA Blank	RCA Snow 1	RCA Snow 2	RCA Snow Avg.
Li	< 7.80E-08	< 7.80E-08	< 7.80E-08	< 7.80E-08
Be	< 2.22E-08	< 2.22E-08	< 2.22E-08	< 2.22E-08
B	1.11E-07	7.82E-08	1.50E-07	1.14E-07
Al	1.79E-08	1.49E-07	2.43E-07	1.96E-07
Ti	< 1.93E-07	< 1.93E-07	< 1.93E-07	< 1.93E-07
V	< 9.84E-09	< 9.84E-09	< 9.84E-09	< 9.84E-09
Cr	< 4.59E-09	< 4.59E-09	< 4.59E-09	< 4.59E-09
Mn	< 3.64E-08	< 3.64E-08	< 3.64E-08	< 3.64E-08
Fe	< 9.76E-08	< 9.76E-08	< 9.76E-08	< 9.76E-08
Co	< 8.48E-09	< 8.48E-09	< 8.48E-09	< 8.48E-09
Ni	< 3.25E-08	< 3.25E-08	< 3.25E-08	< 3.25E-08
Cu	< 2.27E-08	< 2.27E-08	< 2.27E-08	< 2.27E-08
Zn	2.87E-07	< 5.52E-08	1.06E-07	8.06E-08
Ga	< 1.80E-08	< 1.80E-08	< 1.80E-08	< 1.80E-08
As	< 2.67E-09	< 2.67E-09	< 2.67E-09	< 2.67E-09
Se	< 2.90E-08	< 2.90E-08	< 2.90E-08	< 2.90E-08
Rb	< 8.11E-09	< 8.11E-09	< 8.11E-09	< 8.11E-09
Sr	< 1.38E-08	< 1.38E-08	< 1.38E-08	< 1.38E-08
Zr	< 1.07E-08	< 1.07E-08	< 1.07E-08	< 1.07E-08
Nb	< 5.38E-09	< 5.38E-09	< 5.38E-09	< 5.38E-09
Mo	< 2.14E-08	< 2.14E-08	< 2.14E-08	< 2.14E-08
Pd	< 2.10E-08	< 2.10E-08	< 2.10E-08	< 2.10E-08
Ag	< 3.58E-09	< 3.58E-09	< 3.58E-09	< 3.58E-09
Cd	< 1.39E-08	< 1.39E-08	< 1.39E-08	< 1.39E-08
Sn	< 1.74E-08	< 1.74E-08	< 1.74E-08	< 1.74E-08
Sb	< 2.87E-09	< 2.87E-09	< 2.87E-09	< 2.87E-09
Cs	< 3.76E-09	< 3.76E-09	< 3.76E-09	< 3.76E-09
Ba	< 6.48E-08	< 6.48E-08	< 6.48E-08	< 6.48E-08
La	< 1.44E-09	< 1.44E-09	< 1.44E-09	< 1.44E-09
Ce	< 1.61E-09	< 1.61E-09	< 1.61E-09	< 1.61E-09
Pr	< 1.42E-09	< 1.42E-09	< 1.42E-09	< 1.42E-09
Nd	< 8.07E-09	< 8.07E-09	< 8.07E-09	< 8.07E-09
W	< 4.11E-09	< 4.11E-09	< 4.11E-09	< 4.11E-09
Tl	< 3.32E-09	< 3.32E-09	< 3.32E-09	< 3.32E-09
Pb	< 1.84E-09	< 1.84E-09	< 1.84E-09	< 1.84E-09
Th	< 8.62E-10	< 8.62E-10	< 8.62E-10	< 8.62E-10
U	< 8.46E-10	< 8.46E-10	< 8.46E-10	< 8.46E-10

Table XXX: Calibrated meteoric EQ3 input for EQ3/6 models.

Species	Concentration (mol/kg)
H^{+}	3.98E-06
Li^{+}	1.84E-04
Be^{+2}	2.22E-08
$B(OH)_3$ (aq)	1.14E-07
HCO_3^{-}	1.30E-08
$NH4^{+}$	1.00E-07
NO_3^{-}	9.19E-07
O_2 (aq)	1.00E-07
F^{-}	1.00E-03
Na^{+}	5.05E-04
Mg^{+2}	2.14E-05
Al^{+3}	1.96E-07
SiO_2 (aq)	1.00E-05
HPO_4^{-2}	2.11E-06
SO_4^{-2}	5.20E-05
HS^{-}	1.00E-06
Cl^{-}	8.01E-05
K^{+}	1.10E-05
Ca^{+2}	5.82E-07
Ti^{+4}	1.93E-07
VO^{+2}	9.84E-09
Mn^{+2}	3.64E-08
Fe^{+2}	9.76E-07
Cu^{+2}	2.27E-08
Zn^{+2}	8.06E-08
Ga^{+3}	1.80E-08
$H_2AsO_4^{-}$	2.67E-09
SeO_3^{-2}	2.90E-08
Br^{-}	1.25E-06
Rb^{+}	8.11E-09
Sr^{+2}	1.38E-08
NbO_3^{-}	5.38E-09
MoO_4^{-2}	2.14E-08
SbO_2^{-}	2.87E-09
Cs^{+}	3.76E-09
Ba^{+2}	6.48E-08
$WO4^{-2}$	4.11E-09
Tl^{+}	3.32E-09
Th^{+4}	8.62E-10
U^{+4}	8.46E-10

13. Appendix G: Sensitivity Analyses of EQ3 and EQ3/6

Table XXXI: EQ3 sensitivity analysis of error on geochemical inputs for 3 of a Kind: select species.

Species	Low (mol/kg)	Mid (mol/kg)	High (mol/kg)	Δ *mid - low*	Δ *mid - high*
H^+	3.33E-08	3.38E-08	3.42E-08	*4.63E-10*	*-4.54E-10*
Li^+	3.53E-04	3.57E-04	3.62E-04	*4.65E-06*	*-4.64E-06*
$B(OH)_3$ (aq)	2.51E-04	2.61E-04	2.71E-04	*9.94E-06*	*-9.95E-06*
BO_2^-	1.39E-05	1.43E-05	1.47E-05	*3.86E-07*	*-3.83E-07*
HCO_3^-	4.73E-03	4.82E-03	4.91E-03	*8.95E-05*	*-8.91E-05*
CO_2 (aq)	2.59E-04	2.67E-04	2.75E-04	*7.94E-06*	*-7.94E-06*
$CO3^{-2}$	1.91E-05	1.93E-05	1.95E-05	*1.88E-07*	*-1.88E-07*
NH_3 (aq)	5.82E-06	6.22E-06	6.61E-06	*3.99E-07*	*-3.93E-07*
NH_4^+	7.18E-06	7.78E-06	8.38E-06	*6.01E-07*	*-6.07E-07*
NO_3^-	7.69E-07	8.06E-07	8.43E-07	*3.71E-08*	*-3.71E-08*
F^-	7.79E-04	8.40E-04	9.02E-04	*6.13E-05*	*-6.13E-05*
Na^+	1.18E-02	1.21E-02	1.25E-02	*3.80E-04*	*-3.80E-04*
$NaHCO_3$ (aq)	5.03E-04	5.27E-04	5.52E-04	*2.46E-05*	*-2.51E-05*
$NaHSiO_3$(aq)	2.23E-05	2.34E-05	2.45E-05	*1.10E-06*	*-1.12E-06*
NaCl (aq)	1.48E-05	1.54E-05	1.59E-05	*5.75E-07*	*-5.81E-07*
NaF (aq)	1.53E-06	1.70E-06	1.87E-06	*1.69E-07*	*-1.76E-07*
$NaCO_3^-$	1.86E-07	1.93E-07	2.00E-07	*6.89E-09*	*-6.95E-09*
AlO_2^-	6.77E-06	7.35E-06	7.93E-06	*5.80E-07*	*-5.80E-07*
$HAlO_2$ (aq)	9.99E-08	1.10E-07	1.20E-07	*9.82E-09*	*-9.97E-09*
SiO_2 (aq)	3.63E-03	3.74E-03	3.85E-03	*1.12E-04*	*-1.13E-04*
$HSiO_3^-$	1.36E-04	1.39E-04	1.41E-04	*2.61E-06*	*-2.60E-06*
SO_4^{-2}	1.71E-04	1.72E-04	1.74E-04	*1.36E-06*	*-1.36E-06*
HS^-	2.30E-07	2.30E-07	2.31E-07	*8.00E-10*	*-8.20E-10*
Cl^-	5.30E-03	5.34E-03	5.39E-03	*4.87E-05*	*-4.88E-05*
K^+	1.95E-04	1.97E-04	1.99E-04	*1.94E-06*	*-1.93E-06*
$KHCO_3$ (aq)	1.98E-06	2.03E-06	2.08E-06	*5.18E-08*	*-5.20E-08*
KSO_4^-	2.79E-07	2.83E-07	2.86E-07	*3.42E-09*	*-3.45E-09*
KCO_3^-	2.68E-08	2.72E-08	2.75E-08	*3.87E-10*	*-3.91E-10*
KCl (aq)	1.23E-08	1.25E-08	1.27E-08	*2.00E-10*	*-2.02E-10*
Ca^{+2}	4.55E-06	4.60E-06	4.66E-06	*5.94E-08*	*-5.93E-08*
$Ca(CO_3)$ (aq)	3.40E-07	3.44E-07	3.49E-07	*4.34E-09*	*-4.37E-09*
$Ca(HCO_3)^+$	2.99E-07	3.07E-07	3.15E-07	*8.13E-09*	*-8.18E-09*
$CaSO_4$ (aq)	8.17E-08	8.26E-08	8.34E-08	*8.63E-10*	*-8.67E-10*
CaF^+	2.76E-08	3.01E-08	3.25E-08	*2.42E-09*	*-2.45E-09*
$HAsO_4^{-2}$	1.49E-05	1.55E-05	1.60E-05	*5.67E-07*	*-5.68E-07*
$H_2AsO_4^-$	2.04E-06	2.14E-06	2.24E-06	*9.64E-08*	*-9.69E-08*
Br^-	9.06E-06	9.18E-06	9.30E-06	*1.19E-07*	*-1.19E-07*

Italics indicate values calculated from modeling outputs.

Table XXXII: EQ3 sensitivity analysis of logfO_2 (± 0.50 log bars) for 3 of a Kind: select species.

Species	Low (mol/kg)	Mid (mol/kg)	High (mol/kg)	Δ *mid - low*	Δ *mid - high*
H^+	3.38E-08	3.38E-08	3.38E-08	*-1.00E-12*	*0.00E+00*
Li^+	3.57E-04	3.57E-04	3.57E-04	*0.00E+00*	*0.00E+00*
$B(OH)_3$ (aq)	2.61E-04	2.61E-04	2.61E-04	*0.00E+00*	*0.00E+00*
BO_2^-	1.43E-05	1.43E-05	1.43E-05	*0.00E+00*	*-1.00E-09*
HCO_3^-	4.82E-03	4.82E-03	4.82E-03	*0.00E+00*	*0.00E+00*
CO_2 (aq)	2.67E-04	2.67E-04	2.67E-04	*-1.00E-08*	*0.00E+00*
$CO3^{-2}$	1.93E-05	1.93E-05	1.93E-05	*1.00E-09*	*0.00E+00*
NH_3 (aq)	6.22E-06	6.22E-06	6.22E-06	*1.00E-10*	*0.00E+00*
NH_4^+	7.78E-06	7.78E-06	7.78E-06	*-1.00E-10*	*1.00E-10*
NO_3^-	8.06E-07	8.06E-07	8.06E-07	*0.00E+00*	*0.00E+00*
F^-	8.40E-04	8.40E-04	8.40E-04	*0.00E+00*	*0.00E+00*
Na^+	1.21E-02	1.21E-02	1.21E-02	*0.00E+00*	*0.00E+00*
$NaHCO_3$ (aq)	5.27E-04	5.27E-04	5.27E-04	*0.00E+00*	*0.00E+00*
$NaHSiO_3$(aq)	2.34E-05	2.34E-05	2.34E-05	*0.00E+00*	*-1.00E-09*
NaCl (aq)	1.54E-05	1.54E-05	1.54E-05	*0.00E+00*	*0.00E+00*
NaF (aq)	1.70E-06	1.70E-06	1.70E-06	*0.00E+00*	*0.00E+00*
$NaCO_3^-$	1.93E-07	1.93E-07	1.93E-07	*0.00E+00*	*0.00E+00*
AlO_2^-	7.35E-06	7.35E-06	7.35E-06	*0.00E+00*	*0.00E+00*
$HAlO_2$ (aq)	1.10E-07	1.10E-07	1.10E-07	*0.00E+00*	*0.00E+00*
SiO_2 (aq)	3.74E-03	3.74E-03	3.74E-03	*0.00E+00*	*0.00E+00*
$HSiO_3^-$	1.39E-04	1.39E-04	1.39E-04	*0.00E+00*	*0.00E+00*
SO_4^{-2}	1.72E-04	1.72E-04	1.72E-04	*0.00E+00*	*0.00E+00*
HS^-	2.30E-07	2.30E-07	2.30E-07	*0.00E+00*	*0.00E+00*
Cl^-	5.34E-03	5.34E-03	5.34E-03	*0.00E+00*	*0.00E+00*
K^+	1.97E-04	1.97E-04	1.97E-04	*0.00E+00*	*0.00E+00*
$KHCO_3$ (aq)	2.03E-06	2.03E-06	2.03E-06	*0.00E+00*	*0.00E+00*
KSO_4^-	2.83E-07	2.83E-07	2.83E-07	*0.00E+00*	*0.00E+00*
KCO_3^-	2.72E-08	2.72E-08	2.72E-08	*1.00E-12*	*0.00E+00*
KCl (aq)	1.25E-08	1.25E-08	1.25E-08	*0.00E+00*	*0.00E+00*
Ca^{+2}	4.60E-06	4.60E-06	4.60E-06	*0.00E+00*	*0.00E+00*
$Ca(CO_3)$ (aq)	3.44E-07	3.44E-07	3.44E-07	*1.00E-11*	*0.00E+00*
$Ca(HCO_3)^+$	3.07E-07	3.07E-07	3.07E-07	*0.00E+00*	*0.00E+00*
$CaSO_4$ (aq)	8.26E-08	8.26E-08	8.26E-08	*0.00E+00*	*0.00E+00*
CaF^+	3.01E-08	3.01E-08	3.01E-08	*0.00E+00*	*0.00E+00*
$HAsO_4^{-2}$	1.55E-05	1.55E-05	1.55E-05	*0.00E+00*	*0.00E+00*
$H_2AsO_4^-$	2.14E-06	2.14E-06	2.14E-06	*0.00E+00*	*1.00E-10*
Br^-	9.18E-06	9.18E-06	9.18E-06	*0.00E+00*	*0.00E+00*

Italics indicate values calculated from modeling outputs.

Table XXXIII: EQ3/6 sensitivity analysis of starting temperature, cooled to 92.2°C: select species.

Species	Low (mol/kg)	Mid (mol/kg)	High (mol/kg)	Δ *mid - low*	Δ *mid - high*
Starting T (^{0}C)	167.8	250	350	---	---
H^+	1.91E-08	1.91E-08	1.91E-08	*9.00E-12*	*2.00E-12*
C Total	1.20E-02	1.20E-02	1.20E-02	*0.00E+00*	*0.00E+00*
HCO_3^-	1.05E-02	1.05E-02	1.05E-02	*0.00E+00*	*0.00E+00*
CO_2 (aq)	3.31E-04	3.32E-04	3.32E-04	*1.70E-07*	*5.00E-08*
CO_3^{-2}	7.42E-05	7.41E-05	7.42E-05	*-3.40E-08*	*-9.00E-09*
F Total	1.00E-03	1.00E-03	1.00E-03	*0.00E+00*	*0.00E+00*
F^-	1.00E-03	1.00E-03	1.00E-03	*0.00E+00*	*0.00E+00*
Na Total	1.21E-02	1.21E-02	1.21E-02	*-3.00E-07*	*-5.00E-07*
Na^+	1.10E-02	1.10E-02	1.10E-02	*0.00E+00*	*0.00E+00*
$NaHCO_3$ (aq)	1.05E-03	1.05E-03	1.05E-03	*1.00E-07*	*1.00E-07*
$NaHSiO_3$ (aq)	7.27E-06	7.27E-06	7.27E-06	*-2.00E-09*	*3.00E-10*
NaF (aq)	1.84E-06	1.84E-06	1.84E-06	*2.00E-10*	*1.00E-10*
$NaCO_3^-$	6.77E-07	6.76E-07	6.77E-07	*-3.70E-10*	*-1.60E-10*
NaOH (aq)	1.72E-07	1.72E-07	1.72E-07	*-1.00E-11*	*5.00E-11*
Al Total	1.26E-06	1.26E-06	1.26E-06	*1.10E-10*	*6.10E-10*
AlO_2^-	1.25E-06	1.25E-06	1.25E-06	*1.00E-10*	*6.00E-10*
$HAlO_2$ (aq)	1.06E-08	1.06E-08	1.06E-08	*2.00E-12*	*3.00E-12*
Si Total	7.80E-04	7.80E-04	7.80E-04	*1.20E-07*	*1.44E-07*
SiO_2 (aq)	7.25E-04	7.25E-04	7.25E-04	*1.20E-07*	*1.30E-07*
$HSiO_3^-$	4.74E-05	4.74E-05	4.74E-05	*-6.00E-09*	*1.10E-08*
S Total	5.30E-05	5.30E-05	5.30E-05	*0.00E+00*	*-1.00E-10*
SO_4^{-2}	5.26E-05	5.26E-05	5.26E-05	*0.00E+00*	*-3.00E-09*
HS^-	2.13E-07	2.13E-07	2.11E-07	*-2.30E-10*	*1.71E-09*
H_2S (aq)	1.01E-08	1.01E-08	9.97E-09	*-7.00E-12*	*8.08E-11*
HSO_4^-	4.72E-10	4.72E-10	4.72E-10	*3.50E-13*	*1.70E-13*
K Total	3.51E-04	3.51E-04	3.51E-04	*1.35E-07*	*-2.60E-08*
K^+	3.43E-04	3.43E-04	3.43E-04	*1.30E-07*	*-3.00E-08*
$KHCO_3$ (aq)	7.76E-06	7.76E-06	7.76E-06	*4.50E-09*	*1.00E-09*
KCO_3^-	1.83E-07	1.83E-07	1.83E-07	*1.00E-11*	*-1.00E-11*
KSO_4^-	1.51E-07	1.52E-07	1.52E-07	*8.00E-11*	*0.00E+00*
KOH (aq)	5.12E-09	5.12E-09	5.12E-09	*2.00E-12*	*1.50E-12*
Ca Total	2.75E-06	2.69E-06	2.43E-06	*-5.52E-08*	*2.67E-07*
Ca^{+2}	1.89E-06	1.85E-06	1.67E-06	*-3.79E-08*	*1.84E-07*
$CaCO_3$ (aq)	5.52E-07	5.41E-07	4.87E-07	*-1.12E-08*	*5.37E-08*
$CaHCO_3^+$	2.78E-07	2.72E-07	2.45E-07	*-5.54E-09*	*2.70E-08*
CaF^+	1.48E-08	1.45E-08	1.31E-08	*-2.96E-10*	*1.44E-09*
$CaSO_4$ (aq)	1.05E-08	1.03E-08	9.29E-09	*-2.10E-10*	*1.02E-09*
$CaOH^+$	3.34E-09	3.27E-09	2.95E-09	*-6.64E-11*	*3.26E-10*

Italics indicate values calculated from modeling outputs.

Table XXXIV: EQ3/6 sensitivity analysis of starting time, cooled to 92.2°C: select species.

Species	Short (mol/kg)	Mid (mol/kg)	Long (mol/kg)	Δ *mid - short*	Δ *mid - long*
Time Length (ka)	0.5	1.5	2.5	---	---
H^+	1.91E-08	1.91E-08	1.91E-08	*0.00E+00*	*0.00E+00*
C Total	1.20E-02	1.20E-02	1.20E-02	*0.00E+00*	*0.00E+00*
HCO_3^-	1.05E-02	1.05E-02	1.05E-02	*0.00E+00*	*0.00E+00*
CO_2 (aq)	3.31E-04	3.31E-04	3.31E-04	*0.00E+00*	*0.00E+00*
CO_3^{-2}	7.42E-05	7.42E-05	7.42E-05	*-1.00E-09*	*-1.00E-09*
F Total	1.00E-03	1.00E-03	1.00E-03	*0.00E+00*	*0.00E+00*
F^-	1.00E-03	1.00E-03	1.00E-03	*0.00E+00*	*0.00E+00*
Na Total	1.21E-02	1.21E-02	1.21E-02	*0.00E+00*	*0.00E+00*
Na^+	1.10E-02	1.10E-02	1.10E-02	*0.00E+00*	*0.00E+00*
$NaHCO_3$ (aq)	1.05E-03	1.05E-03	1.05E-03	*0.00E+00*	*0.00E+00*
$NaHSiO_3$ (aq)	7.27E-06	7.27E-06	7.27E-06	*0.00E+00*	*0.00E+00*
NaF (aq)	1.84E-06	1.84E-06	1.84E-06	*0.00E+00*	*0.00E+00*
$NaCO_3^-$	6.77E-07	6.77E-07	6.77E-07	*0.00E+00*	*0.00E+00*
NaOH (aq)	1.72E-07	1.72E-07	1.72E-07	*0.00E+00*	*0.00E+00*
Al Total	1.26E-06	1.26E-06	1.26E-06	*1.00E-11*	*1.00E-11*
AlO_2^-	1.25E-06	1.25E-06	1.25E-06	*0.00E+00*	*0.00E+00*
$HAlO_2$ (aq)	1.06E-08	1.06E-08	1.06E-08	*0.00E+00*	*0.00E+00*
Si Total	7.80E-04	7.80E-04	7.80E-04	*2.00E-09*	*2.00E-09*
SiO_2 (aq)	7.25E-04	7.25E-04	7.25E-04	*1.00E-08*	*1.00E-08*
$HSiO_3^-$	4.74E-05	4.74E-05	4.74E-05	*0.00E+00*	*0.00E+00*
S Total	5.30E-05	5.30E-05	5.30E-05	*0.00E+00*	*0.00E+00*
SO_4^{-2}	5.26E-05	5.26E-05	5.26E-05	*0.00E+00*	*0.00E+00*
HS^-	2.13E-07	2.13E-07	2.13E-07	*0.00E+00*	*0.00E+00*
H_2S (aq)	1.01E-08	1.01E-08	1.01E-08	*0.00E+00*	*0.00E+00*
HSO_4^-	4.72E-10	4.72E-10	4.72E-10	*1.00E-14*	*1.00E-14*
K Total	3.51E-04	3.51E-04	3.51E-04	*1.00E-09*	*1.00E-09*
K^+	3.43E-04	3.43E-04	3.43E-04	*0.00E+00*	*0.00E+00*
$KHCO_3$ (aq)	7.76E-06	7.76E-06	7.76E-06	*0.00E+00*	*0.00E+00*
KCO_3^-	1.83E-07	1.83E-07	1.83E-07	*0.00E+00*	*0.00E+00*
KSO_4^-	1.51E-07	1.51E-07	1.51E-07	*0.00E+00*	*0.00E+00*
KOH (aq)	5.12E-09	5.12E-09	5.12E-09	*0.00E+00*	*0.00E+00*
Ca Total	2.75E-06	2.75E-06	2.75E-06	*0.00E+00*	*0.00E+00*
Ca^{+2}	1.89E-06	1.89E-06	1.89E-06	*0.00E+00*	*0.00E+00*
$CaCO_3$ (aq)	5.52E-07	5.52E-07	5.52E-07	*0.00E+00*	*0.00E+00*
$CaHCO_3^+$	2.78E-07	2.78E-07	2.78E-07	*1.00E-11*	*1.00E-11*
CaF^+	1.48E-08	1.48E-08	1.48E-08	*1.00E-12*	*1.00E-12*
$CaSO_4$ (aq)	1.05E-08	1.05E-08	1.05E-08	*0.00E+00*	*0.00E+00*
$CaOH^+$	3.34E-09	3.34E-09	3.34E-09	*1.00E-13*	*1.00E-13*

Italics indicate values calculated from modeling outputs.

14. Appendix H: Modeling Outputs (EQ3 and EQ3/6)

Table XXXV: Total dissolved solids and ionic strength from EQ3 models of Y-5 thermal features.

Sample	TDS (mg/kg)	Ionic strength (mol/kg)
3 of a Kind	1125	0.012
Uther	1227	0.014
Pendragon	1120	0.011
Gwenivere	1076	0.012
Merlin's Beard	738	0.008
Mordrid	1230	0.012
Grizzly Pool	866	0.012

Table XXXVI: Calibrated EQ3/6 outputs compared with EQ3 speciation: select species (mol/kg), 3 of a Kind and Uther.

	EQ3/6	3 of a Kind	*Δ 3 of a Kind - EQ3/6*	Uther	*Δ Uther - EQ3/6*
T (°C)	92.2	92.2	*0.0*	92.2	*0.0*
H^+	1.91E-08	3.38E-08	*-1.47E-08*	1.10E-07	*9.08E-08*
pH	7.719	7.471	*0.248*	6.959	*-0.760*
C Total	1.20E-02	5.64E-03	*6.37E-03*	6.06E-03	*-5.95E-03*
HCO_3^-	1.05E-02	4.82E-03	*5.72E-03*	4.68E-03	*-5.86E-03*
CO_2 (aq)	3.31E-04	2.67E-04	*6.41E-05*	8.34E-04	*5.02E-04*
CO_3^{-2}	7.42E-05	1.93E-05	*5.49E-05*	5.90E-06	*-6.83E-05*
F Total	1.00E-03	8.42E-04	*1.60E-04*	1.12E-03	*1.19E-04*
F^-	1.00E-03	8.40E-04	*1.62E-04*	1.12E-03	*1.16E-04*
Na Total	1.21E-02	1.27E-02	*-6.51E-04*	1.35E-02	*1.43E-03*
Na^+	1.10E-02	1.21E-02	*-1.14E-03*	1.29E-02	*1.92E-03*
$NaHCO_3$ (aq)	1.05E-03	5.27E-04	*5.22E-04*	5.37E-04	*-5.12E-04*
$NaHSiO_3$ (aq)	7.27E-06	2.34E-05	*-1.61E-05*	9.25E-06	*1.98E-06*
NaF (aq)	1.84E-06	1.70E-06	*1.46E-07*	2.37E-06	*5.30E-07*
$NaCO_3^-$	6.77E-07	1.93E-07	*4.84E-07*	6.11E-08	*-6.16E-07*
NaOH (aq)	1.72E-07	1.07E-07	*6.48E-08*	3.50E-08	*-1.37E-07*
Al Total	1.26E-06	7.46E-06	*-6.20E-06*	2.37E-06	*1.11E-06*
AlO_2^-	1.25E-06	7.35E-06	*-6.10E-06*	2.27E-06	*1.01E-06*
$HAlO_2$ (aq)	1.06E-08	1.10E-07	*-9.92E-08*	1.09E-07	*9.82E-08*
Si Total	7.73E-04	3.88E-03	*-3.11E-03*	4.58E-03	*3.81E-03*
SiO_2 (aq)	7.25E-04	3.74E-03	*-3.02E-03*	4.53E-03	*3.81E-03*
$HSiO_3^-$	4.74E-05	1.39E-04	*-9.12E-05*	5.22E-05	*4.85E-06*
S Total	5.28E-05	1.73E-04	*-1.20E-04*	1.73E-04	*1.21E-04*
SO_4^{-2}	5.26E-05	1.72E-04	*-1.20E-04*	1.70E-04	*1.17E-04*
HS^-	2.13E-07	2.30E-07	*-1.74E-08*	2.12E-06	*1.90E-06*
H_2S (aq)	1.01E-08	1.92E-08	*-9.13E-09*	5.66E-07	*5.56E-07*
K Total	3.51E-04	1.99E-04	*1.52E-04*	1.90E-04	*-1.61E-04*
K^+	3.43E-04	1.97E-04	*1.46E-04*	1.88E-04	*-1.55E-04*
$KHCO_3$ (aq)	7.76E-06	2.03E-06	*5.73E-06*	1.85E-06	*-5.91E-06*
KSO_4^-	1.51E-07	2.83E-07	*-1.31E-07*	2.59E-07	*1.07E-07*
KCO_3^-	1.83E-07	2.72E-08	*1.56E-07*	7.72E-09	*-1.75E-07*
KOH (aq)	5.12E-09	1.66E-09	*3.46E-09*	4.86E-10	*-4.63E-09*
Ca Total	2.75E-06	5.39E-06	*-2.65E-06*	3.62E-05	*3.35E-05*
Ca^{+2}	1.89E-06	4.60E-06	*-2.72E-06*	3.25E-05	*3.06E-05*
$CaCO_3$ (aq)	5.52E-07	3.44E-07	*2.08E-07*	7.07E-07	*1.55E-07*
$CaHCO_3^+$	2.78E-07	3.07E-07	*-2.92E-08*	2.05E-06	*1.77E-06*
$CaSO_4$ (aq)	1.05E-08	8.26E-08	*-7.20E-08*	5.46E-07	*5.36E-07*
CaF^+	1.48E-08	3.01E-08	*-1.52E-08*	2.75E-07	*2.61E-07*
$CaOH^+$	3.34E-09	4.57E-09	*-1.23E-09*	9.80E-09	*6.46E-09*

Italics indicate values calculated from modeling outputs.

Table XXXVII: Calibrated EQ3/6 outputs compared with EQ3 speciation: select species (mol/kg), Pendragon and Gwenivere.

	EQ3/6	Pendragon	*Δ Pendragon - EQ3/6*	EQ3/6	Gwenivere	*Δ Gwenivere - EQ3/6*
T (°C)	83.9	83.9	*0.0*	79.8	79.8	*0.0*
H^+	1.45E-08	4.22E-08	*2.76E-08*	1.26E-08	3.13E-09	*-9.47E-09*
pH	7.838	7.375	*-0.463*	7.899	8.504	*0.604*
C Total	1.20E-02	5.89E-03	*-6.11E-03*	1.20E-02	5.65E-03	*-6.36E-03*
HCO_3^-	1.07E-02	5.11E-03	*-5.58E-03*	1.08E-02	4.99E-03	*-5.77E-03*
CO_2 (aq)	2.41E-04	3.36E-04	*9.56E-05*	2.05E-04	2.36E-05	*-1.81E-04*
CO_3^{-2}	9.79E-05	1.59E-05	*-8.21E-05*	1.12E-04	2.09E-04	*9.70E-05*
F Total	1.00E-03	7.37E-04	*-2.65E-04*	1.00E-03	7.00E-04	*-3.02E-04*
F^-	1.00E-03	7.35E-04	*-2.67E-04*	1.00E-03	6.99E-04	*-3.04E-04*
Na Total	1.22E-02	1.08E-02	*-1.43E-03*	1.23E-02	1.17E-02	*-5.51E-04*
Na^+	1.12E-02	1.03E-02	*-9.17E-04*	1.14E-02	1.11E-02	*-2.20E-04*
$NaHCO_3$ (aq)	9.62E-04	4.26E-04	*-5.36E-04*	9.21E-04	4.19E-04	*-5.02E-04*
$NaHSiO_3$ (aq)	8.12E-06	1.99E-05	*1.18E-05*	8.59E-06	1.69E-04	*1.60E-04*
NaF (aq)	1.71E-06	1.16E-06	*-5.47E-07*	1.64E-06	1.12E-06	*-5.19E-07*
$NaCO_3^-$	9.72E-07	1.47E-07	*-8.25E-07*	1.17E-06	2.14E-06	*9.70E-07*
NaOH (aq)	1.60E-07	5.06E-08	*-1.09E-07*	1.54E-07	6.06E-07	*4.52E-07*
Al Total	1.01E-06	2.71E-06	*1.70E-06*	9.01E-07	8.19E-06	*7.29E-06*
AlO_2^-	1.00E-06	2.65E-06	*1.65E-06*	8.94E-07	8.17E-06	*7.28E-06*
$HAlO_2$ (aq)	8.15E-09	6.30E-08	*5.49E-08*	7.09E-09	1.61E-08	*9.03E-09*
Si Total	6.62E-04	4.87E-03	*4.21E-03*	6.10E-04	3.73E-03	*3.12E-03*
SiO_2 (aq)	6.15E-04	4.75E-03	*4.14E-03*	5.63E-04	2.81E-03	*2.25E-03*
$HSiO_3^-$	4.64E-05	1.23E-04	*7.62E-05*	4.57E-05	9.17E-04	*8.71E-04*
S Total	5.28E-05	1.60E-04	*1.07E-04*	5.29E-05	1.39E-04	*8.63E-05*
SO_4^{-2}	5.26E-05	1.59E-04	*1.06E-04*	5.26E-05	1.34E-04	*8.14E-05*
HS^-	2.09E-07	4.77E-07	*2.68E-07*	2.07E-07	4.79E-06	*4.59E-06*
H_2S (aq)	7.99E-09	5.32E-08	*4.52E-08*	7.11E-09	4.09E-08	*3.38E-08*
K Total	2.93E-04	1.32E-04	*-1.61E-04*	2.67E-04	1.95E-04	*-7.21E-05*
K^+	2.88E-04	1.31E-04	*-1.57E-04*	2.62E-04	1.93E-04	*-6.93E-05*
$KHCO_3$ (aq)	5.43E-06	1.19E-06	*-4.24E-06*	4.52E-06	1.54E-06	*-2.98E-06*
KSO_4^-	1.15E-07	1.61E-07	*4.60E-08*	1.00E-07	1.88E-07	*8.79E-08*
KCO_3^-	1.83E-07	1.37E-08	*-1.69E-07*	1.82E-07	2.50E-07	*6.79E-08*
KOH (aq)	3.73E-09	5.87E-10	*-3.14E-09*	3.16E-09	9.36E-09	*6.20E-09*
Ca Total	2.75E-06	2.73E-05	*2.45E-05*	2.75E-06	6.46E-06	*3.72E-06*
Ca^{+2}	1.88E-06	2.39E-05	*2.20E-05*	1.88E-06	3.81E-06	*1.94E-06*
$CaCO_3$ (aq)	5.94E-07	1.26E-06	*6.69E-07*	6.16E-07	2.34E-06	*1.72E-06*
$CaHCO_3^+$	2.46E-07	1.52E-06	*1.27E-06*	2.33E-07	2.20E-07	*-1.30E-08*
$CaSO_4$ (aq)	9.36E-09	3.70E-07	*3.61E-07*	8.84E-09	4.59E-08	*3.70E-08*
CaF^+	1.27E-08	1.20E-07	*1.07E-07*	1.18E-08	1.67E-08	*4.93E-09*
$CaOH^+$	2.46E-09	1.09E-08	*8.40E-09*	2.11E-09	1.72E-08	*1.51E-08*

Italics indicate values calculated from modeling outputs.

Table XXXVIII: Calibrated EQ3/6 outputs compared with EQ3 speciation: select species (mol/kg), Merlin's Beard and Mordrid.

	EQ3/6	Merlin's Beard	*Δ Merlin's Beard - EQ3/6*	EQ3/6	Mordrid	*Δ Mordrid - EQ3/6*
T (°C)	74.2	74.2	*0.0*	59.1	59.1	*0.0*
H^+	1.03E-08	3.58E-08	*2.55E-08*	5.69E-09	6.96E-07	*6.91E-07*
pH	7.987	7.446	*-0.541*	8.245	6.157	*-2.088*
C Total	1.20E-02	2.75E-03	*-9.26E-03*	1.20E-02	6.28E-03	*-5.72E-03*
HCO_3^-	1.08E-02	2.46E-03	*-8.37E-03*	1.09E-02	3.04E-03	*-7.90E-03*
CO_2 (aq)	1.64E-04	1.35E-04	*-2.95E-05*	8.92E-05	3.05E-03	*2.96E-03*
CO_3^{-2}	1.36E-04	8.24E-06	*-1.27E-04*	2.25E-04	5.05E-07	*-2.24E-04*
F Total	1.00E-03	7.26E-04	*-2.76E-04*	1.00E-03	1.16E-03	*1.55E-04*
F^-	1.00E-03	7.25E-04	*-2.78E-04*	1.00E-03	1.15E-03	*1.52E-04*
Na Total	1.24E-02	7.66E-03	*-4.74E-03*	1.26E-02	1.14E-02	*-1.19E-03*
Na^+	1.15E-02	7.50E-03	*-4.01E-03*	1.19E-02	1.12E-02	*-6.46E-04*
$NaHCO_3$ (aq)	8.67E-04	1.34E-04	*-7.33E-04*	7.39E-04	1.95E-04	*-5.44E-04*
$NaHSiO_3$ (aq)	9.28E-06	1.15E-05	*2.23E-06*	1.15E-05	1.35E-06	*-1.02E-05*
NaF (aq)	1.56E-06	7.66E-07	*-7.93E-07*	1.36E-06	1.48E-06	*1.28E-07*
$NaCO_3^-$	1.51E-06	6.49E-08	*-1.45E-06*	3.16E-06	6.78E-09	*-3.15E-06*
NaOH (aq)	1.45E-07	2.73E-08	*-1.18E-07*	1.21E-07	9.34E-10	*-1.20E-07*
Al Total	7.67E-07	1.81E-06	*1.04E-06*	4.80E-07	2.34E-06	*1.86E-06*
AlO_2^-	7.62E-07	1.76E-06	*1.00E-06*	4.77E-07	1.29E-06	*8.10E-07*
$HAlO_2$ (aq)	5.79E-09	4.83E-08	*4.25E-08*	3.11E-09	1.03E-06	*1.03E-06*
Si Total	5.42E-04	3.34E-03	*2.80E-03*	3.78E-04	5.07E-03	*4.69E-03*
SiO_2 (aq)	4.96E-04	3.26E-03	*2.76E-03*	3.34E-04	5.06E-03	*4.73E-03*
$HSiO_3^-$	4.47E-05	8.16E-05	*3.69E-05*	4.11E-05	5.06E-06	*-3.60E-05*
S Total	5.29E-05	8.70E-05	*3.42E-05*	5.29E-05	1.38E-04	*8.55E-05*
SO_4^{-2}	5.27E-05	8.55E-05	*3.28E-05*	5.27E-05	1.37E-04	*8.45E-05*
HS^-	2.05E-07	6.76E-07	*4.71E-07*	1.96E-07	2.96E-07	*9.92E-08*
H_2S (aq)	6.07E-09	7.24E-08	*6.63E-08*	3.96E-09	7.34E-07	*7.30E-07*
K Total	2.34E-04	1.97E-04	*-3.64E-05*	1.58E-04	1.54E-04	*-3.61E-06*
K^+	2.30E-04	1.97E-04	*-3.35E-05*	1.56E-04	1.53E-04	*-2.31E-06*
$KHCO_3$ (aq)	3.49E-06	7.08E-07	*-2.78E-06*	1.67E-06	4.59E-07	*-1.21E-06*
KSO_4^-	8.27E-08	1.25E-07	*4.23E-08*	4.84E-08	1.25E-07	*7.71E-08*
KCO_3^-	1.81E-07	1.02E-08	*-1.71E-07*	1.75E-07	3.92E-10	*-1.75E-07*
KOH (aq)	2.50E-09	6.18E-10	*-1.88E-09*	1.23E-09	9.94E-12	*-1.22E-09*
Ca Total	2.75E-06	8.89E-05	*8.62E-05*	2.75E-06	1.00E-05	*7.28E-06*
Ca^{+2}	1.86E-06	8.32E-05	*8.13E-05*	1.81E-06	9.58E-06	*7.77E-06*
$CaCO_3$ (aq)	6.48E-07	2.05E-06	*1.40E-06*	7.40E-07	8.95E-09	*-7.31E-07*
$CaHCO_3^+$	2.15E-07	2.36E-06	*2.14E-06*	1.77E-07	2.62E-07	*8.52E-08*
$CaSO_4$ (aq)	8.19E-09	6.96E-07	*6.88E-07*	6.71E-09	9.41E-08	*8.74E-08*
CaF^+	1.06E-08	3.70E-07	*3.59E-07*	8.22E-09	5.04E-08	*4.22E-08*
$CaOH^+$	1.69E-09	2.26E-08	*2.09E-08*	9.02E-10	3.91E-11	*-8.63E-10*

Italics indicate values calculated from modeling outputs.

Table XXXIX: Grizzly Pool speciation (EQ3): select species (mol/kg).

	Grizzly Pool
T (°C)	17.3
H^+	7.57E-10
pH	9.121
C Total	4.02E-03
HCO_3^-	3.58E-03
CO_2 (aq)	5.60E-06
CO_3^{-2}	2.76E-04
F Total	1.07E-03
F^-	1.07E-03
Na Total	1.14E-02
Na^+	1.10E-02
$NaHCO_3$ (aq)	1.49E-04
$NaHSiO_3$ (aq)	1.90E-04
NaF (aq)	8.99E-07
$NaCO_3^-$	9.55E-06
NaOH (aq)	4.81E-08
Al Total	1.52E-06
AlO_2^-	1.52E-06
$HAlO_2$ (aq)	4.67E-09
Si Total	9.00E-04
SiO_2 (aq)	6.56E-04
$HSiO_3^-$	2.44E-04
S Total	4.16E-05
SO_4^{-2}	4.15E-05
HS^-	9.92E-11
H_2S (aq)	7.87E-13
HSO_4^-	1.63E-12
K Total	2.61E-04
K^+	2.60E-04
$KHCO_3$ (aq)	3.46E-07
KSO_4^-	5.25E-08
KCO_3^-	3.02E-07
KOH (aq)	6.01E-10
Ca Total	3.90E-05
Ca^{+2}	3.11E-05
$CaCO_3$ (aq)	6.75E-06
$CaHCO_3^+$	8.38E-07
$CaSO_4$ (aq)	6.86E-08
CaF^+	1.03E-07
$CaOH^+$	2.09E-09

Table XL: Fluorine speciation (EQ3) in Y-5 thermal features.

Species (mol/kg)	3 of a Kind	Uther	Pendragon	Gwenivere	Merlin's Beard	Mordrid	Grizzly Pool
F Total	8.42E-04	1.12E-03	7.37E-04	7.00E-04	7.26E-04	1.16E-03	1.07E-03
F^-	8.40E-04	1.12E-03	7.35E-04	6.99E-04	7.25E-04	1.15E-03	1.07E-03
NaF (aq)	1.70E-06	2.37E-06	1.16E-06	1.12E-06	7.66E-07	1.48E-06	8.99E-07
HF (aq)	1.32E-07	5.66E-07	1.22E-07	7.86E-09	8.56E-08	1.88E-06	8.54E-10
MgF^+	4.99E-08	6.58E-08	3.97E-08	3.00E-08	1.33E-07	2.35E-08	1.74E-07
CaF^+	3.01E-08	2.75E-07	1.20E-07	1.67E-08	3.70E-07	5.04E-08	1.03E-07
RbF (aq)	7.61E-09	9.80E-09	6.24E-09	6.90E-09	5.11E-09	8.08E-09	8.79E-09
BaF^+	5.18E-10	6.85E-10	4.13E-10	3.33E-10	2.13E-10	2.40E-10	6.07E-11
SrF^+	1.50E-10	2.00E-10	1.25E-10	9.82E-11	1.22E-10	8.78E-11	8.80E-11
HF_2^-	3.78E-11	2.15E-10	3.01E-11	1.82E-12	2.02E-11	6.64E-10	2.02E-13
FeF^{+2}	1.70E-17	8.89E-16	5.86E-17	1.52E-20	2.04E-17	2.04E-12	7.55E-19
FeF^+	5.38E-19	1.05E-17	3.10E-19	6.76E-22	8.73E-20	4.98E-17	1.98E-22
BF_4^-	2.47E-21	2.75E-19	2.68E-21	5.71E-25	7.12E-22	6.25E-17	5.75E-26

Table XLI: Chlorine speciation (EQ3) in Y-5 thermal features.

Species (mol/kg)	3 of a Kind	Uther	Pendragon	Gwenivere	Merlin's Beard	Mordrid	Grizzly Pool
Cl Total	5.36E-03	7.39E-03	4.51E-03	4.17E-03	4.15E-03	7.33E-03	6.06E-03
Cl^-	5.34E-03	7.37E-03	4.50E-03	4.16E-03	4.14E-03	7.32E-03	6.06E-03
NaCl (aq)	1.54E-05	2.23E-05	1.03E-05	9.73E-06	6.43E-06	1.42E-05	8.61E-06
LiCl (aq)	8.73E-08	1.47E-07	6.93E-08	6.23E-08	3.79E-08	9.21E-08	4.97E-08
$CaCl^+$	2.11E-08	2.01E-07	8.14E-08	1.10E-08	2.34E-07	3.53E-08	6.01E-08
CsCl (aq)	1.40E-08	1.91E-08	1.07E-08	9.33E-09	5.39E-09	1.34E-08	4.63E-09
KCl (aq)	1.25E-08	1.62E-08	5.89E-09	7.24E-09	6.71E-09	6.20E-09	2.97E-09
$MgCl^+$	8.79E-09	1.20E-08	6.91E-09	5.14E-09	2.22E-08	4.51E-09	3.20E-08
$BaCl^+$	2.15E-09	2.94E-09	1.59E-09	1.23E-09	7.38E-10	8.68E-10	1.59E-10
RbCl (aq)	1.33E-09	1.78E-09	9.69E-10	9.97E-10	6.66E-10	9.80E-10	5.28E-10
$ZnCl^+$	7.84E-10	3.43E-09	9.56E-10	5.83E-11	5.32E-10	2.30E-09	6.03E-11
$SrCl^+$	4.78E-10	6.62E-10	3.78E-10	2.85E-10	3.33E-10	2.55E-10	1.97E-10
$CaCl_2$ (aq)	2.12E-11	2.74E-10	7.17E-11	9.05E-12	2.05E-10	5.86E-11	1.53E-10
$ZnCl_2$ (aq)	2.14E-12	1.27E-11	2.27E-12	1.28E-13	1.24E-12	1.01E-11	3.85E-13
$ZnCl_3^-$	2.19E-15	1.80E-14	2.11E-15	1.15E-16	1.18E-15	2.06E-14	1.55E-15
ClO^-	2.39E-19	2.18E-19	8.74E-19	8.45E-19	2.28E-19	8.95E-19	4.97E-20
HClO (aq)	1.15E-19	3.37E-19	5.53E-19	4.03E-20	1.33E-19	1.12E-17	1.29E-21
$FeCl^+$	1.03E-19	2.08E-18	5.60E-20	1.18E-22	1.44E-20	8.78E-18	2.82E-23
$FeCl_2$ (aq)	6.63E-27	1.82E-25	1.40E-27	1.80E-30	1.31E-28	2.78E-26	4.85E-34
ClO_3^-	1.08E-27	4.31E-28	1.78E-25	2.94E-25	1.09E-26	1.28E-24	1.34E-25
ClO_2^-	3.54E-29	2.13E-29	6.43E-28	6.95E-28	5.60E-29	6.48E-28	6.29E-30
ClO_4^-	4.22E-30	1.11E-30	5.70E-27	1.36E-26	2.17E-28	2.15E-25	1.26E-25

Table XLII: Bromide speciation (EQ3) in Y-5 thermal features.

Species (mol/kg)	3 of a Kind	Uther	Pendragon	Gwenivere	Merlin's Beard	Mordrid	Grizzly Pool
Br Total	9.19E-06	1.01E-05	8.26E-06	7.71E-06	5.32E-06	9.40E-06	7.42E-06
Br^-	9.18E-06	1.01E-05	8.25E-06	7.70E-06	5.32E-06	9.39E-06	7.42E-06
NaBr (aq)	8.78E-09	1.02E-08	6.11E-09	5.78E-09	2.61E-09	5.50E-09	2.70E-09
KBr (aq)	8.84E-11	9.20E-11	4.64E-11	5.89E-11	3.91E-11	3.96E-11	2.45E-11
CsBr (aq)	2.78E-11	3.05E-11	2.33E-11	2.08E-11	8.46E-12	2.22E-11	8.49E-12
RbBr (aq)	1.35E-12	1.45E-12	1.04E-12	1.08E-12	4.97E-13	7.21E-13	3.56E-13
HBrO (aq)	1.97E-18	4.64E-18	1.35E-17	1.15E-18	3.24E-18	4.94E-16	3.88E-19
BrO^-	5.84E-19	4.27E-19	2.91E-18	3.22E-18	7.18E-19	4.68E-18	1.33E-18
Br_3^-	2.50E-28	2.30E-27	2.41E-27	1.57E-29	3.21E-28	6.25E-24	6.79E-29
BrO_3^-	1.20E-30	3.84E-31	2.29E-28	3.96E-28	1.08E-29	1.48E-27	2.35E-28
BrO_4^-	3.76E-47	7.91E-48	2.61E-44	4.31E-44	2.81E-46	6.08E-44	2.18E-46

Table XLIII: Lithium and boron speciation (EQ3) in Y-5 thermal features.

Species (mol/kg)	3 of a Kind	Uther	Pendragon	Gwenivere	Merlin's Beard	Mordrid	Grizzly Pool
Li Total	3.57E-04	4.42E-04	3.66E-04	3.76E-04	2.35E-04	3.90E-04	3.44E-04
Li^+	3.57E-04	4.42E-04	3.66E-04	3.76E-04	2.35E-04	3.90E-04	3.44E-04
LiCl (aq)	8.73E-08	1.47E-07	6.93E-08	6.23E-08	3.79E-08	9.21E-08	4.97E-08
LiOH (aq)	1.18E-08	4.50E-09	6.66E-09	7.56E-08	3.14E-09	1.18E-10	5.38E-09
$LiCO_3^-$	1.34E-09	4.92E-10	1.50E-09	2.30E-08	7.47E-10	1.32E-10	6.77E-07
B Total	2.76E-04	2.84E-04	2.84E-04	2.85E-04	1.34E-04	2.79E-04	2.49E-04
$B(OH)_3$ (aq)	2.61E-04	2.79E-04	2.73E-04	1.87E-04	1.28E-04	2.79E-04	1.42E-04
BO_2^-	1.43E-05	4.76E-06	1.10E-05	9.84E-05	5.40E-06	5.15E-07	1.07E-04
BF_4^-	2.47E-21	2.75E-19	2.68E-21	5.71E-25	7.12E-22	6.25E-17	5.75E-26

Table XLIV: As, Rb, Mo, Sb, Cs, and W speciation (EQ3) of in Y-5 thermal features.

Species (mol/kg)	3 of a Kind	Uther	Pendragon	Gwenivere	Merlin's Beard	Mordrid	Grizzly Pool
As Total	1.76E-05	1.74E-05	1.75E-05	1.86E-05	8.07E-06	1.76E-05	8.18E-06
$HAsO_4^{-2}$	1.55E-05	1.21E-05	1.50E-05	1.83E-05	7.05E-06	5.06E-06	8.12E-06
$H_2AsO_4^-$	2.14E-06	5.29E-06	2.51E-06	2.19E-07	1.01E-06	1.26E-05	2.44E-08
AsO_4^{-3}	5.61E-09	1.40E-09	4.06E-09	6.70E-08	1.92E-09	6.88E-11	4.25E-08
$HAsO_2$ (aq)	1.32E-26	1.59E-25	7.61E-28	1.89E-30	1.07E-28	2.94E-28	6.18E-38
$H_2AsO_3^-$	1.74E-27	6.52E-27	6.76E-29	2.09E-30	8.83E-30	8.89E-31	4.29E-38
AsO_2^-	1.71E-27	6.41E-27	6.68E-29	2.07E-30	8.78E-30	8.93E-31	4.33E-38
Rb Total	9.98E-07	9.81E-07	9.57E-07	1.14E-06	8.02E-07	8.78E-07	1.15E-06
Rb^+	9.89E-07	9.69E-07	9.50E-07	1.13E-06	7.96E-07	8.68E-07	1.14E-06
RbF (aq)	7.61E-09	9.80E-09	6.24E-09	6.90E-09	5.11E-09	8.08E-09	8.79E-09
RbCl (aq)	1.33E-09	1.78E-09	9.69E-10	9.97E-10	6.66E-10	9.80E-10	5.28E-10
RbOH (aq)	1.43E-11	4.31E-12	7.32E-12	9.46E-11	4.30E-12	9.67E-14	4.42E-12
RbBr (aq)	1.35E-12	1.45E-12	1.04E-12	1.08E-12	4.97E-13	7.21E-13	3.56E-13
Mo Total	8.40E-07	4.68E-07	5.46E-07	6.32E-07	3.25E-07	5.42E-07	5.13E-07
MoO_4^{-2}	8.39E-07	4.66E-07	5.45E-07	6.32E-07	3.25E-07	5.33E-07	5.13E-07
$HMoO_4^-$	1.11E-09	1.95E-09	7.86E-10	6.19E-11	3.56E-10	8.42E-09	6.31E-12
Sb Total	9.74E-07	1.09E-06	1.10E-06	1.09E-06	5.38E-07	1.14E-06	3.92E-07
$HSbO_2$ (aq)	9.71E-07	1.09E-06	1.09E-06	1.07E-06	5.38E-07	1.14E-06	3.88E-07
SbO_2^-	2.48E-09	8.62E-10	1.84E-09	2.22E-08	8.24E-10	6.20E-11	4.64E-09
Cs Total	2.06E-06	2.07E-06	2.02E-06	2.01E-06	1.19E-06	2.09E-06	1.46E-06
Cs^+	2.04E-06	2.05E-06	2.01E-06	2.00E-06	1.19E-06	2.07E-06	1.45E-06
CsCl (aq)	1.40E-08	1.91E-08	1.07E-08	9.33E-09	5.39E-09	1.34E-08	4.63E-09
CsBr (aq)	2.78E-11	3.05E-11	2.33E-11	2.08E-11	8.46E-12	2.22E-11	8.49E-12
CsOH (aq)	1.99E-12	6.13E-13	9.72E-13	1.01E-11	3.70E-13	1.15E-14	1.71E-13
W Total	7.56E-06	7.78E-06	7.97E-06	7.80E-06	4.12E-06	8.50E-06	6.17E-06
WO_4^{-2}	7.56E-06	7.77E-06	7.97E-06	7.80E-06	4.12E-06	8.48E-06	6.17E-06
HWO_4^-	1.81E-09	5.91E-09	2.05E-09	1.36E-10	7.94E-10	2.28E-08	1.16E-11

Table XLV: Carbon speciation (EQ3) in Y-5 thermal features.

Species (mol/kg)	3 of a Kind	Uther	Pendragon	Gwenivere	Merlin's Beard	Mordrid	Grizzly Pool
C total	5.64E-03	6.06E-03	5.89E-03	5.65E-03	2.75E-03	6.28E-03	4.02E-03
HCO_3^-	4.82E-03	4.68E-03	5.11E-03	4.99E-03	2.46E-03	3.04E-03	3.58E-03
$NaHCO_3$ (aq)	5.27E-04	5.37E-04	4.26E-04	4.19E-04	1.34E-04	1.95E-04	1.49E-04
CO_2 (aq)	2.67E-04	8.34E-04	3.36E-04	2.36E-05	1.35E-04	3.05E-03	5.60E-06
CO_3^{-2}	1.93E-05	5.90E-06	1.59E-05	2.09E-04	8.24E-06	5.05E-07	2.76E-04
$KHCO_3$ (aq)	2.03E-06	1.85E-06	1.19E-06	1.54E-06	7.08E-07	4.59E-07	3.46E-07
$Ca(CO_3)$ (aq)	3.44E-07	7.07E-07	1.26E-06	2.34E-06	2.05E-06	8.95E-09	6.75E-06
$Ca(HCO_3)^+$	3.07E-07	2.05E-06	1.52E-06	2.20E-07	2.36E-06	2.62E-07	8.38E-07
$NaCO_3^-$	1.93E-07	6.11E-08	1.47E-07	2.14E-06	6.49E-08	6.78E-09	9.55E-06
$Mg(HCO_3)^+$	1.38E-07	1.33E-07	1.33E-07	1.03E-07	2.18E-07	2.98E-08	2.82E-07
$BaHCO_3^+$	1.16E-07	1.12E-07	1.02E-07	8.00E-08	2.27E-08	1.64E-08	2.87E-09
$Mg(CO_3)$ (aq)	4.02E-08	1.19E-08	3.05E-08	3.13E-07	5.64E-08	3.41E-10	1.13E-06
$SrHCO_3^+$	3.80E-08	3.70E-08	3.34E-08	2.50E-08	1.34E-08	5.64E-09	3.10E-09
KCO_3^-	2.72E-08	7.72E-09	1.37E-08	2.50E-07	1.02E-08	3.92E-10	3.02E-07
$Ba(CO_3)$ (aq)	8.59E-09	2.54E-09	6.25E-09	6.69E-08	1.69E-09	6.14E-11	6.30E-09
$Sr(CO_3)$ (aq)	2.94E-09	8.81E-10	2.17E-09	2.21E-08	1.05E-09	2.24E-11	6.74E-09
$NH_4CO_3^-$	1.68E-09	7.24E-10	1.53E-09	5.44E-09	7.76E-10	3.23E-11	1.08E-08
$FeCO_3$ (aq)	5.63E-17	2.45E-16	3.27E-17	9.97E-19	5.46E-18	1.22E-16	3.60E-19
$FeHCO_3^+$	6.38E-18	9.05E-17	4.12E-18	8.89E-21	5.19E-19	1.99E-16	6.83E-22
$Fe(CO_3)_2^{-2}$	1.82E-20	2.43E-20	9.28E-21	3.88E-21	8.81E-22	1.46E-21	5.67E-21
CO (aq)	1.08E-39	5.08E-39	2.07E-41	3.48E-43	1.04E-42	3.96E-44	1.07E-53
OCN^-	2.44E-58	4.00E-57	4.01E-63	1.50E-65	5.78E-64	8.64E-70	5.27E-84

Table XLVI: Nitrogen speciation (EQ3) in Y-5 thermal features.

Species (mol/kg)	3 of a Kind	Uther	Pendragon	Gwenivere	Merlin's Beard	Mordrid	Grizzly Pool
N total	1.48E-05	1.48E-05	1.48E-05	1.73E-05	1.54E-05	1.02E-05	1.42E-05
NH_4^+	7.78E-06	1.12E-05	9.79E-06	2.89E-06	1.07E-05	9.93E-06	9.83E-06
NH_3 (aq)	6.22E-06	2.76E-06	4.21E-06	1.36E-05	3.32E-06	6.91E-08	4.16E-06
NO_3^-	8.06E-07	8.06E-07	8.06E-07	8.06E-07	1.42E-06	1.61E-07	1.61E-07
$NH_4CO_3^-$	1.68E-09	7.24E-10	1.53E-09	5.44E-09	7.76E-10	3.23E-11	1.08E-08
HNO_3 (aq)	4.96E-15	1.60E-14	5.20E-15	3.50E-16	6.44E-15	9.79E-15	4.20E-18
NO_2^-	1.30E-15	1.97E-15	8.80E-17	4.49E-17	1.21E-16	4.84E-19	1.54E-21
N_2 (aq)	9.73E-16	7.99E-14	3.42E-20	2.68E-23	7.17E-19	6.51E-23	1.67E-32
HNO_2 (aq)	2.53E-20	1.23E-19	2.29E-21	8.92E-23	2.98E-21	2.67E-22	1.90E-27
$HN_2O_2^-$	1.53E-53	2.58E-52	4.62E-58	2.50E-60	5.57E-58	3.09E-64	1.75E-76
$H_2N_2O_2$ (aq)	1.53E-54	8.31E-53	6.35E-59	2.66E-62	7.50E-59	9.71E-64	1.45E-78
$N_2O_2^{-2}$	3.61E-56	1.92E-55	7.67E-61	5.36E-62	8.78E-61	1.99E-68	2.57E-78

Table XLVII: Phosphorus speciation (EQ3) in Y-5 thermal features.

Species	3 of a Kind	Uther	Pendragon	Gwenivere	Merlin's Beard	Mordrid	Grizzly Pool
P Total	1.57E-06	1.05E-06	1.05E-06	1.05E-06	2.11E-07	2.11E-07	2.11E-07
HPO_4^{-2}	1.14E-06	4.83E-07	7.26E-07	1.02E-06	1.52E-07	2.72E-08	2.09E-07
$H_2PO_4^-$	4.25E-07	5.70E-07	3.27E-07	3.29E-08	5.88E-08	1.83E-07	1.78E-09
PO_4^{-3}	5.68E-11	7.66E-12	2.78E-11	5.34E-10	6.09E-12	5.73E-14	2.08E-10
H_3PO_4 (aq)	3.94E-12	1.70E-11	3.42E-12	2.40E-14	4.72E-13	2.28E-11	1.52E-16
$HP_2O_7^{-3}$	1.84E-13	1.07E-13	6.43E-14	7.93E-15	1.57E-15	5.37E-16	8.27E-18
$H_2P_2O_7^{-2}$	1.39E-14	2.53E-14	5.96E-15	5.21E-17	1.29E-16	7.35E-16	1.36E-20
$P_2O_7^{-4}$	4.46E-15	8.45E-16	1.36E-15	2.49E-15	3.90E-17	9.46E-19	1.22E-17
$H_3P_2O_7^-$	8.42E-20	4.87E-19	4.43E-20	2.78E-23	8.29E-22	8.03E-20	1.48E-27
$H_4P_2O_7$ (aq)	1.62E-25	3.02E-24	9.81E-26	4.34E-30	1.44E-27	2.23E-24	2.96E-35
HPO_3^{-2}	4.59E-43	2.94E-43	3.50E-45	1.04E-45	6.83E-47	1.25E-50	2.77E-57
$H_2PO_3^-$	1.79E-44	3.62E-44	1.62E-46	3.40E-48	2.64E-48	8.05E-51	1.87E-60
H_3PO_3 (aq)	4.93E-50	3.22E-49	5.26E-52	7.90E-55	6.95E-54	3.56E-55	6.90E-68

Table XLVIII: Sulfur speciation (EQ3) in Y-5 thermal features.

Species (mol/kg)	3 of a Kind	Uther	Pendragon	Gwenivere	Merlin's Beard	Mordrid	Grizzly Pool
S Total	1.73E-04	1.73E-04	1.60E-04	1.39E-04	8.70E-05	1.38E-04	4.16E-05
SO_4^{-2}	1.72E-04	1.70E-04	1.59E-04	1.34E-04	8.55E-05	1.37E-04	4.15E-05
KSO_4^-	2.83E-07	2.59E-07	1.61E-07	1.88E-07	1.25E-07	1.25E-07	5.25E-08
HS^-	2.30E-07	2.12E-06	4.77E-07	4.79E-06	6.76E-07	2.96E-07	9.92E-11
$CaSO_4$ (aq)	8.26E-08	5.46E-07	3.70E-07	4.59E-08	6.96E-07	9.41E-08	6.86E-08
H_2S (aq)	1.92E-08	5.66E-07	5.32E-08	4.09E-08	7.24E-08	7.34E-07	7.87E-13
$MnSO_4$ (aq)	5.32E-09	7.21E-09	5.39E-09	9.84E-12	2.15E-09	1.34E-09	5.07E-13
HSO_4^-	2.71E-09	8.49E-09	2.45E-09	1.33E-10	8.73E-10	1.59E-08	1.63E-12
$KHSO_4$ (aq)	9.77E-16	2.88E-15	4.68E-16	3.29E-17	1.95E-16	1.73E-15	9.36E-20
$FeSO_4$ (aq)	9.63E-19	1.35E-17	5.87E-19	1.11E-21	9.38E-20	4.72E-17	4.71E-23
HSO_5^-	5.77E-28	1.19E-27	1.43E-27	6.42E-29	8.29E-29	1.35E-27	5.23E-34
HSO_3^-	4.63E-39	2.19E-38	8.26E-41	1.22E-42	5.06E-42	2.58E-43	1.86E-53
SO_3^{-2}	4.06E-39	6.06E-39	6.79E-41	1.49E-41	5.64E-42	2.12E-44	2.50E-51
$S_2O_8^{-2}$	1.10E-42	7.21E-42	2.03E-42	4.52E-45	3.20E-44	6.40E-42	4.61E-53
SO_2 (aq)	5.55E-44	8.45E-43	9.77E-46	9.45E-49	3.95E-47	2.49E-47	7.19E-61
$S_2O_6^{-2}$	1.06E-59	1.59E-58	1.13E-61	7.39E-65	1.44E-63	5.86E-64	2.06E-79

Table XLIX: EQ3/6 relative abundances (comprising 99% or greater) for select elements in Y-5 thermal features.

Species	EQ3/6 92.2°C	EQ3/6 83.9°C	EQ3/6 79.8°C	EQ3/6 74.2°C	EQ3/6 59.1°C
Li^+	99.99	99.99	99.99	99.99	99.98
$B(OH)_3$ (aq)	91.19	89.42	88.40	86.84	81.47
BO_2^-	8.81	10.58	11.60	13.16	18.53
HCO_3^-	87.80	89.10	89.63	90.23	91.18
$NaHCO_3$ (aq)	8.74	8.02	7.67	7.23	6.16
CO_2 (aq)	2.76	2.00	1.71	1.37	0.00
CO_3^{-2}	0.00	0.00	0.00	1.13	1.87
N_2 (aq)	86.49	85.08	84.36	83.35	80.62
NH_3 (aq)	7.92	8.27	8.43	8.61	10.46
NH_4^+	5.58	6.64	7.21	8.03	8.90
F^-	99.81	99.82	99.83	99.84	99.86
HPO_4^{-2}	82.53	86.74	88.52	90.65	94.81
$H_2PO_4^-$	17.47	13.25	11.47	9.34	5.16
SO_4^{-2}	99.27	99.35	99.39	99.43	99.52
Cl^-	99.74	99.75	99.76	99.77	99.79
$HAsO_2$ (aq)	68.49	65.95	64.63	62.75	57.30
$H_2AsO_3^-$	15.89	17.11	17.75	18.66	21.40
AsO_2^-	15.62	16.93	17.61	18.58	21.29
Br^-	99.91	99.92	99.92	99.93	99.94
Rb^+	99.08	99.12	99.13	99.15	99.20
MoO_4^{-2}	99.92	99.95	99.96	99.97	99.99
$HSbO_2$ (aq)	99.55	99.51	99.49	99.45	99.34
Cs^+	99.99	99.99	99.99	99.99	99.99
WO_4^{-2}	99.99	99.99	99.99	99.99	100.00

SIGNATURE PAGE

This is to certify that the thesis prepared by Shanna Lynn Law entitled "Hydrothermal water-rock reaction modeling with microbial considerations: Rabbit Creek Area, Yellowstone National Park, WY" has been examined and approved for acceptance by the Department of Chemistry and Geochemistry, Montana Tech of The University of Montana, on this 24th day of July, 2018.

Alysia Cox, PhD, Assistant Professor
Department of Chemistry and Geochemistry
Chair, Examination Committee

Christopher Gammons, PhD, Professor
Department of Geological Engineering
Member, Examination Committee

Katherine Zodrow, PhD, Assistant Professor
Department of Environmental Engineering
Member, Examination Committee